JOURNAL OF PETROLOGY | VOLUME 52 | NUMBER 10 | PAGES 2009–2045 | 2011 | doi:10.1093/petrology/egr038

Volatile-rich Metasomatism in Montferrier Xenoliths (Southern France): Implications for the Abundances of Chalcophile and Highly Siderophile Elements in the Subcontinental Mantle

OLIVIER ALARD[1,2]*, JEAN-PIERRE LORAND[3], LAURIE REISBERG[4], JEAN-LOUIS BODINIER[1], JEAN-MARIE DAUTRIA[1] AND SUZANNE Y. O'REILLY[2]

[1]GÉOSCIENCES MONTPELLIER, CNRS UMR 5243, UNIVERSITÉ DE MONTPELLIER II, cc060, PL. E. BATAILLON, 34095 MONTPELLIER, FRANCE

[2]GEMOC, DEPARTMENT OF EARTH AND PLANETARY SCIENCES, MACQUARIE UNIVERSITY, SYDNEY, 2109 NSW, AUSTRALIA

[3]LABORATOIRE DE MINÉRALOGIE ET COSMOCHIMIE DU MUSÉUM NATIONAL D'HISTOIRE NATURELLE, CNRS UMR 7202, 61 RUE BUFFON, 75005 PARIS, FRANCE

[4]CRPG, CNRS, BP20, 54501 VANDOEUVRE-LES-NANCY, FRANCE

RECEIVED SEPTEMBER 12, 2009; ACCEPTED JULY 12, 2011

Despite a relatively 'uniform' fertile composition ($Al_2O_3 = 2{\cdot}19$–$4{\cdot}47$ wt %; Fo% = 89·2 ± 0·3%; $Cr\#_{Spl} = 8{\cdot}9 \pm 1{\cdot}5\%$), the Montferrier peridotite xenoliths show a wide range of S contents (22–590 ppm). Most sulphides are interstitial and show peculiar pyrrhotite–pentlandite intergrowths and low abundances of Cu-rich phases. Sulphide-rich samples are characterized by strong enrichment in the light rare earth elements and large ion lithophile elements without concomitant enrichment of the high field strength elements. Such trace-element fractionation is commonly ascribed to metasomatism by volatile-rich melts and/or carbonatitic melts. S and Se (11–67 ppb), as well as S/Se (up to ≈12 000), are correlated with La/Sm. Cu, however, remains broadly constant (30 ± 5 ppm). These features strongly suggest that the percolation–reaction of such volatile-rich fluids has led to sulphide enrichment with an atypical signature marked by strong fractionation of the chalcophile elements (i.e. S vs Se and Cu). S-rich xenoliths are also characterized by high $(Pd/Ir)_N$ (1·2–1·9; where subscript N indicates normalized to chondrite), $(Pd/Pt)_N$ between 1·5 and 2·2, and $(Os/Ir)_N$ up to 1·85. Despite the relative uniform fertile composition of the xenoliths, Re/Os ranges between 0·02 and 0·18. $^{187}Os/^{188}Os$ is extremely variable even within a single sample and can be as high as 0·1756 for the most S-rich samples. Sulphides show highly fractionated and variable abundances of the highly siderophile elements (HSE) $[0{\cdot}03 \leq (Pd/Ir)_N < 1283]$ and Re–Os isotopic composition $(0{\cdot}115 < {}^{187}Os/{}^{188}Os < 0{\cdot}172)$. Such variation can be observed at the thin-section scale. Whole-rock and in situ sulphide data demonstrate that chalcophile and HSE systematics and the Os isotopic composition of the upper mantle could be significantly modified through metasomatism, even with volatile-rich fluids. These features highlight the complex behaviour of the HSE in fluid–rock percolation–reaction models and suggest a complex interplay between sulphide addition (crystallization or sulphidation) and partial equilibration of pre-existing sulphide. The specific fractionations observed in chemical proxies such as S and Se, Os and Ir, and Pd and Pt, as

*Corresponding author. Present address: Géosciences Montpellier, CNRS UMR 5243, Université De Montpellier II, cc060, Pl. E. Bataillon, 34095 Montpellier, France. Telephone: +33 (0)467149311. Fax: +33 (0)467143603. E-mail: oalard@univ-montp2.fr

well as the low abundance of Cu-rich sulphides, suggest that sulphide addition may not have occurred via sulphide melts. Rather, we infer that S was present as a dissolved species in a (supercritical) oxidizing, volatile-rich fluid (C–O–H–S ± Cl) along with other chalcophile and siderophile elements such as Os, Pd, Re and Au. The highly radiogenic Os composition of this fluid ($^{187}Os/^{188}Os > 0{\cdot}17$) would imply that such fluids are derived from an uncommon type of mantle source possibly related to carbonatite melts.

KEY WORDS: *peridotite; sulphide; metasomatism; mantle; highly siderophile elements; chalcophile elements*

INTRODUCTION

The highly siderophile elements (HSE: Os, Ir, Ru, Rh, Pt, Pd, Au and Re) have recently been added to the suite of trace elements commonly analyzed in upper mantle samples. Unlike lithophile trace elements, which are controlled by major silicate and minor oxide phases, the HSE are carried by a set of trace phases including low melting point Cu–Fe–Ni sulphides (Lorand *et al.*,2008*a*, and references therein). The effects of metasomatism on HSE abundances and those of their companion chalcophile elements (including the semi-metals Se, Te, Bi and As) have been debated for the past 10 years. Integrated studies coupling mineralogical data on sulphides with whole-rock and *in situ* analyses of HSE and Re–Os isotopes provide compelling evidence that the chalcophile elements and HSE potentially offer an excellent opportunity to monitor the multistage metasomatic history of the lithospheric mantle in ways that are different from but complementary to those provided by incompatible lithophile elements (e.g. Alard *et al.*, 2000, 2002; Lorand *et al.*, 2008*a*). This stems from the extremely mobile and reactive nature of Cu–Fe–Ni sulphides in the mantle, and the high solubility of S in magmas and C–H–O–S fluids.

The estimated S content of the primitive mantle is about 250 ± 50 ppm (McDonough & Sun, 1995). Although the S contents of fertile peridotites from orogenic massifs support this estimate, peridotites hosted in alkali basalts commonly contain only a few tens of ppm S (Lorand, 1990; Ionov *et al.*, 1992; Lorand *et al.*, 2003*a*). However, several xenoliths from the Montferrier volcano (Herault valley, southern France) have very high S abundances (up to 2000 ppm) with intergranular sulphides predominating over enclosed sulphides (Lorand & Conquéré, 1983). Given the geochemical characteristics of the Montferrier peridotites and the pronounced sulphide enrichment already documented (Lorand & Conquéré, 1983; Cabanes & Briqueu, 1986; Fabries *et al.*, 1987; Cabanes & Mercier, 1988; Lorand & Alard, 2001; Lorand *et al.*, 2003*a*), this xenolith suite offers a promising opportunity to shed some new light on metasomatic processes and on their consequences for the systematics of the HSE and $^{187}Os/^{188}Os$ in metasomatized subcontinental lithospheric mantle (SCLM). Therefore we have carried out an extensive study of 23 selected xenoliths from the Montferrier locality, including major-element and lithophile trace-element analyses, and detailed studies of sulphide and chalcogenide (S, Se) element geochemistry. HSE abundances and Os isotopic compositions of whole-rocks and sulphides were determined for key samples.

SAMPLES AND GEOLOGICAL BACKGROUND

Montferrier is a Tertiary volcano (Bellon, 1976) located near Montpellier (Languedoc, Southern France, Fig. 1). Gastaud (1981) obtained two K–Ar ages of 23·6 ± 0·6 and 26·6 ± 0·7 Ma for the Montferrier lava and the nearby Pouget dyke, respectively. The lava is basanitic ($SiO_2 \approx 45$ wt %; Mg-number = 60, $Ne_{Norm} \approx 10\%$) in composition. Along with other discrete volcanic bodies, mainly isolated dykes, it forms the small Montpellier volcanic province, which lies within an Oligocene graben delimited by two major fault systems, which are probably of Hercynian origin, the Nimes faults (oriented N-20°) and the Cevennes Fault network (Fig. 1). The age, location and chemistry of these magmatic rocks indicate that this volcanism is not related to that of the Massif Central volcanic province (Dautria *et al.*, 2010). Recent studies suggest that the Montpellier province is instead part of the Languedoc volcanic domain, which extends from the shore of the Mediteranean Sea (Agde) to the Causses. This domain is characterized by a long (Jurassic to Quaternary) history of sporadic volcanic activity (small volumes $<2\ km^3$) now exposed mainly as plugs and dykes. Both the lavas and their entrained mantle xenoliths display Sr–Nd–Pb isotopic signatures intermediate between those of the French Massif Central (FMC) volcanic province and the Pyrenean peridotite massifs (Dautria *et al.*, 2010).

Two main volcanic products crop out at Montferrier: (1) phreatomagmatic hyaloclastic breccias of yellowish colour; (2) massive basanite lava occurring in a series of small intrusions. Both types of outcrop contain abundant peridotitic and very rare pyroxenitic xenoliths (Fabries *et al.*, 1987). The largest xenoliths occur in the breccias (up to 25 cm in diameter), and have an ovoid form (Luguet & Lorand, 1998). In contrast, the basanite-hosted xenoliths are angular and smaller (≤15 cm in diameter); they are fresher than those hosted by the breccias, which exhibit a yellow-brownish colour owing to olivine alteration. However, the basanite-hosted xenoliths can have loss on ignition (LOI) values as high as those from the breccias (Table 1). Observation of several tens of hand-sample specimens suggests that overall the Montferrier peridotite

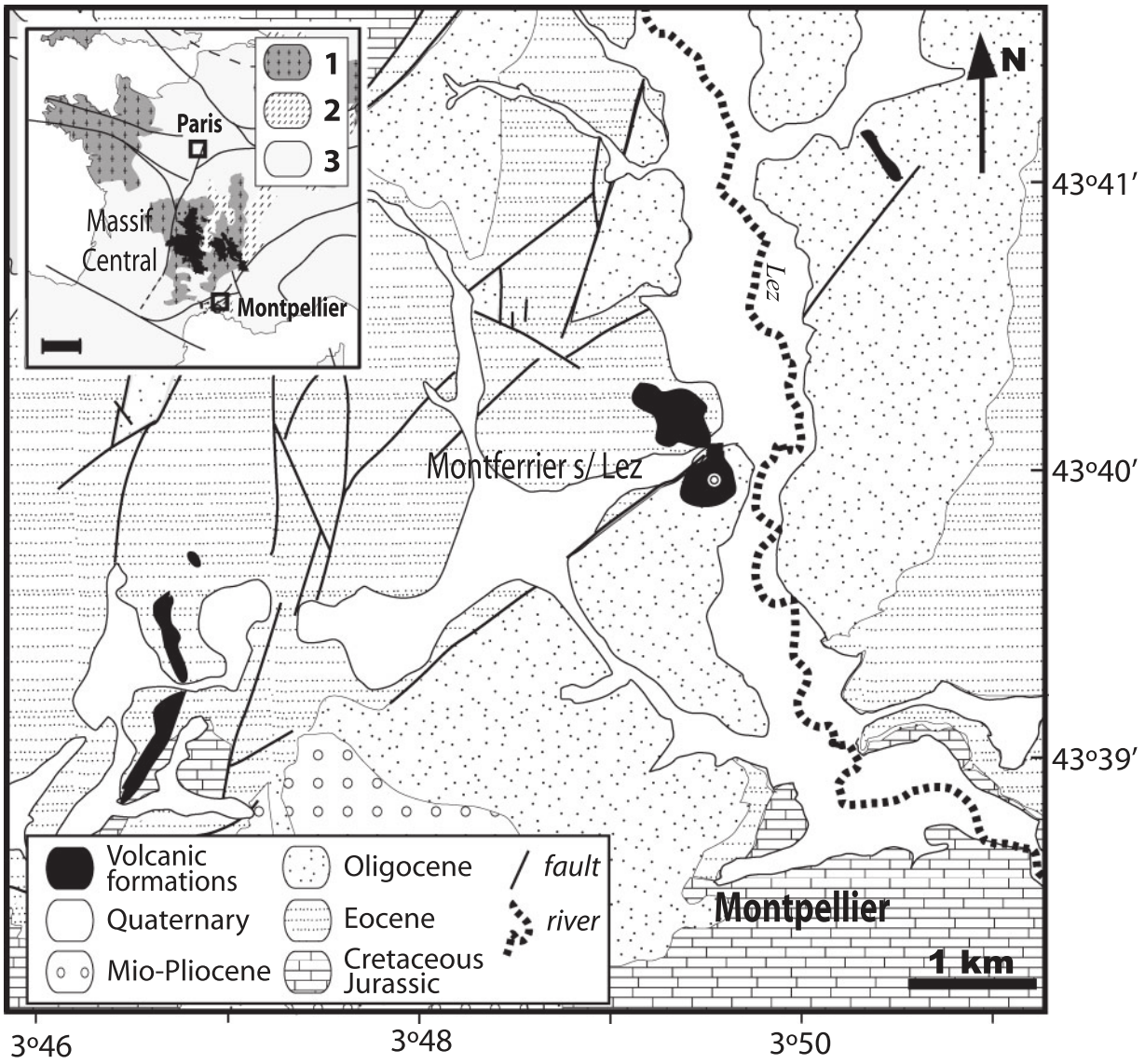

Fig. 1. Simplified geological map showing the location of the Montferrier volcano. 1, Hercynian massifs; 2, Oligo-Miocene peri-Alpine rifts; 3, Meso-Cenozoic cover; dashed line, Variscan tectonic front; continuous black lines, main faults. Scale bar is 200 km in main map; modified from Cabanes & Briqueu (1986).

xenoliths are relatively fertile and are mainly lherzolitic in composition, with a large proportion of cpx-rich lherzolites (cpx% = 15–20), and contain up to ≈10% amphibole (± phlogopite).

ANALYTICAL METHODS

One to three thin (≈30 μm) and thick sections (100–200 μm) were made for each sample. Sulphide modal abundance was obtained by point counting using a grid or by image processing of chemical maps obtained by electron microprobe using a LINK energy-dispersive system in the GEMOC Analytical Unit (GAU). Results obtained by both methods are comparable. Silicate compositions when not reported previously (Cabanes & Briqueu, 1986; Fabries *et al.*, 1987; Cabanes & Mercier, 1988) were obtained by electron microprobe analysis using a Cameca SX-50 electron microprobe at the GAU or a Cameca SX100 at the Service MicrosondeSud of Montpellier II University. Analytical conditions for silicates and oxides were: accelerating voltage 15 kV, sample current 20×10^{-9} A, beam diameter ≈1 μm, 10s peak counting and 5s background counting on either side of the peaks. New sulphide compositions [i.e. not reported by Fabries *et al.* (1987)] were obtained at the GAU using the CAMECA SX50 operated at the following conditions: accelerating voltage ≈20 kV,

sample current 20×10^{-9} A, beam diameter ≈2 μm; peak counting varied between 10 and 20s, and background counting was performed for 5–10s on each side of the peak.

To obtain sample powders for whole-rock analysis, the xenoliths were first sawn into 1–2 cm thick slabs. The slabs were carefully inspected for veins or impregnation areas. Then, the cores (taken several centimetres from the xenolith rim) of 2–4 slabs were crushed and powdered in an agate mortar. Contamination between samples was minimized by careful and extensive washing with MQ water

Table 1: Major and trace element compositions of the bulk-rock xenoliths and key parameters

Sample:	Pg	Pg-6	Pg-41	80-442	Pg-43	Pg-1	Pg-5	Pg-42	80-441	80-438	Mtf-10	Mtf-C1	Mtf-20	Mtf-21
Hosted:	β	β	β	β	β	β	β	β	β	β	β	β	β	β
Amp:	++	++++	+++	+++	+++	++	++	++	+	+	+	+	+	+
Al_2O_3	n.a.	4·47	3·02	2·59	3·73	n.a.	4·31	4·20	3·73	2·19	3·89	3·76	n.a.	n.a.
CaO	n.a.	3·57	3·13	2·02	3·42	n.a.	3·61	3·83	3·48	2·69	3·66	3·34	n.a.	n.a.
Fo%		89·2	89·5	90·0	89·0	n.a.	89·2	88·7	89·0	90·5		89·3	89·8	
$Cr\#_{Spl}$%		6·8	10·2	10·4	9·6	n.a.	8·2	5·5	9·5	11·0		9·0	8·3	
$T_{BK90} \pm 1SD$	857 ± 12	846 ± 12	863 ± 26	846 ± 7	n.a.	854 ± 21	867 ± 34							
Rb (ppm)	0·211	0·546	2·005	1·104	0·459	0·242	0·299	0·718	0·716	0·185	0·724	n.a.	n.a.	n.a.
Sr	21·0	49·8	48·5	48·9	11·4	23·4	13·5	12·9	20·1	1·4	28·1	—	—	—
Y	3·06	4·02	2·67	1·91	3·41	2·56	3·42	3·72	3·08	1·97	3·22	—	—	—
Zr	5·30	4·01	2·07	3·62	5·78	4·11	5·84	7·46	5·82	0·68	6·13	—	—	—
Nb	0·053	0·028	0·062	0·055	0·048	0·082	0·099	0·045	0·024	0·040	0·038	—	—	—
Cs	0·0064	0·0199	0·0172	0·0491	0·0049	0·0104	0·0181	0·0087	0·0364	0·0019	0·0484	—	—	—
Ba	1·48	21·6	24·3	54·9	0·55	7·39	1·86	0·99	4·96	0·32	12·2	—	—	—
La	1·66	3·96	3·12	4·04	0·221	1·18	0·283	0·248	0·569	0·012	1·24	—	—	—
Ce	2·64	5·79	5·24	3·38	0·736	2·08	0·537	0·724	0·975	0·033	1·87	—	—	—
Pr	0·243	0·291	0·412	0·190	0·126	0·236	0·118	0·138	0·132	0·010	0·198	—	—	—
Nd	0·921	0·883	1·217	0·642	0·802	0·942	0·724	0·842	0·738	0·116	0·938	—	—	—
Sm	0·281	0·307	0·238	0·182	0·307	0·247	0·290	0·324	0·283	0·095	0·310	—	—	—
Eu	0·119	0·136	0·097	0·073	0·128	0·107	0·130	0·137	0·126	0·047	0·131	—	—	—
Gd	0·477	0·540	0·352	0·274	0·483	0·373	0·478	0·525	0·459	0·221	0·462	—	—	—
Tb	0·0860	0·1066	0·0679	0·0519	0·0902	0·0694	0·0911	0·0974	0·0863	0·0466	0·0894	—	—	—
Dy	0·611	0·758	0·490	0·380	0·644	0·488	0·659	0·705	0·637	0·379	0·663	—	—	—
Ho	0·132	0·172	0·110	0·0851	0·144	0·108	0·147	0·157	0·142	0·0883	0·146	—	—	—
Er	0·378	0·497	0·319	0·253	0·420	0·313	0·415	0·460	0·411	0·264	0·430	—	—	—
Tm	0·0586	0·0756	0·0492	0·0399	0·0647	0·0477	0·0656	0·0684	0·0635	0·0419	0·0657	—	—	—
Yb	0·383	0·497	0·338	0·264	0·421	0·311	0·425	0·457	0·405	0·278	0·425	—	—	—
Lu	0·0620	0·0839	0·0575	0·0463	0·0696	0·0526	0·0717	0·0742	0·0692	0·0468	0·0708	—	—	—
Hf	0·203	0·197	0·110	0·122	0·217	0·144	0·199	0·230	0·203	0·047	0·214	—	—	—
Ta	0·0054	0·0015	0·0073	0·0023	0·0073	0·0088	0·0123	0·0035	0·0017	0·0008	0·0045	—	—	—
Th	0·186	0·381	0·655	0·913	0·002	0·205	0·016	0·002	0·065	0·001	0·193	—	—	—
U	0·0539	0·0699	0·142	0·333	0·0195	0·0811	0·0291	0·0136	0·0249	0·0028	0·0778	n.a.	n.a.	n.a.
S (ppm)	180	592	451	427	153	71	111	122	307	241	196	158		130
Cu (ppm)	30	35	33	20	33	26	31	30	26	23	32	n.a.		n.a.
Se (ppb)	67	50	48	n.a.	30	28	29	n.a.	n.a.	n.a.	40	n.a.		n.a.
S/Se	2687	11840	9396	—	5100	2536	3828	—	—	—	4900	—		—
Alt-S%	8·5	5·0	11·7	0·2	3·6	11·1	16·7	3·9	0·2	0·2	7·4	6·5	?	20·6
S* (ppm)	195	622	504	428	159	79	130	127	308	241	211	168		157
S*/Se	2915	12432	10495	—	5284	2817	4467	—	—	—	5263	—		—

(continued)

Table 1: Continued

Sample:	Mtf-37	Pg-3	Pg-45	Pg-46	Mtf-F	Pg-2	Pg-2n	Mtf-15	Mtf-17
Hosted:	Bc	Bc	Bc	Bc	Bc	Bc	Bc	Bc	Bc
Amp:	+++	+++	++	++	+	+	+	+	+
Al_2O_3	4·24	4·03	3·21	3·78	3·04	n.a.	n.a.	3·67	3·16
CaO	3·75	4·26	3·01	3·28	2·96	n.a.	n.a.	3·58	2·49
Fo%	89·3	89·3	89·4	89·2	90·0	89·0	89·1	89·7	89·6
$Cr\#_{Spl}$%	8·7	10·1	10·6	9·1	8·3	8·5	9·5	9·5	10·0
$T_{BK90} \pm 1SD$	834 ± 35	871 ± 10	858 ± 19	887 ± 31		903 ± 35	831 ± 40		
Rb (ppm)	0·120	0·410	0·045	0·095	0·118	0·099	0·166	0·117	n.a.
Sr	12·3	69·1	3·41	18·0	6·6	12·2	6·7	13·0	—
Y	3·20	3·46	3·06	2·97	2·61	3·41	2·40	3·16	—
Zr	6·09	5·81	2·18	4·86	3·75	5·83	2·33	5·84	—
Nb	0·030	0·061	0·046	0·053	0·051	0·041	0·037	0·036	—
Cs	0·0053	0·0184	0·0013	0·0037	0·0019	0·0074	0·0063	0·0079	—
Ba	1·56	32·53	0·57	4·34	2·22	1·19	1·03	1·94	—
La	0·284	3·79	0·071	0·932	0·249	0·289	0·280	0·290	—
Ce	0·601	9·23	0·362	1·69	0·408	0·611	0·496	0·577	—
Pr	0·140	1·078	0·103	0·182	0·083	0·128	0·094	0·134	—
Nd	0·770	3·902	0·573	0·766	0·497	0·742	0·522	0·786	—
Sm	0·291	0·590	0·210	0·239	0·199	0·287	0·189	0·301	—
Eu	0·127	0·201	0·087	0·102	0·087	0·133	0·078	0·135	—
Gd	0·461	0·599	0·350	0·389	0·337	0·477	0·306	0·464	—
Tb	0·0859	0·0985	0·0658	0·0735	0·0607	0·0888	0·0607	0·0871	—
Dy	0·603	0·663	0·478	0·541	0·461	0·641	0·447	0·655	—
Ho	0·138	0·144	0·108	0·121	0·0975	0·146	0·0979	0·143	—
Er	0·399	0·413	0·329	0·360	0·278	0·409	0·296	0·430	—
Tm	0·0610	0·0631	0·0505	0·0556	0·0417	0·0629	0·0458	0·0640	—
Yb	0·401	0·410	0·329	0·369	0·267	0·415	0·305	0·409	—
Lu	0·0680	0·0693	0·0566	0·0617	0·0443	0·0684	0·0518	0·0697	—
Hf	0·200	0·193	0·107	0·163	0·148	0·207	0·105	0·203	—
Ta	0·0075	0·0072	0·0044	0·0030	0·0057	0·0026	0·0041	0·0035	—
Th	0·001	0·381	0·003	0·115	0·023	0·001	0·021	0·004	—
U	0·0286	0·124	0·0053	0·143	0·0340	0·0278	0·0335	0·0338	n.a.
S (ppm)	55	327	27	108	80	68	89	42	22
Cu (ppm)	39	33	29	32	34	28	22	34	n.a.
Se (ppb)	25	46	11	51	27	48	35	27	n.a.
S/Se	2200	7109	2455	2118	2963	1417	2543	1556	—
Alt-S%	72·7	13·8	47·3	45·2	54·0	68·0	26·8	46·0	73·7
S* (ppm)	95	372	40	157	123	114	113	61	38
S*/Se	3800	8090	3615	3075	4563	2380	3224	2271	—

Bc, breccia-hosted xenolith; β, basalt-hosted xenolith; Amp, amphibole abundances determined either through whole-rock and mineral major element content inversion or by point counting: +, Amp ≤ 1%; ++, 1 < Amp ≤ 2·5; +++, 2·5 < Amp ≤ 5%; ++++, Amp > 5%. $T_{B\&K91}$ is the average core pyroxene equilibrium temperature using the Brey & Köhler (1990) formulation; SD, standard deviation. Alt-S% denotes the degree of sulphide alteration in per cent and is the total Fe-hydroxide area divided by the total sulphide area (including Fe-hydroxide); both data are obtained by point counting

and ethanol, and by buffering the mortar with a discarded aliquot of the sample. Major-element contents were obtained at the analytical service (SARM) of the Centre de Recherche Pour la Géologie (Nancy) by inductively coupled plasma optical emission spectrometry and at the Open University, UK, by X-ray fluorescence. Whole-rock trace elements [Rb, Sr, Y, Zr, Nb, Cs, Ba, rare earth elements (REE), Hf, Ta, Th and U] were obtained by inductively coupled plasma mass spectrometry (ICP-MS) (VG PQ2+) at the University of Montpellier. We followed the procedures described by Ionov *et al.* (1992) and Godard *et al.* (2000), who documented the accuracy and reproducibility of the method based on repeated analyses of international peridotite standards.

Sulphur was analyzed at the Muséum National d'Histoire Naturelle de Paris (Luguet & Lorand, 1998) by iodometric titration of the SO_2 produced by combustion of 1 g powder aliquots (Gros *et al.*, 2005). During this study three analyses of the international reference matériel SY-2 yielded 116 ± 5 ppm and four analyses of JP-1 yielded $26{\cdot}5 \pm 1{\cdot}5$ ppm. Selenium was determined from 10 g powder aliquots by hydride generation and flameless atomic absorption spectroscopy (AAS) at Geoscience Laboratories (Ontario, Canada); two analyses of JP-1 yielded $7{\cdot}28 \pm 0{\cdot}52$ ppb.

Five platinum group elements (PGE: Ir, Ru, Rh, Pt, Pd) and gold were determined on 10–15 g aliquots with a VG 353 PlasmaQuad ICP-MS system (University of Montpellier II) with external calibration standards. PGE and Au were preconcentrated by NiS-fire assay and Te-coprecipitation as described by Gros *et al.* (2002) and Lorand *et al.* (2008*b*). Replicate analyses of an in-house peridotite standard (FON B-93) are reported below and attest to the excellent reproducibility of the method (Gros *et al.*, 2002; Meisel & Moser, 2004; Lorand *et al.*, 2008*b*).

Whole-rock Re–Os data were obtained over a period of *c.* 10 years in three laboratories: CRPG (Nancy, France); the Open University (Milton Keynes, UK); GEMOC (Sydney, Australia).

At the CRPG (Nancy, France; 1998–2000), about 2 g of sample powder were spiked with ^{185}Re and ^{190}Os tracer solutions. In most cases, the samples were then desilicified in a reducing (HF–HBr) solution. This solution was dried down and redissolved in concentrated HCl, and then again dried down to drive off excess HF. The residue was digested in a Carius tube (Shirey & Walker, 1995) at 230°C using a 2:1 mixture of HCl and HNO_3. Os was extracted by double distillation (Shirey & Walker, 1995) and further purified through microdistillation (Birck *et al.*, 1997). For duplicates, Os was separated into Br_2 liquid (Birck *et al.*, 1997). Osmium was analyzed as negative ions (Creaser *et al.*, 1991) on a Finnigan MAT 262 mass spectrometer in peak-jumping mode using an electron multiplier. Re was then extracted on one AG1X8 anion column following the procedure described by Reisberg *et al.* (1991) and then analyzed by isotope dilution on an Elan 6000 ICP-MS system. Seventy measurements of the DTM standard made during the period of the study yielded an average of $0{\cdot}17398 \pm 0{\cdot}00040$ (Peslier *et al.*, 2000). Os and Re blanks were $(6 \pm 1) \times 10^{-12}$ g g^{-1} and $(18 \pm 12) \times 10^{-12}$ g g^{-1}, respectively. For duplicates, performed later in 2000, Os and Re blanks were in the range of $(0{\cdot}5–2{\cdot}5) \times 10^{-12}$ g g^{-1} and $(4–8) \times 10^{-12}$ g g^{-1}, respectively.

The Open University technique consists of the digestion of 1–2 g of sample and ^{185}Re–^{190}Os spike in inverse aqua regia in Carius tubes followed by solvent extraction (Shirey & Walker, 1995; Cohen & Waters, 1996). Re separation was achieved after further solvent extraction and an anion column pass (Cohen & Waters, 1996). Samples were run on a Finnigan MAT-261 mass spectrometer in negative thermal ionization mass spectrometry (N-TIMS) mode (Creaser *et al.*, 1991). Four analyses of $2{\cdot}5 \times 10^{-9}$ g of J&M Os standard solution yielded $^{187}Os/^{188}Os = 0{\cdot}14914 \pm 0{\cdot}00008$. Replicate digestion and analyses of UB-N ($n = 3$) yielded $Os = (3{\cdot}36 \pm 0{\cdot}19) \times 10^{-9}$ g g^{-1} (2 SD); $^{187}Os/^{188}Os = 0{\cdot}12857 \pm 0{\cdot}00045$ (2SD) and $Re = (0{\cdot}206 \pm 0{\cdot}010) \times 10^{-9}$ g g^{-1} (2SD, $n = 2$), in agreement with published data (Meisel *et al.*, 2003). Two total procedural blanks gave $Os = (0{\cdot}35 \pm 0{\cdot}12) \times 10^{-12}$ g g^{-1} and $^{187}Os/^{188}Os = 0{\cdot}2188 \pm 0{\cdot}0082$ (2SD, $n = 2$); therefore the Os blank represents much less than 0·2% of the total Os loaded ($>2 \times 10^{-9}$ g g^{-1}).

Further Re concentrations were conducted at GEMOC (Sydney, Australia). One gram of powder and the appropriate amount of ^{185}Re spike were digested in Savillex pressure vessels with HF–HBr at ≈140°C for several days. This step was repeated once. Then the dried-down solution was dissolved in double-distilled concentrated HCl. Once the HCl was dried down on a hot plate, the residue was taken into solution with 2 N HNO_3. Re was then separated by solvent extraction following the method described by Birck *et al.* (1997) and then analyzed by isotope dilution on an Agilent HP7500c ICP-MS system. RSD on 10 ppt Re is 4·1 ±1·0%; blanks are *c.* $(3{\cdot}2 \pm 1{\cdot}4) \times 10^{-12}$ g g^{-1} ($n = 3$). Four aliquots of UB-N yielded an average Re concentration of $(0{\cdot}2064 \pm 0{\cdot}0093) \times 10^{-9}$ g g^{-1} in agreement with published data (Meisel *et al.*, 2003).

In situ PGE analyses were performed with the GEMOC laser ablation (LAM)-ICP-MS system (Alard *et al.*, 2000). The six PGE, Au, and Se were determined with a custom-built laser ablation system linked to an Agilent HP 4500 ICP-MS system (RF power, 1050 W). The laser is a Continuum Surelite I-20 Q-switched quadrupled frequency Nd:YAG laser delivering a 266 nm ultraviolet beam (Norman *et al.*, 1996). Ablation was carried out in a pure He atmosphere (0·85 l min^{-1}). The laser ablation system was operated at 4 Hz with a beam energy ≈0·5 mJ

per pulse and beam diameter of ≈60 μm. Raw data were processed online using the GLITTER software package (Griffin *et al.*, 2008). Sulphur determined by electron microprobe (as indicated above) was used as internal standard. The level of $^{63}Cu^{40}Ar$ interference on ^{103}Rh (monoisotopic) was determined by ablating a pure Cu metal several times during the run. The accuracy of the correction is checked by correcting ^{105}Pd for $^{65}Cu^{40}Ar$ interference and comparing it with ^{106}Pd, which is free of major interference, except for $^{66}Zn^{40}Ar$. However, Zn abundance in mantle sulphides is generally low (<0·3 wt %) and thus the effect on ^{106}Pd is negligible. A quenched NiS bead (PGE-A) doped with PGE, Se and Au was used as the external standard for Se, PGE and Au. Another NiS bead (ReOsOA#4) with similar stoichiometry was used for Re. The similarity of the matrix between the standard and the analyzed sulphide allows straightforward processing of the data. Typical detection limits, for the conditions described above, are lower than 30 ppb for all PGE except Ru and Rh, which showed an average detection limit of *c.* 60 ppb (see below).

In situ Re–Os data on sulphides were obtained using a Nu Plasma multi-collector ICP-MS system (Nu005) coupled to a laser ablation system at the GAU, following the method described by Pearson *et al.* (2002). The laser ablation system is a Merchantek LUV266 nm operating at 5 Hz, with a beam energy of about 3–5 mJ per pulse; the spot size varied between 60 and 120 μm. Ablation was carried out in a He atmosphere. Measurements were made in static collection mode; masses 194, 193, 192, 191, 190, 189, 188 and 186 were measured in Faraday cups, whereas masses 187 and 185 were measured in ion counters. This detector setting allows simultaneous measurement of Os, Re and Ir (Pt?) and permits analysis of low-Os sulphides (down to ≈10 ppm for a 5% 2SE on $^{187}Os/^{188}Os$). This detector array allows efficient correction of the ^{187}Re overlap on the ^{187}Os up to $^{187}Re/^{188}Os \approx 1{\cdot}6$ (Pearson *et al.*, 2002); the validity of this correction has been recently reassessed by Pearson *et al.* (2009). Ir is introduced to the Ar component of the nebulizer gas stream, as a 'dry' vapour produced by desolvating an Ir solution (100 ppb) in a CETAC MCN6000, and is used to measure the mass bias of the instrument for correction of Re and Os. Daily analysis of Ir–Os, Ir–Re and Re–Os solutions shows that the fractionation behaviour and relative fractionation coefficients for Os, Re and Ir are internally consistent (Pearson *et al.*, 2002). Repeated analyses of synthetic sulphide standards yielded $^{187}Os/^{188}Os$ in agreement with N-TIMS measurements. Twenty-eight analyses of PGEA analysed during this study yielded $^{187}Os/^{188}Os = 0{\cdot}10642 \pm 0{\cdot}00018$ (2SD), in agreement with TIMS analyses ($^{187}Os/^{188}Os = 0{\cdot}106443 \pm 0{\cdot}000082$; $n = 4$, I. Horn, personal communication; O. Alard, unpublished data). ReOsGS#3 yielded $^{187}Re/^{188}Os = 0{\cdot}352 \pm 0{\cdot}037$ and $^{187}Os/^{188}Os = 0{\cdot}18364 \pm 0{\cdot}00021$, compared with $^{187}Os/^{188}Os = 0{\cdot}18360 \pm 0{\cdot}00002$ ($n = 3$; 2SD) obtained by N-TIMS analysis (N. J. Pearson, personal communication).

SILICATE PETROGRAPHY AND GEOCHEMISTRY

Petrography

The 23 peridotite xenoliths investigated during this study were all equilibrated in the spinel facies. Calculated equilibrium temperatures from pyroxene core compositions (Brey & Köhler, 1990) yield a very narrow range, from 830 to 900°C (average $T_{BK90} = 860 \pm 21$ °C; uncertainty is 1SD; $n = 12$). A garnet–spinel-bearing pyroxenite was reported by Fabries *et al.* (1987) with equilibrium conditions of $T_{BK90} = 860 \pm 28$°C and $P_{N\&G85} = 14 \pm 1$ kbar (Nickel & Green, 1985). The homogeneous temperature conditions suggest that all xenoliths were derived from a restricted volume of mantle at relatively shallow depth (≈40 km); however, fO_2 is highly variable [$-2{\cdot}7 \leq \Delta \log fO_2 \leq +0{\cdot}6$, relative to the Fayalite–Magnetite–Quartz (FMQ) buffer, estimated using the formulation of Balhaus *et al.* (1991)]. Although equant and tabular granuloblastic microstructures occur occasionally, most (70–80%) of the peridotites have a porphyroclastic microstructure (Fig. 2). The relative proportions of porphyroclasts and neoblasts, as well as their average sizes, are variable, and textures range from coarse deformed to sheared varieties. The former exhibit spinels still associated with large orthopyroxenes. Porphyroclasts are large (≈0·5–1 cm) and contiguous, and the proportion of neoblasts (100–500 μm) is below 20%. The sheared microstructure is characterized by a much higher proportion (*c.* 80%) of small neoblasts (100–50 μm) and elongated porphyroblasts aligned with scattered spinel (Cabanes & Briqueu, 1986; Fabries *et al.*, 1987). These previous studies ascribed the extremely deformed sheared microstructure of the xenoliths to low-temperature (≈800°C), high-stress deformation related to the tectonic activation of the nearby Cevennes–Nimes fault system (Fig. 1), suggesting a lithospheric scale for these crustal faults.

As suggested by the systematic study of hand-sample specimens, all the xenoliths are fertile lherzolites with a roughly constant modal composition: olivine 50 ± 10% (Ol, ±1SD), orthopyroxene 29 ± 7% (Opx), clinopyroxene 15 ± 3% (Cpx) and spinel *c.* 1·5 ± 0·7% (Spl). The proportion of pale brown amphibole ranges from 0 to ≈10%. This uniform fertile bulk composition is reflected in the mineral compositions: forsterite contents vary between 88·7 and 90·0% (average = 89·3 ± 0·3) and $Cr\#_{Spl}$ [100Cr/(Cr + Al)] is confined to a narrow range between 5·5 and 10·6 (average 8·9 ± 1·5). Amphibole occurs as disseminated crystals (not as veinlets) within the neoblast matrix and is a Ti (calcic)-pargasite (CaO = 10·4 ± 0·2 wt %).

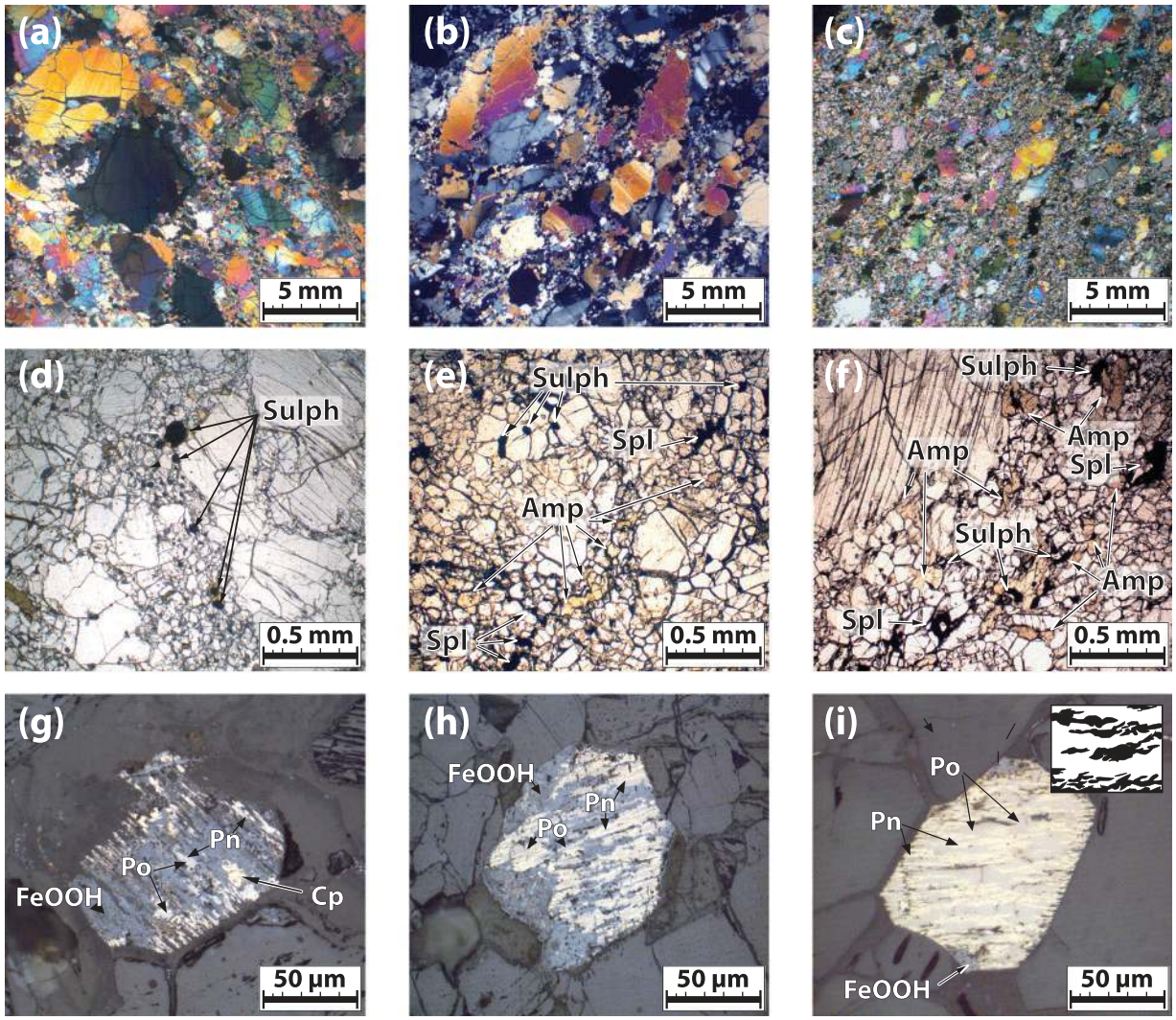

Fig. 2. Photomicrographs of the Montferrier xenoliths showing microstructural features and sulphide occurrence and mineralogy. (a–c) Photomicrographs in cross-polarized light, illustrating the range of microstructures (porphyroclastic to mylonitic). (d–f) Photomicrographs in transmitted light, showing the relationship between sulphide and the main rock-forming silicates (porphyroclast and neoblast) and amphibole; Sulph, sulphide; Spl, spinel; Amp, amphibole. (g–i) illustrate various degrees of sulphide alteration (reflected light); FeOOH, iron-oxyhydroxide, Po, pyrrhotite; Pn, pentlandite; Cp, chalcopyrite; inset in (i) shows the peculiar microstructural relationships between pn (black) and po (white) specific to Montferrier S-rich peridotites, in which pn forms flame-like exsolution lamellae within a Ni-rich po.

Minor amounts of phlogopite (<1%) also occur. Microstructural evidence led Cabanes and co-workers (Cabanes & Briqueu, 1986; Cabanes & Mercier, 1988) to conclude that amphibole crystallization was synchronous with the deformation leading to the sheared microstructure.

Major elements and lithophile trace elements

In agreement with the petrographic observations, whole-rock major-element contents (Table 1) indicate that these xenoliths are all fertile. Al_2O_3 varies between 2·19 and 4·47 wt % and averages *c.* 3·59 ± 0·61% ($n = 20$). The heavy REE (HREE) show a limited range of variation (e.g. $0{\cdot}264 \leq Yb \leq 0{\cdot}497$ ppm; Table 2) and confirm the fertile nature of these samples [average $Lu_N = 2{\cdot}56 \pm 0{\cdot}44$, where subscript N indicates chondrite normalized; values after McDonough & Sun (1995)]. The chondrite-normalized REE patterns could be described as a continuum between two 'end-members', with 'depleted' and 'enriched' REE patterns (Fig. 3). The 'depleted' pattern as in Pg-42 is characterized by a smooth negatively sloping pattern from the HREE to the light REE [LREE; $(La/Sm)_N = 0{\cdot}49$; $(Sm/Yb)_N = 0{\cdot}70$]. However, with the exception of sample 80-438 [$(La/Sm)_N = 0{\cdot}08$; $Al_2O_3 = 2{\cdot}19$ wt %], the amount of depletion, as shown by the REE

Table 2: Typical analyses of sulphide phases obtained by electron microprobe

Sample:	Mtf-20					Mtf-37		Pg-5		Pg-6			Pg-41		
Phase:	e(Opx)-Mss1	e(Opx)-Mss2	i-Po	i-Pn	i-Cp	i-Po	i-Pn	i-Po	i-Pn	i-Po	i-Pn	i-Cp	i-Po	i-Pn	i-Cp
wt %															
S	39·25	38·32	37·57	32·85	34·95	36·63	32·84	37·38	32·67	38·01	32·63	34·22	37·02	33·52	34·12
Fe	49·58	40·75	61·61	32·49	31·47	62·23	31·82	61·71	33·77	61·37	33·04	31·26	62·38	34·85	31·59
Cu				0·05	33·53	0·04	0·02	0·00	0·10	0·07	0·00	34·21	0·00	0·00	33·31
Co	0·17	0·34	0·46	0·70	—	0·00	0·68	0·00	0·59	0·00	0·57	0·00	0·02	0·43	0·00
Ni	9·45	20·42	0·03	33·31	—	0·49	33·98	0·35	32·44	0·37	33·77	0·32	0·22	31·34	0·30
O	—	—	—	—	—	0·44	0·28	0·62	0·67	0·77	0·42	0·40	0·50	0·47	0·56
Total	98·45	99·83	99·67	99·40	99·95	99·83	99·60	100·05	100·24	100·59	100·43	100·41	100·14	100·60	99·89
at. %															
S	53·79	52·45	51·32	46·86	49·97	50·34	46·88	51·20	46·04	51·73	45·89	49·16	50·34	47·29	49·28
Fe	39·01	32·03	48·32	26·61	25·83	49·26	26·08	48·54	27·92	47·96	27·73	25·79	49·48	28·23	26·20
Ni	7·07	15·27	0·02	25·95	0·00	0·37	26·50	0·26	25·51	0·27	25·94	0·25	0·16	24·15	0·24
Cu	0·00	0·00	0·00	0·04	24·19	0·02	0·01	0·00	0·07	0·04	0·00	24·80	0·00	0·00	24·28
Co	0·13	0·25	0·34	0·54	0·00	0·00	0·53	0·00	0·46	0·00	0·43	0·00	0·01	0·33	0·00
Total	100·00	100·00	100·00	100·00	100·00	100·00	100·00	100·00	100·00	100·00	100·00	100·00	100·00	100·00	100·00
M/S	0·859	0·906	0·949	1·134	1·001	0·986	1·133	0·953	1·172	0·933	1·179	1·034	0·986	1·115	1·029
(Ni + Co)/Fe	0·185	0·485	0·008	0·996	0·000	0·008	1·036	0·005	0·930	0·378	0·042	0·019	0·071	0·004	1·005

e, enclosed sulphide; i, intergranular sulphide; Mss, monosulphide solid solution; Pn, pentlandite; Po, pyrrhotite; Cp, chalcopyrite; M/S, metal to sulphur ratio (Fe + Ni + Co + Cu)/S computed in at. %.

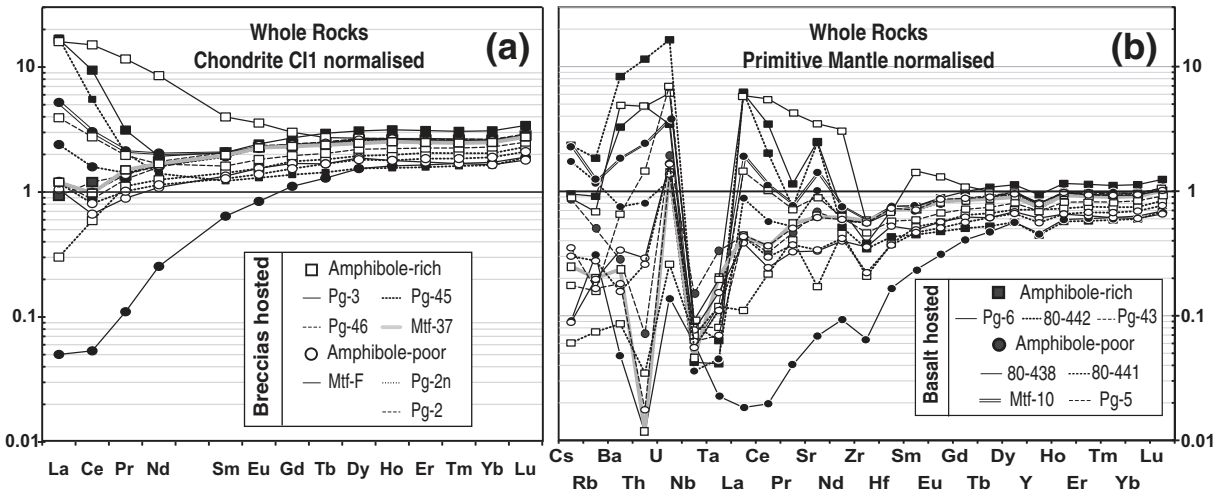

Fig. 3. Whole-rock incompatible trace-element patterns: (a) rare earth elements normalized to chondrite; (b) extended incompatible trace-element patterns normalized to primitive mantle values. Black squares, basalt-hosted amphibole-rich (>1%) xenoliths; white squares, breccia-hosted amphibole-rich (>1%) xenoliths; black circles, basalt-hosted amphibole-poor xenoliths (<1%); white circles, breccia-hosted amphibole-poor (<1%) xenoliths; chondrite and primitive mantle values are from McDonough & Sun (1995).

fractionations, remains weak and suggests that these rocks have experienced only very limited melt extraction (≤5%). The 'enriched' pattern is characterized by a HREE–MREE (middle REE) segment similar to that displayed by the 'depleted' samples – and a steep LREE segment with $(La/Sm)_N$ as high as 14·4. Figure 3a shows that as the patterns evolve progressively from the 'depleted' towards the 'enriched' types, first only La is enriched

relative to Ce (e.g. Pg-5; Mtf-37), then the enrichment 'moves to the right' and the less incompatible LREE such as Nd and Pr are affected (e.g. Mtf-10, Pg-6). Ultimately, as in Pg-3, the most incompatible of the MREE (i.e. Sm, Eu ± Gd) are affected. The 'depleted' or 'enriched' nature of the xenoliths does not correlate with the type of host volcanic rock. The most LREE-enriched xenoliths (e.g. Pg-3; Pg-6) are amphibole-rich, yet several amphibole-poor samples (e.g. Mtf-10) also show $(La/Sm)_N > 1$. Conversely, several amphibole-rich samples have $(La/Sm)_N < 1$ (e.g. Pg-43).

The extended trace-element patterns (Fig. 3b) show that the LREE-depleted samples also have low Th, Nb and Ta abundances but display a significant positive U anomaly relative to Th, leading to $(U/Th)_{PM}$ as high as 124 [where PM indicates primitive mantle; values after McDonough & Sun (1995)]. The other large ion lithophile elements (LILE) such as Cs, Rb and Ba show variable enrichment relative to Th. In contrast, the 'enriched' patterns are characterized by high abundances of U and Th with $(U/Th)_{PM}$ about unity. However, the high field strength elements (HFSE, i.e. Nb, Ta, Zr and Hf) display abundances similar to those in the 'depleted' patterns, and thus define pronounced 'negative' Nb–Ta anomalies [$(Nb/Ce)_{PM}$ as low as 0·012]. Many samples (e.g, Pg-45; 80-441) show characteristics intermediate between these two end-members. Figure 3 shows that the evolution from one pattern to another is continuous and is mainly driven by the variation of the LREE and LILE (especially Th) contents whereas the levels of HREE (± MREE) and HFSE remain constant throughout the enrichment process (Fig. 4). Both U and Th are enriched as La rises relative to Sm, but Th shows a much steeper trend.

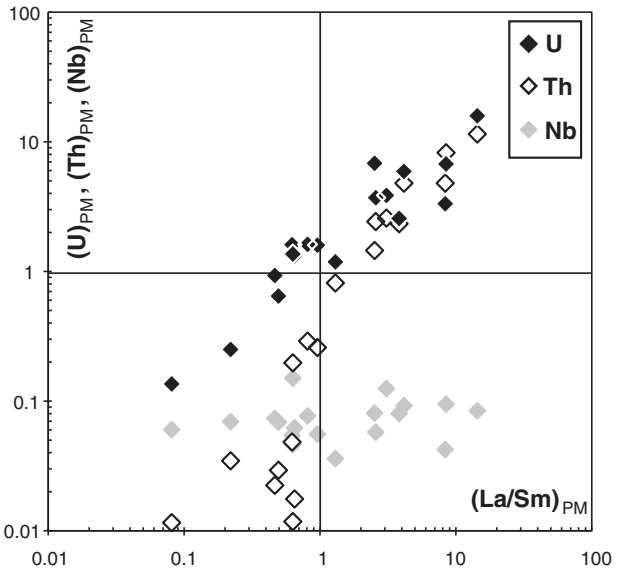

Fig. 4. Variation of primitive mantle (PM) normalized U, Th and Nb vs La/Sm. Primitive mantle values after McDonough & Sun (1995).

SULPHIDE OCCURRENCE AND COMPOSITION

The modal abundance of sulphides in the xenoliths, as estimated by point counting, varies from 0·013 to 0·19% (relative error is estimated at *c.* 20%). Given the relatively uniform fertility of the Montferrier xenoliths, such a large variation is unexpected. Furthermore, although low modal abundances of sulphide are common in alkali-basalt hosted peridotite xenoliths (Lorand, 1990; Ionov *et al.*, 1992), the upper part of the range is extremely unusual. For comparison, the sulphide content of the primitive mantle can be estimated to be *c.* 0·070 ± 0·015%, assuming 250 ± 50 ppm of sulphur (McDonough & Sun, 1995) and a typical monosulphide solid solution (S_{mss} = 36 wt %). Overall, sulphides are abundant (i.e. >0·02%) to extremely abundant (i.e. >0·07%) in the Montferrier xenoliths relative to neighbouring localities in the Massif Central and Languedoc (Lorand & Conquéré, 1983; Lorand, 1990; Lorand & Alard, 2001; Lorand *et al.*, 2003*a*). In addition, the sulphide occurrence, grain size and mineralogy (and thus composition) are unusual in many aspects. Most strikingly, 99% of the investigated sulphides are interstitial; few sulphides (n = 5; Lorand & Conquéré, 1983) have been found as inclusions in the primary silicates.

The rare enclosed sulphides were found in porphyroclasts. They have spherical shapes, with diameters ranging between 20 and 50 μm. Their petrographic characteristics are similar to those of primary sulphide inclusions in other mantle-derived xenoliths; that is, Type-1 sulphide of Alard *et al.* (2000, 2002) and Lorand & Alard (2001) for the Massif Central and the Languedoc xenoliths. Enclosed sulphides are formed of Ni-rich and Ni-poor mss (Table 2, Fig. 5) in roughly equal proportions, with minor amounts of pentlandite and chalcopyrite (not analysed). Such modal compositions are typical of primary inclusions in moderately depleted peridotites from the subcontinental lithosphere (Lorand & Conquéré, 1983). The sulphide inclusions are devoid of low-temperature alteration phases such as iron hydroxide. The major-element compositions of the Ni-rich mss (Ni up to 15·2 wt %) and Ni-poor mss (Ni *c.* 7 wt %) as well as the compositions of the pentlandite and chalcopyrite are provided in Table 2. Combining the modal abundances of the sulphide phases and their compositions yields a bulk composition for the silicate-enclosed sulphides; this composition is characterized by a S content of *c.* 38·5 wt %, a metal to sulphide ratio (M/S) of about 0·9, and a (Ni + Co)/Fe atomic ratio of *c.* 0·37.

Interstitial sulphides have shapes, sizes and mineralogy significantly different from those that are enclosed. They display angular forms in textural equilibrium with the

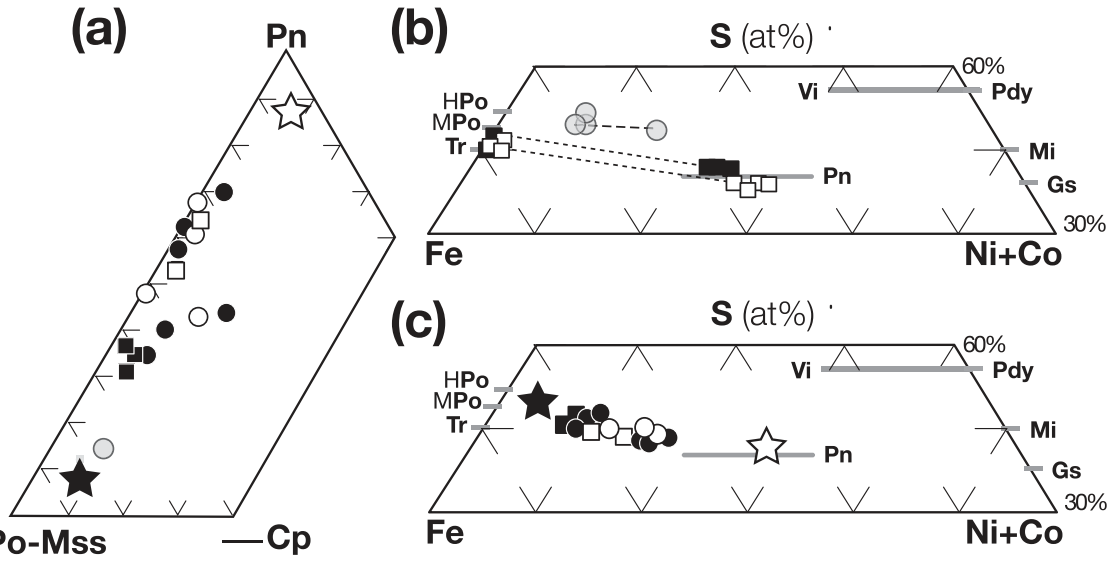

Fig. 5. (a) Average modal abundances of sulphide by sample for the Montferrier xenoliths (see Table 3). Grey circles, silicate-hosted sulphide (Fabries *et al.*, 1987); black squares, basalt-hosted amphibole-rich samples; open squares, basalt-hosted amphibole-poor samples; black circles, breccia-hosted amphibole-rich samples; open circles, breccia-hosted amphibole-poor xenoliths; black star, average composition of sulphide inclusions in peridotite xenoliths from the Massif Central and neighbouring volcanic districts (Lorand & Conquéré, 1983); open star, average composition of interstitial sulphide in the Pyrenees orogenic peridotite massifs (Lorand, 1989). (b) Single sulphide analyses obtained by electron microprobe (Table 2). Grey circles, sulphides enclosed in silicates (Fabries *et al.*, 1987); black square, interstitial sulphides in Pg-6 (a basalt-hosted amphibole-rich sample); open squares, interstitial sulphides in Mtf-37 (a breccia-hosted amphibole-rich sample); dashed lines link the coexisting phases; HPo, hexagonal pyrrhotite; MPo, monoclinic pyrrhotite; Tr, troilite; Pn, pentlandite; Pdy; polydymite; Mi, millerite; Gs, godlevskite; Vi, violarite; at% denotes atomic per cent. (c) Average bulk sulphide composition by sample; symbols as in (a) and mineral name abbreviations as in (b) (see Tables 2 and 3).

surrounding olivine neoblasts (Figs 2 and 7). They are also fairly large, most being several hundred micrometres across; a few sulphides, such as those in Pg-4l, are up to a millimetre across. Although sulphides and amphiboles both occur within the matrix, there is no systematic relationship between these two phases; a sulphide–amphibole spatial association is observed only occasionally, in samples in which amphibole is particularly abundant (i.e. >5%, e.g. Pg-6; Fig. 2). The polygonal and interstitial sulphides are mainly composed of Ni-poor (Ni < 1 wt %; M/S = 0·95 ± 0·05 at. %) pyrrhotite (po; Table 2) associated with pentlandite (pn, Ni/Fe = 0·96 ± 0·13 at. %, Table 2, Figs 5 and 7). Chalcopyrite (cp; Table 2) occurs in various proportions. Minor amounts (<5%) of secondary sulphides, such as smythite (Fe_9S_{11}) replacing pyrrhotite, valleriite and mackinawite films coating silicate grain boundaries, and violarite replacing pentlandite, testify to partial desulphidation of intergranular sulphides at low temperature (<200°C). In almost all samples, Cu–Fe–Ni sulphides are pseudomorphosed by amorphous Fe-oxyhydroxides [$FeO(OH)$,5–6H_2O]. Although the degree of alteration from grain to grain within one sample is extremely variable (Fig. 2), marked differences in the average abundance of Fe-oxyhydroxides between breccias and basalt-hosted xenoliths have been demonstrated by Luguet & Lorand (1998) and are confirmed here (Fig. 6). The breccia-hosted xenoliths contain large amounts of Fe-hydroxides (up to 75% of sulphide grains are altered); in contrast, the lava-hosted xenoliths contain a smaller proportion of altered sulphide grains (0–20%). We found no correlation between LOI and the degree of alteration of the sulphide (Table 1).

Major sulphide phases (i.e. po, pn and cp) occur in bimodal (i.e. pn–cp) or trimodal (po–pn–cp) assemblages. These two sulphide assemblages are characterized by two different microstructures (Lorand & Conquéré, 1983, fig. 9). Two-phase grains are composed of blocky pn and cp, both sulphides representing primary precipitates. Three-phase grains invariably display a pyrrhotite matrix containing abundant flame-like pentlandite exsolution blebs (up to 40–50 vol. %; Figs 2i and 7). Chalcopyrite occurs either as thin films at the po margin or cross-cutting the po. The relative proportions of the major sulphide phases are extremely variable from sample to sample. Furthermore, for the breccia-hosted xenoliths, accurate estimates are difficult to obtain owing to the effects of supergene weathering. Recast from unaltered sulphides, po proportions vary from 31 to 70%, pn from 32 to 63% and cp from 0 to 17% of the total sulphide (Table 3). Figure 8a shows that the relative proportion of po varies positively with the modal abundance of sulphides; Pn shows the opposite behaviour (Fig. 8b). Cp modal abundances do

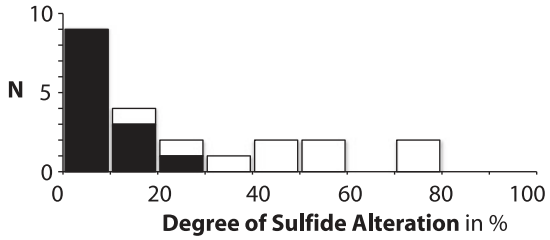

Fig. 6. Average degree of sulphide weathering (Alt-S) in per cent per sample. Degree of sulphide alteration is the ratio of the area of Fe-hydroxide to the total sulphide area (including Fe-oxyhydroxide); N, number of samples; black, basalt-hosted xenolith; white, breccia-hosted xenoliths.

not show such correlations (Fig. 8c), partly because of low-temperature alteration that remobilized Cu as vallerite. Two-phase sulphide grains (pn–cp) have been observed in the pn-rich but sulphide-poor lherzolites, whereas three-phase sulphide grains (po–pn–cp) are pyrrhotite-rich and predominate in sulphide-rich lherzolites. Although the major-element composition of each phase is relatively constant in all samples, the strong modal evolution produces significant variations in the bulk composition of the sulphide. As sulphur contents and sulphide abundances increase, the M/S and (Ni + Co)/Fe of the bulk sulphide decrease (Fig. 8e and f).

CHALCOGENIDE (S, Se) AND CHALCOPHILE (Cu) ELEMENT ABUNDANCES

Whole-rock S contents vary from 7 to 592 ppm, and are well correlated with sulphide modal abundance. Five samples have S contents higher than that estimated for the primitive mantle (i.e. 250 ± 50 ppm; McDonough & Sun, 1995). However, S content varies irrespective of fertility indices such as Al_2O_3 (Fig. 9), CaO%, Fo%, $Cr\#_{Spl}$, or HREE content (not shown). The lack of covariation between S and fertility indices is common for alkali-basalt hosted xenotliths and has often been ascribed to S-loss by late, low-temperature weathering (Lorand, 1990). This issue could be significant, especially for the breccia-hosted xenoliths, for which sulphide alteration can be as high as 73%. Alteration-corrected sulphur contents (S*, see Table 1) range between 38 and 621 ppm (Fig. 10). This range is far too large to be reconciled with the modest variability in fertility that characterizes our sample suite, and the relationship between S* and Al_2O_3 remains poor. In contrast, there is a good correlation between S* and REE fractionation as monitored by the La/Sm ratio (Fig. 11a).

Cu varies between 20 and 38 ppm and averages 30 ± 5 ppm ($n = 17$, 1SD), which is similar to the primitive mantle value (≈28 ppm; McDonough & Sun, 1995). This is in agreement with the overall fertile nature of the

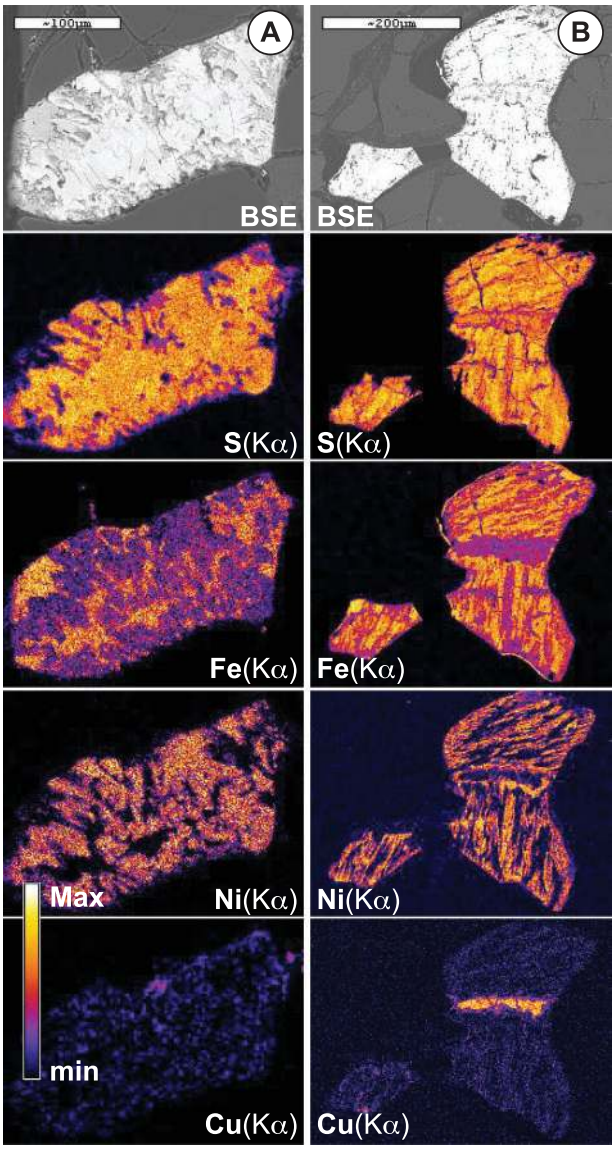

Fig. 7. Backscattered-electron (BSE) images and chemical maps of typical Montferrier sulphides. Chemical maps were produced using a LINK energy-dispersive X-ray detector coupled to a CAMECA SX-50 microprobe in the GAU. Shading indicates the relative abundance of a given element. (a) Pg-41 sulphide; (b) sulphide in sample Pg-6.

Montferrier xenoliths. Thus the extreme S enrichment is not accompanied by a concomitant Cu enrichment. This confirms our previous observations regarding cp abundance, which was found to be low and independent of sulphide abundances in the most sulphide-enriched samples (Fig. 8c). Furthermore, although there is some scatter, Cu shows a rough correlation with Al_2O_3 as in the Pyrenean orogenic lherzolites (Fig. 9b). No correlation was found between Cu and $(La/Sm)_N$.

Se concentrations display a large range, between 11 and 67 ppb, and average 37·5 ± 14·2 (Table 1). In contrast

Table 3: Sulphide abundances, mineralogy and composition

Sample	Sulf wt %	%S-Alt	%Po	%Pn	%Cp	Other	S wt %	Fe	Ni	Co	Cu	Total	M/S
Amphibole-rich, basalt-hosted xenoliths													
Pg-6	0·192	5·0	63·2	31·2	5·1	Vall, Sm,	36·3	51·4	10·7	0·2	1·7	100·3	1·00
Pg-41	0·115	11·7	60·8	36·7	2·2		36·1	50·8	12·5	0·2	0·7	100·3	0·99
80-442	0·140	0·2	60·7	34·9	4·4	Vall	36·8	49·2	11·8	0·3	1·4	99·4	1·04
Pg-43	0·050	3·6	31·5	62·0	6·5								
H204	0·12 ± 0·1	0	57 ± 3	33 ± 3	10 ± 5	Mw, Vall	36·5	44·91	14·923	0·32	3·75		0·98
Amphibole-poor, basalt-hosted xenoliths													
Pg-5	0·032	16·7	37·2	62·0	0·8		34·5	44·2	21·0	0·4	0·3	100·4	0·92
Pg-42	0·034	3·9	41·2	57·8	1·2		34·7	45·3	19·7	0·3	0·4	100·3	0·93
80-441	0·060	0·2	51·9	39·8	7·6	Mw, Vall	36·4	46·6	13·4	0·3	2·7	99·5	1·02
80-438	0·040	0·2	39·0	43·8	17·1	Mw	35·8	42·9	14·7	0·3	5·8	99·6	1·00
Mtf-10	0·066	6	44·0	47	9	Vall				n.d.			
Mtf-C1	0·055	6·5	32·8	69·6	3·6	Vall	34·9	40·6	23·3	0·5	1·1	100·5	0·94
Mtf-20	0·060	n.d.	58·0	35·0	7·0	Vall	35·5	49·8	12·4	0·2	2·3	100·2	0·97
Mtf-21	0·051	20·6		n.d.						n.d.			
Amphibole-rich, breccia-hosted xenolith													
Mtf-37	0·029	72·7	34·2	63·4	>0·1	Mw, Vall	35·2	41·7	21·2	0·5	0·9	99·4	0·97
Pg-3	0·097	13·8	55·1	41·1	3·8		35·7	49·1	13·8	0·2	1·3	100·1	0·98
Pg-45	0·013	47·3		n.d.						n.d.			
Pg-46	0·044	36·2	41·2	53·6	3·1		34·7	45·5	18·7	0·3	1·1	100·3	0·93
Amphibole-poor, breccia-hosted xenoliths													
Mtf-F	0·047	54·0	32·3	67·7	>0·1		35·1	41·1	22·7	0·5	0·1	99·5	0·96
Pg-2	0·052	58·0		n.d.						n.d.			
Pg-2 N	0·016	26·8		n.d.						n.d.			
Mtf-15	0·034	46·0	36·8	60·4	2·72	Vall	35·4	42·5	20·0	0·4	1·0	99·4	0·98
Mtf-17	0·038	73·7	51·5	48·5	>0·1		36·2	46·4	16·4	0·4	0·0	99·4	1·01

Sulf (wt %), abundance of sulphide determined by petrographic observation including Fe-hydroxide, given in weight per cent; Alt-S%, degree of sulphide alteration in per cent (see Table 1); Po%, Pn%, Cp%, average modal proportion of pyrrhotite, pentlandite and chalcopyrite respectively obtained for the sulphide grains for a given sample corrected of Alt-S%; 'Other', other sulphide phases observed representing <1% of the sulphide mode; Vall, vallerite; Sm, smithite; Mw, mackinawite; n.d., not determined; S/M, sulfur-metal ratio [S/(Fe + Ni + Co + Cu)] computed in at. %. Data were compiled from Fabriès *et al.*, (1987), Luguet & Lorand (1998), Lorand *et al.* (2003) and the present study.

to S abundances, Se abundances do not exceed the primitive-mantle estimate (i.e. 75 ± 15 ppm; McDonough & Sun, 1995). However, Se concentrations vary irrespective of fertility indices (Fig. 9c) and are broadly correlated with La/Sm_N (Fig. 11b) as observed for S, whereas Cu and Se are not correlated. The relationship between Se and S or S* is not straightforward (Fig. 10). Breccia-hosted xenoliths, which show high degrees of sulphide alteration, have S contents below 110 ppm and S/Se below 3000 (averaging 2178 ± 547; $n = 7$). However, for the same samples, the S*/Se ratio averages 3275 ± 806. These values agree with the S/Se ratio of *c.* 3120 for the UM reference peridotite xenolith suite of the Basaltic Volcanic Study Project (Morgan, 1986) and are within error of the chondritic ratio (2500 ± 200; Dreibus *et al.*, 1995). Many of these samples have $(La/Sm)_N \leq 1$ (Fig. 11c). In contrast, basalt-hosted xenoliths, which show low degrees of sulphide alteration but high S contents, have S/Se ratios much higher than ≈3000, up to 12 000. These samples are also characterized by pronounced LREE enrichment relative to the MREE (Fig. 3, Table 1). The S/Se ratio shows a positive correlation with fO_2 (Table 1).

WHOLE-ROCK HSE ABUNDANCES AND $^{187}Os/^{188}Os$ COMPOSITION

Whole-rock HSE (Ir, Ru, Rh, Pt, Pd, Au) contents have been obtained for seven of the Montferrier xenoliths

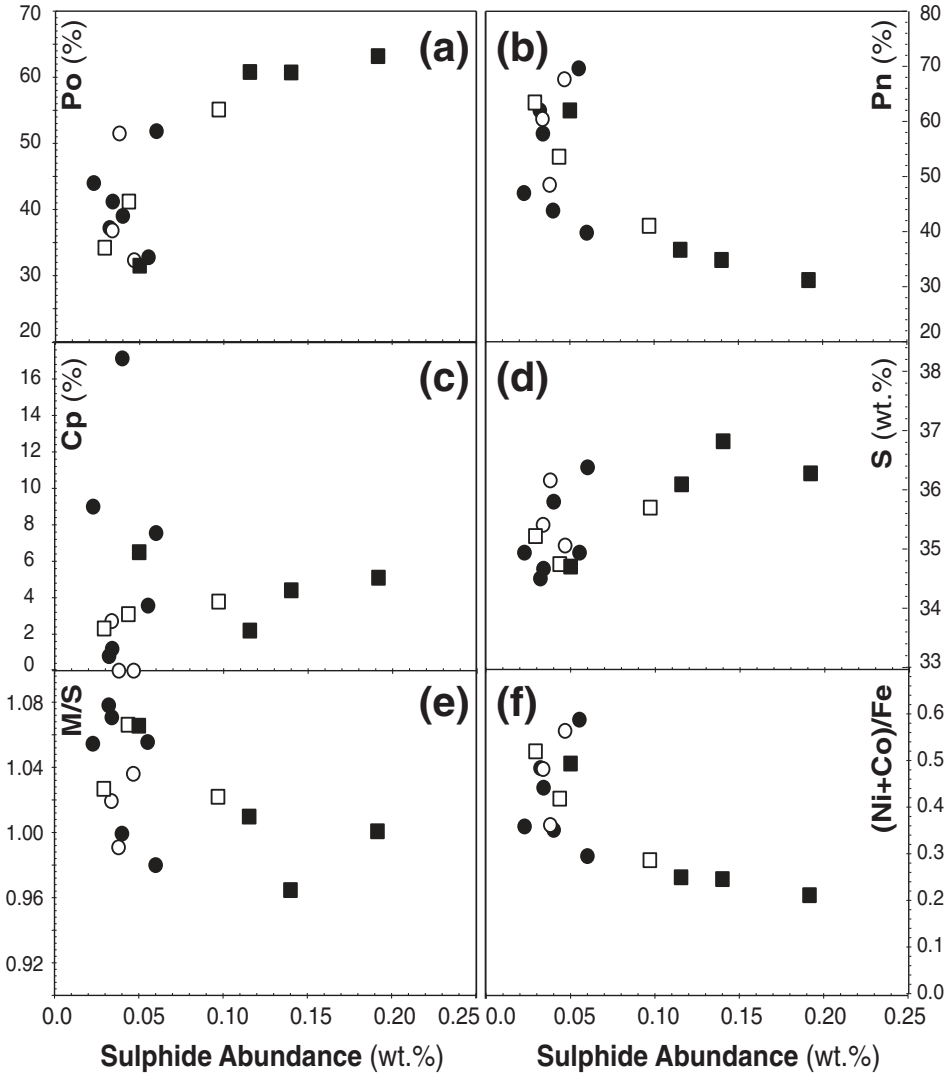

Fig. 8. Average mineralogical and bulk composition vs sulphide modal abundance. Black squares, basalt-hosted amphibole-rich samples; open squares, basalt-hosted amphibole-poor samples; black circles, breccia-hosted amphibole-rich samples; open circles, breccia-hosted amphibole-poor xenoliths. (a) Average pyrrhotite abundance (Po%) vs sulphide abundance by sample (see Table 3); (b) average pentlandite abundance (Pn%) vs sulphide abundance per sample (see Table 3); (c) average chalcopyrite abundance (Cp%) vs sulphide abundance per sample (see Table 3); (d) S bulk sulphide composition in wt % vs sulphide modal abundance; (e) bulk metal to sulphur ratio [M/S = (Fe + Ni + Co + Cu)/S in at. %] vs sulphide modal abundance; (f) (Ni + Co)/Fe vs sulphide modal abundance. Bulk sulphide compositions were obtained for each sample by recombining electron microprobe point analyses (Table 2) and modal abundances of sulphide phases obtained by point counting or image processing (Table 3) for more than eight sulphide grains (≥50 mm) per section.

spanning the range of S contents. Data are reported in Table 4. Re and Os abundances and the $^{187}Os/^{188}Os$ compositions of nine samples have also been determined but not on the same powder aliquots, and are also reported in Table 4. The seven xenoliths analyzed show a narrow range of PGE concentrations (ΣPGE = 20–28·2 ppb) broadly similar to those obtained for the Massif Central xenoliths (Lorand & Alard, 2001) and the Pyrenean orogenic massifs (Lorand *et al.*, 1999). PGE contents and fractionation patterns are independent of the degree of sulphide weathering and of the fertility indices of the xenoliths (Fig. 12). Ir varies between 2·3 and 4·6 ppb, and $(Ru/Ir)_N$ and $(Rh/Ir)_N$ ratios are remarkably constant (1·05 ± 0·10 and 1·22 ± 0·06, respectively). Relative to the Massif Central xenoliths, Pd contents are high, but similar to the Pd-rich Pyrenean peridotites. In terms of HSE fractionation the Montferrier samples resemble the average HSE pattern obtained for the Pyrenean lherzolites (Lorand *et al.*, 1999; Becker *et al.*, 2006). $(Pd/Ir)_N$ and $(Pd/Pt)_N$ are suprachondritic, and vary between 1·18 and 1·87 and between 1·46 and 2·17, respectively. $(Os/Ir)_N$ varies between 0·77 and 1·85. In contrast to the Pyrenean suite, the

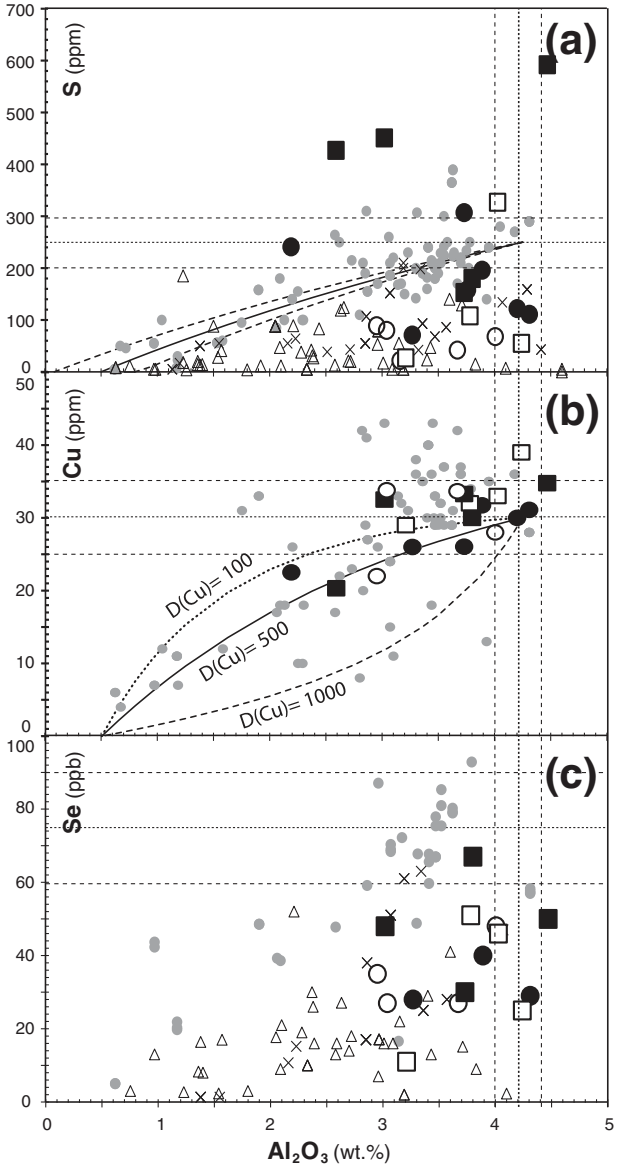

Fig. 9. Whole-rock variation of S, Cu and Se relative to Al_2O_3 as a fertility index. Symbols for the Montferrier xenoliths as in Figs 4 and 7; grey circles, Pyrenees peridotite massifs (J.-M. Lorand & O. Alard, unpublished data); open triangles, French Massif Central peridotite xenoliths (Lorand & Alard, 2001; Lorand *et al.*, 2003*a*); ×, ultramafic xenolith suites and Kilbourne Hole peridotite xenoliths (Morgan *et al.*, 1986; O. Alard, unpublished data); dashed thin lines denote the primitive mantle abundance and associated uncertainties after McDonough & Sun (1995). (a) Al_2O_3 vs S; continuous and dashed bold curves are melting curves calculated with mass-balance equations for fractional melting of the sulphide phase for a S saturation of *c.* 1000 ± 100 ppm (continuous and dashed lines respectively) and for an S primitive mantle abundance *c.* 250 ppm; (b) Al_2O_3 vs Cu, melting curves are calculated with mass-balance equations for fractional melting of the sulphide phase, assuming all of the Cu residing in the sulphides, for a S saturation of *c.* 1000 ppm, and $D(\mathrm{Cu}) = 100$ (dotted line), 500 (continuous line) and 1000 (dashed line); (c) Al_2O_3 vs Se.

Pd/Ir ratio is independent of the Al_2O_3 content. However, $(\mathrm{Pd/Ir})_N$, $(\mathrm{Pd/Pt})_N$ and $(\mathrm{Os/Ir})_N$ are positively correlated with S (Fig. 12), Se, S/Se and La/Sm. The increase of the Pd/Ir, Pd/Pt and Os/Ir ratios is due to the decrease of Ir, Ru, Rh and Pt contents with increasing S, whereas the Pd and Os contents remain roughly constant. This 'differential dilution' effect is also shown by the relationship between ΣPGE and S (Fig. 12). The Os/Ir ratios should be viewed with some caution as Os and Ir concentrations were obtained from separate powder aliquots by different techniques. However, the Os–Ir fractionation is supported by the existence of similar Os–Ir fractionation in the sulphides (see below). All samples have Au contents significantly higher than those of the Massif Central xenoliths (Lorand & Alard, 2001), falling in the upper part of the range for Pyrenean peridotites (Lorand *et al.*, 1999). Re (0·156–0·464 ppb) and Re/Os (0·030–0·180) are not correlated with Al_2O_3 but increase with S and Se and thus La/Sm (Fig. 12).

The $^{187}Os/^{188}Os$ for the nine samples analysed varies between 0·1246 and 0·1756 (Fig. 13). The Os contents (and isotopic composition) are extremely variable between replicates, especially for the most S-rich samples (see Table 4). For instance, the Os content varies from 2·3 to 4·6 ppb for two aliquots of Pg-41 and two aliquots of Pg-6 yield $^{187}Os/^{188}Os$ *c.* 0·1363 and 0·1756, respectively. These features suggest that the Os carrier phase in the 'enriched' peridotites is extremely heterogeneously distributed and/or has extremely variable composition. There is no correlation between $^{187}Re/^{188}Os$ and $^{187}Os/^{188}Os$, and thus the extremely radiogenic compositions are not supported by high Re contents; this observation suggests that Re enrichment was recent. Conversely, samples having low $^{187}Re/^{188}Os$ do not show unradiogenic $^{187}Os/^{188}Os$. No correlations are observed between Os abundances (or 1/Os), Al_2O_3 and $^{187}Os/^{188}Os$. However, the two samples (80-438 and 80-442) with $Al_2O_3 < 3$ wt % have $^{187}Os/^{188}Os$ (0·12576 and 0·12462, respectively) significantly below the estimates for carbonaceous chondrites (0·12753; Walker *et al.*, 2002). Although $^{187}Os/^{188}Os$ is not correlated with S*, the most radiogenic values have been found in the samples most enriched in S* and incompatible trace elements.

SULPHIDE HSE ABUNDANCES AND Re–Os ISOTOPIC COMPOSITION

HSE abundances

In situ HSE analyses of Cu–Fe–Ni sulphides have been obtained for one 'depleted' sample [Mtf-37; $(\mathrm{La/Sm})_N = 0{\cdot}63$, S = 55 ppm], one intermediate sample [Pg-5; $(\mathrm{La/Sm})_N = 0{\cdot}63$, S = 111 ppm], and the two most LREE-enriched samples [Pg-41 and Pg-6; $(\mathrm{La/Sm})_N >$

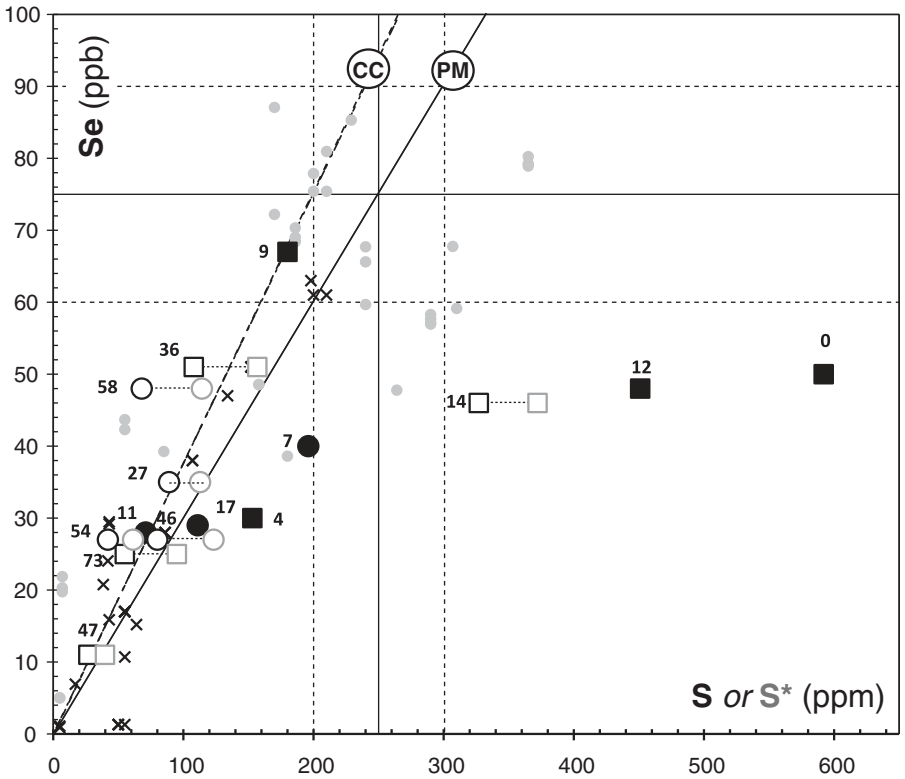

Fig. 10. Whole-rock Se and S (and S*) abundance for the Montferrier xenoliths. Symbols as in Figs 4 and 8; point labels denote the sulphide alteration percentage determined through petrographic observation (Table 3); grey open circles and open squares, Se abundances plotted against S* (S content corrected for the effect of alteration) for the breccia-hosted xenoliths; grey filled circles; Pyrenees peridotite massifs (J.-M. Lorand & O. Alard, unpublished data); ×, ultramafic xenolith suites and Kilbourne Hole peridotite xenoliths (Morgan *et al.*, 1986; O. Alard, unpublished data); continuous and dashed fine lines denote the primitive mantle abundance and associated uncertainties after McDonough & Sun (1995); continuous bold line and PM, primitive mantle S/Se ratio of *c.* 3300 (McDonough & Sun, 1995); dashed bold line and CC, carbonaceous chondrite S/Se ratio (S/Se ≈ 2600) after Dreibus *et al.* (1995).

8·3; S > 450 ppm]. Data are reported in Table 5, and abundances normalized to primitive mantle values are shown in Fig. 14.

There are significant differences in both absolute and relative concentrations between Mtf-37 and the other three samples. Mtf-37 sulphides have relatively homogeneous contents of the iridium group of the PGE (IPGE; Os, Ir, Ru) (i.e. $4 \leq Ir \leq 39$ ppm), sub-chondritic Ru/Ir and Rh/Ir, and variable Pd and Re abundances [$0{\cdot}05 < (Pd/Ir)_N < 8{\cdot}1$; $0{\cdot}04 < (Re/Os)_N < 4{\cdot}2$]. HSE patterns of the Mtf-37 sulphides are otherwise marked by negative Pt and Au anomalies. The HSE concentrations and patterns of the Mtf-37 sulphides are reminiscent of those of intergranular pentlandite from orogenic peridotites (Alard *et al.*, 2000; Lorand *et al.*, 2008*a*, 2008*b*). The distribution of some HSE and other chalcophile elements (e.g. Se, As) has been mapped using the CSIRO–GEMOC Scanning Nuclear Microprobe facility (courtesy of C. Ryan). Ru, Rh and Pd determined by LA-ICP-MS for Mtf-37-S1 and Mtf-37-S3 agree well with the proton probe analysis of the same grain (Table 5; Fig. 14). However, the proton probe analyses of the same sulphides do not show negative Pt anomalies. As shown in Fig. 15, Pt resides in a $PtAs_2$ micronugget in the S3 sulphide. The proton probe analyses the whole sulphide imaged down to ≈70 μm depth and thus includes the $PtAs_2$ nugget. In contrast, the LA-ICP-MS analyses are restricted to an area of 50 μm in diameter and a depth ranging between 40 and 60 μm, and obviously did not include the Pt nugget. Thus clearly the Pt-anomaly problem so often reported in LA-ICP-MS analyses of sulphide is a problem of volume sampling, and is thus ironically a caveat on the use of the high spatial resolution of the LA-ICP-MS technique.

Sulphides in Pg-5, Pg-41 and Pg-6 samples show two distinct HSE patterns (Fig. 14). The first type (Type-1) has IPGE abundances similar to those of the Mtf-37 sulphides ($9 \leq Ir \leq 45$ ppm) and overall the normalized abundances of the HSE decrease smoothly from Rh to Au (Pd/Ir ≤ 0·55). $(Re/Os)_N$ is lower than chondrite but varies widely between 0·02 and 0·81. Such negatively sloped patterns are reminiscent of the patterns of mss residual after melting (Alard *et al.*, 2000). Except for sulphide Pg-6-z3sF

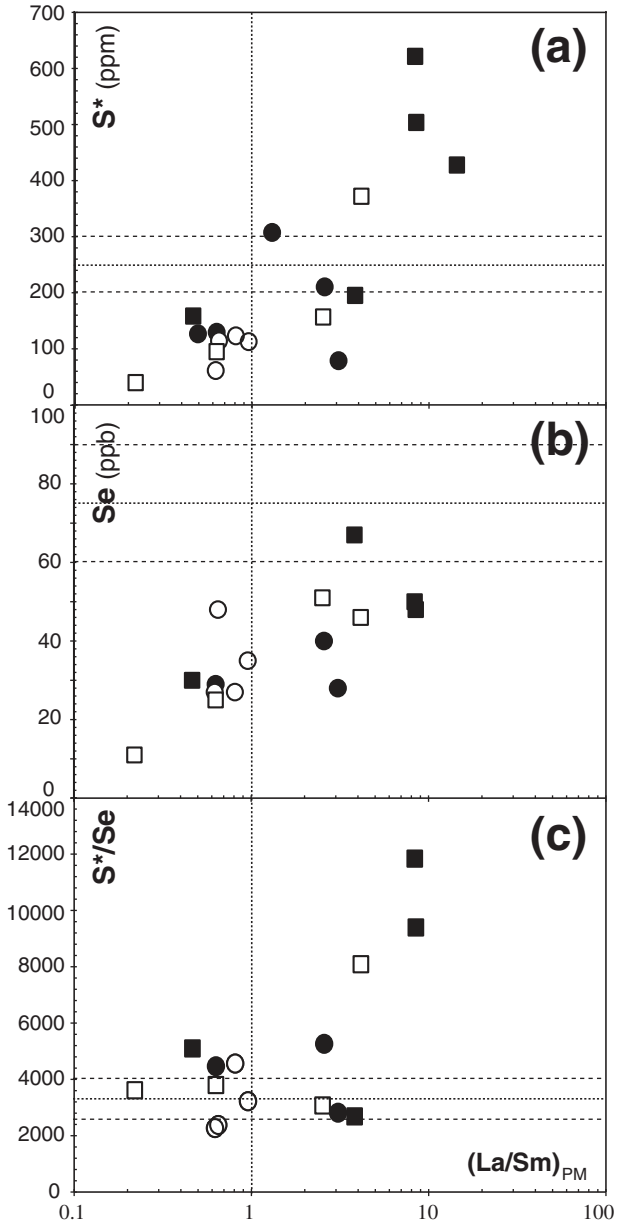

Fig. 11. S*, Se, and S*/Se vs La/Sm. Symbols as in Fig. 4; PM, primitive mantle-normalized ratio; dashed fine lines denote the primitive mantle (PM) abundance and associated uncertainties after McDonough & Sun (1995).

no Type-1 sulphides have Pt negative anomalies. Au seems to form a negative 'kink' between Pt and Re. The second pattern (Type-2) is characterized by strongly positive slopes ($4 < Pd/Ir \leq 1487$), extremely low Ir abundance (0·65 ppm) and high yet widely variable $(Re/Os)_N$ (1·8–603). Although highly variable within a single sample, Pd/Ir decreases as the proportion of Type-2 sulphides increases (see Fig. 14 caption) from Pg-5 ($Pd/Ir = 243 - 1428$), to Pg-41 (24–80) and Pg-6 (4–70). Osmium is clearly enriched relative to Ir [$2 < (Os/Ir)_N < 60$]. Although Au/Ir is highly variable owing to the Au negative anomaly, ratios as high as 246 have been obtained. Type-1 sulphides have higher Se abundances ($\approx 148 \pm 11$ ppm) than Type-2 sulphides (69 ± 17 ppm). It should be noted that the two sulphide patterns cannot be distinguished in terms of microstructural occurrence or the modal abundances and composition of the sulphides (i.e. pn + cp or po + pn + cp grains).

Taking into account the modal abundances of sulphides, mixing in various proportions of Type-1 and Type-2 sulphides accounts within error for the whole-rock abundances of Ir, Ru, Rh, Pd and Re in Pg-5, Pg-41 and Pg-6 (Fig. 14). In contrast, whole-rock Os contents cannot be reproduced by the sulphide analyses; although Type-2 sulphides have high Os/Ir, their rather low Os abundances cannot explain the high whole-rock Os/Ir (See Table 5). This deficit suggests a missing carrier of Os (another mineral and/or fluid and/or mineral surfaces?). The highly variable abundances of Pd, Au and Re preclude such a calculation for Mtf-37, but the Mtf-37 sulphide composition and the estimated sulphide abundances broadly account for the whole-rock abundances of Os, Ir, Ru and Rh. Unexpectedly, the agreement between the whole-rock and the estimated bulk sulphide Pt content is reasonable. However, this may be due to analytical artefacts related either to the NiS fire assay technique, which does not ensure a 100% collection of Pt-rich micronuggets (Lorand *et al.*, 2008*b*), or to the sampling bias inherent in the high spatial resolution of the LA-ICP-MS technique (see above). For Au, the measured sulphide abundances clearly are much too low to explain the whole-rock abundances. Au is thus inferred to reside in another microphase not detected by the analytical methods used here.

Re–Os isotopic composition of single sulphide grains

Re–Os isotopic compositions were obtained on 64 sulphide grains in eight samples. Sulphides analysed for Re–Os isotopes were not previously analysed for HSE abundances. Data are reported in Table 6 and plotted in Fig. 16. In considering these data, the reader must be aware of the limitations inherent in the LA-MC (multicollector)-ICP-MS technique and of the bias that these analytical limitations induce. Reliable $^{187}Os/^{188}Os$ measurements can only be obtained for sulphides having Re/Os ratios <0·33 (i.e. $^{187}Re/^{188}Os \leq 1{\cdot}6$), as shown by Pearson *et al.* (2002), and Os beams higher than 10^{-3} V. Although the Os beam intensity depends on several factors such as laser output energy, laser pulse frequency and laser beam diameter (related to sulphide size), ultimately it is the sulphide Os content that is the main limiting factor. Thus sulphides with Os contents below the ppm level and/or high Re/Os do not yield reliable $^{187}Os/^{188}Os$ data and these are not reported. Therefore *in situ* Os-isotope data are always biased towards high-Os, low-Re/Os sulphides. In the present

Table 4: HSE whole-rock content and Re–Os isotopic composition of Montferrier peridotites

Sample	Group	Os (ppb)	Ir	Ru	Rh	Pt	Pd	Au	Re	$^{187}Re/^{188}Os$	$^{187}Os/^{188}Os$	±2σ
Pg-6	A.r-β	4·57*	2·3	3·9	0·86	4·4	5·2	1·8	0·464*	0·491	0·17556*	0·00022
Replicate		3·34*	—	—	—	—	—	—	—	—	0·13630*	0·00010
Pg-41	A.r-β	2·33*	2·8	4·4	1	5·12	4·9	—	0·419†	0·857	0·12730*	0·00016
Replicate		4·61‡	—	—	—	—	—	—	0·430‡	0·444	0·14637‡	0·00007
80-442	A.r-β	3·80‡	—	—	—	—	—	—	0·431‡	0·541	0·12462‡	0·00010
Pg-43	A.r-β	4·12*	3·0	4·9	1·03	5·4	5·3	1·2	0·315*	0·368	0·15235*	0·00034
Replicate		3·94*	—						0·317†	0·384	0·12750*	0·00030
Pg-5	A.p-β	3·61*	2·6	4·4	0·9	4·5	4·5	1	0·268†	0·353	0·12741*	0·00016
80-338	A.p-β	4·01*							0·369‡	0·438	0·12576*	0·00020
Mtf-37	A.r-Bc	5·24§	4·6	7·5	1·56	8·3	6·6	2·2	0·156§	0·144	0·12770§	n.g.
Replicate				5·0	8·2	1·60	7·5	6·4	2·8			
Pg-45	A.r-Bc	3·93‡	—	—	—	—	—	—	0·096†	0·116	0·12520‡	0·00018
Mtf-F	A.p-Bc	—	2·8	5·3	0·98	5·5	4·6	1·3	—	—	—	—
Mtf-15	A.p-Bc	3·82‡	3·5	4·8	1·13	6·3	5·0	2·0	0·170‡	0·212‡	0·12781‡	0·00008
FON-B	STD		3·23	5·85	1·16	6·74	6·34	1·60				
	$n=3$		±0·12	±0·32	±0·12	±0·23	±0·24	±0·14				

A.r, amphibole rich; A.p, amphibole poor; β, basalt-hosted xenolith; Bc, breccia-hosted xenolith.
*Os and Re determined at CRPG (Nancy, France) after Carius tube digestion and TIMS, and isotope dilution (ID) ICP-MS analyses, respectively.
†Re determined by ID-ICP-MS at the GEMOC laboratory (Australia).
‡Os and Re determined after Carius tube digestion and TIMS analyses at the Open University.
§Meisel *et al*. (2001) Carius-tube and TIMS analyses. n.g., not given.

study, this bias was significant. Indeed, from Fig. 14 and Table 6 reliable $^{187}Os/^{188}Os$ cannot be obtained for Type-2 HSE sulphide; consequently, the 'yield' for S-poor samples is about 52% and it is less than 30% for S-rich samples.

For the 64 sulphide grains that were successfully analysed $^{187}Re/^{118}Os$ varies between 0·012 and 0·89, and $^{187}Os/^{188}Os$ ranges between 0·115 and 0·172. However, there are striking differences in Re–Os systematics from one sample to another. First, samples Pg-5, Pg-45, Pg and Pg-46 show a positive correlation between $^{187}Re/^{188}Os$ and $^{187}Os/^{188}Os$ (Fig. 16). The slopes of these trends are usually shallow. The range of $^{187}Os/^{188}Os$ is limited between 0·117 and 0·131. Where whole-rock data are available, the whole-rock value is within the trend defined by the sulphide data. These samples show otherwise moderate S abundances (27–180 ppm), S*/Se *c.* 3000 and $(La/Sm)_N$ between 0·6 and 3·8.

In contrast, as shown by Alard *et al*. (2002), sample Mtf-37 is characterized in $^{187}Re/^{188}Os$–$^{187}Os/^{188}Os$ space by an unusual inverse correlation (Fig. 16). Pg-2 shows the same systematics. Both samples are LREE-depleted [$(La/Sm)_N$ *c.* 0·6] but show high $(U/Th)_{PM}$, *c.* 80 and 123, respectively. Both samples have highly altered sulphides and have S/Se ratios significantly below the PM and carbonaceous chondrite ratios. Sulphides can reach fairly radiogenic Os compositions (up to 0·145). The whole-rock Re–Os composition of Mtf-37 is consistent with the sulphide systematics. Sulphides in Pg-43, which has S/Se much higher than the chondritic value (≈5500) and a high $(U/Th)_{PM}$ ratio (*c.* 44), display extremely diverse Re–Os isotopic compositions: highly radiogenic Os compositions (i.e. $^{187}Os/^{188}Os \geq 0{\cdot}14$) are found in both low-Re/Os and high-Re/Os sulphides. As a result of (1) the extreme variation obtained between aliquots of the whole-rock sample powder, (2) the low success rate of sulphide analyses and (3) the extreme variation of sulphide composition, we can hardly discuss the relationships between sulphides and whole-rock. Keeping on the safe side, it can only be said that both whole-rock and sulphide Re–Os composition are not mutually exclusive.

For Pg-6, the most S- and LREE-rich sample studied here, $^{187}Re/^{188}Os$ and $^{187}Os/^{188}Os$ of sulphides vary in the range 0·10–0·90 and 0·120–0·172, respectively. $^{187}Os/^{188}Os$ is roughly correlated with $^{187}Re/^{188}Os$. One whole-rock analysis (0·136) plots on the trend defined by the sulphides; the other more radiogenic whole-rock data point does not. However, for the same reasons as advocated for Pg-43, we cannot here discuss the relationships between sulphides and whole-rock on a solid basis.

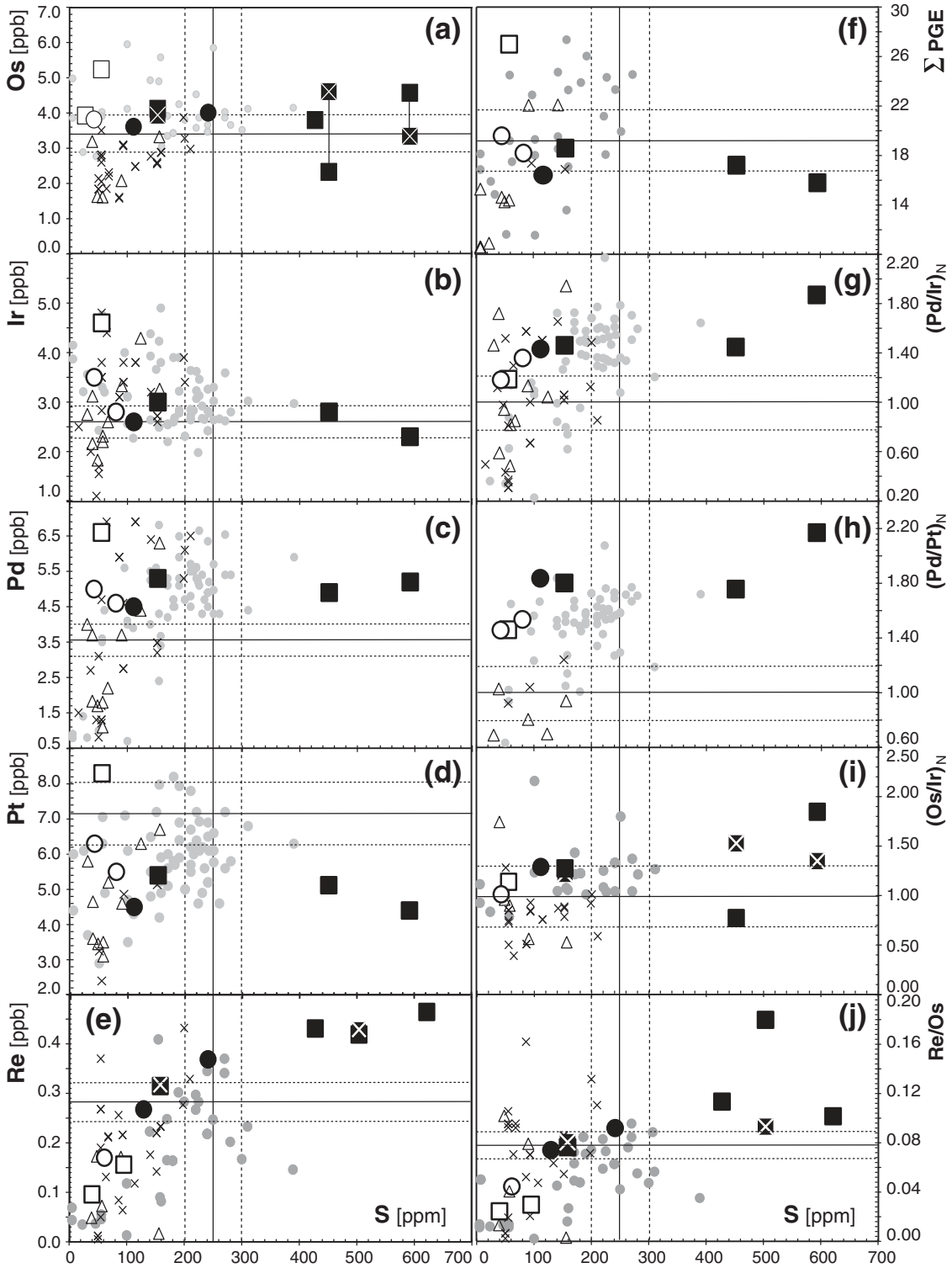

Fig. 12. Whole-rock contents and relative abundances of the HSE vs S content. Symbols as in Fig. 8 except for the white cross over black filled squares, which denotes replicate analyses; N, CI-chondrite-normalized; continuous and dashed fine lines denote the primitive mantle abundance and associated uncertainties; primitive mantle and CI chondrite values after McDonough & Sun (1995).

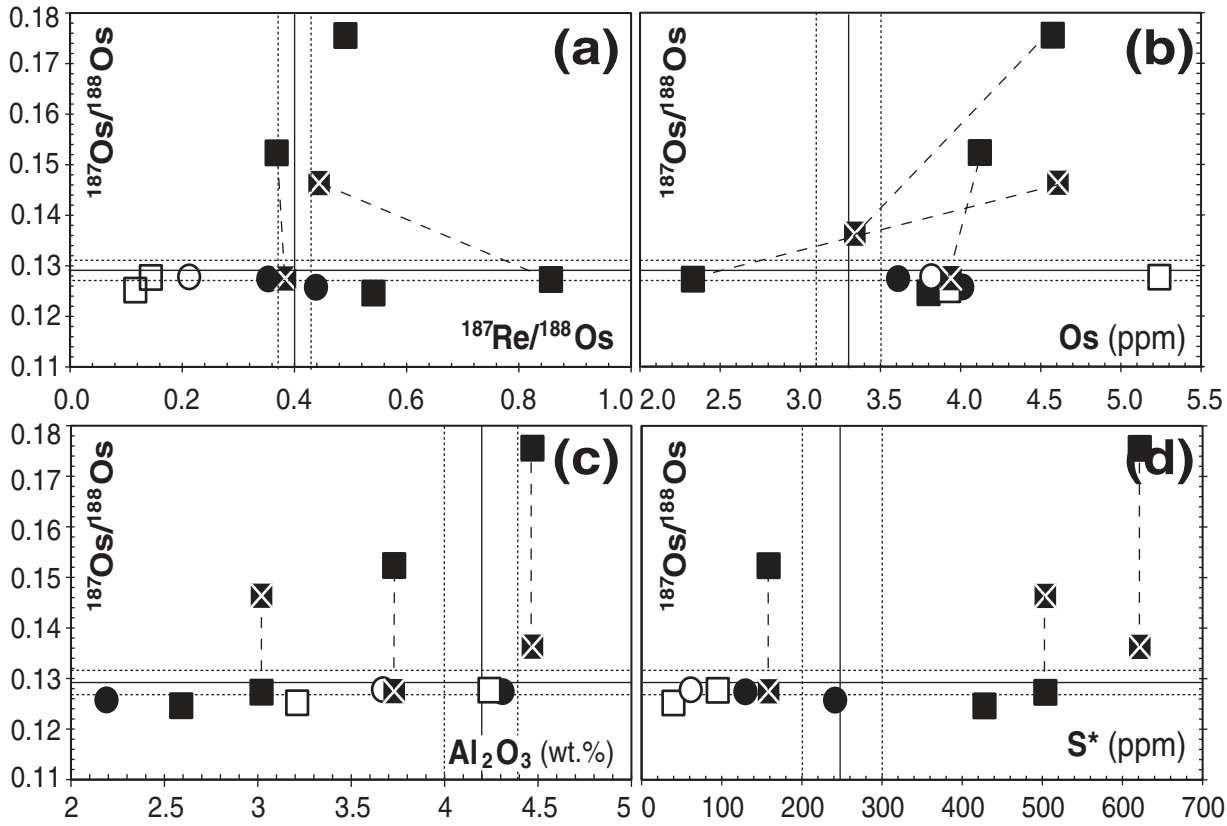

Fig. 13. Whole-rock $^{187}Os/^{188}Os$ composition relative to (a) $^{187}Re/^{188}Os$, (b) Os, (c) Al_2O_3 (wt %) and (d) S*. Symbols as in Fig. 11; long dashed lines connect replicate analyses; continuous and dashed fine lines denote the primitive mantle abundances and associated uncertainties after McDonough & Sun (1995).

DISCUSSION

An overview of the literature shows that the compositions of mantle samples can generally be accounted for by the superimposition of at least two processes: the first involves variable degrees of melt extraction during partial melting, whereas the second is related to the percolation (± reaction) of a melt or a fluid through the peridotite matrix (i.e. metasomatism; Frey & Green, 1974). Sulphur displays moderately incompatible behaviour during partial melting, roughly comparable with that of Al or the HREE, as shown by the positive correlation between Al_2O_3, Yb and S in orogenic peridotites (e.g. Lorand *et al.*, 1999) and ultramafic xenoliths (Morgan, 1986). The large variation of S abundances in the Montferrier samples could be interpreted within this framework: low S abundances result from partial melt depletion, whereas S abundances higher than estimated for the primitive mantle (PM) would be related to metasomatic enrichment. However, based on the data presented above this is clearly an oversimplified interpretation, which will be discussed further below.

Late-stage alteration

The low S abundance in some xenoliths (as low as 22 ppm) would require high degrees of partial melting (i.e. $F \approx 20\%$; Fig. 9) which does not agree with the uniformly fertile compositions of the studied samples ($F \leq 5\%$). The detailed investigation of sulphide mineralogy has revealed the occurrence of two 'secondary' assemblages attesting to different stages of alteration. The first assemblage is characterized by the widespread but quantitatively limited formation of valleriite and mackinawite owing to serpentinization, inducing reduction and partial redistribution of Cu, Fe and S. The occurrence and abundance of this assemblage is independent of the nature of the host-rock of the xenoliths. This low-T reaction did not significantly disturb the Cu and S whole-rock contents, which vary irrespectively of the occurrence of valleriite and/or mackinawite (Table 3).

In contrast, except for Pg-3, all breccia-hosted samples with S contents below 110 ppm show high abundances of hydrous iron hydroxide (i.e. >25%). The abundance of hydrous iron hydroxide is dependent on the nature of the host-rock (Fig. 6) and is probably due to the higher

Table 5: HSE abundances of Montferrier sulphides obtained by LA-ICP-MS and proton probe

Sample:	Mtf-37									
Sulf no.:	s1	s1*	s3	s3*	s4	s7	s11	s15	s13	s9
Cu	1500	n.a.	5303	n.a.	n.a.	n.a.	n.a.	n.a.	n.a.	n.a.
Se	92·9	82·7	110	92·4	199	65·1	92·4	122	138	116
Os	32·2	n.a.	16·2	n.a.	13·2	15·8	13·6	6·83	15·6	12·4
Ir	38·8	n.a.	12·2	n.a.	9·73	15·9	15·7	4·50	12·3	12·2
Ru	48·2	37·6	24·9	20·5	16·7	21·4	19·2	7·50	18·5	16·7
Rh	6·86	6·54	4·70	2·89	1·06	2·76	2·16	0·160	1·1	1·61
Pt	5·33	25·9	0·41	18·5	<0·041	0·18	8·19	0·140	1·7	<0·038
Pd	2·83	4·62	13·9	8·59	24·2	1·84	2·88	44·2	57	0·690
Au	0·218	n.a.	0·772	n.a.	<0·042	0·110	0·220	0·105	0·070	0·170
Re	2·13	n.a.	0·528	n.a.	1·383	0·062	0·042	2·06	5·42	0·108

Sample:	Pg-5										
Sulf no.:	s3	s8	s5	s6	s4	s5	s2	s7	sA	sC	sF
Cu	6533	393	4287	12994	680	8759	1533	2082	n.a.	n.a.	n.a.
Se	149	145	138	144	149	173	80·7	84·3	73·6	65·1	66·7
Os	158	31·9	13·7	25·6	19·6	46·1	0·120	0·083	1·22	0·51	0·60
Ir	175	35·8	10·8	28·1	19·6	45·2	0·018	0·016	0·019	0·015	0·014
Ru	224	54·5	17·5	48·8	26·1	65·3	0·128	0·080	0·31	0·29	0·18
Rh	58	8·86	2·51	8·96	4·64	11·9	0·035	0·079	0·1	0·20	0·16
Pt	152	35·5	10·8	32·2	19·7	46·8	0·081	0·260	0·12	0·31	0·13
Pd	6·38	3·94	2·38	13·6	1·41	6·89	4·39	22·8	15·6	18·7	21·7
Au	0·390	0·336	0·048	0·048	<0·062	0·046	0·030	0·730	2·65	2·63	3·44
Re	0·430	0·053	0·333	0·638	0·136	0·159	0·6	4·08	0·990	2·21	2·52

Sample:	Pg-41				Pg-6							
Sulf no.:	s8	s11	s23	s25	z1sB	z2sD	z2sE	z2sF	z3sA	z3SB	z3sF	z3sG
Cu	530	2703	3596	15481	70477	6193	9090	60350	4430	1664	2110	5651
Se	133	41·5	43·7	45·3	59·4	80·4	78·1	98·9	73·9	71·5	155	150
Os	10·8	0·036	0·085	0·276	0·654	0·200	0·180	0·370	0·450	0·357	7·10	8·14
Ir	11·2	0·016	0·023	0·096	0·131	0·083	0·092	0·106	0·127	0·157	9·03	9·09
Ru	15·7	0·076	0·090	0·426	0·321	0·550	0·345	0·555	0·840	0·343	12·3	11·5
Rh	2·61	0·030	0·041	0·168	0·180	0·090	0·152	0·302	0·0590	0·0712	3·06	3·13
Pt	15·4	0·076	0·480	5·13	0·230	0·100	0·150	0·680	0·280	0·220	26·1	1·45
Pd	3·87	0·392	1·84	6·92	5·29	1·94	2·88	4·73	8·86	0·720	3·25	4·98
Au	0·193	0·278	0·108	<0·026	<0·850	0·260	1·400	<0·279	0·035	0·164	0·640	0·070
Re	0·364	0·409	0·188	0·504	0·616	0·440	0·640	0·480	0·112	0·160	0·148	0·541

All data are given in ppm. n.a., not analysed; <, below detection limit.
*Bulk proton probe analysis (see Fig. 14); uncertainty is *c*. 10% (1σ).

permeability of the volcanic breccias to meteoric water (Luguet & Lorand, 1998). Thus, along with the amorphous nature of the hydrous iron hydroxide demonstrated by X-ray diffraction (Luguet & Lorand, 1998), the relationship between the abundance of this phase and the host-rock type attests to the supergene nature of this alteration (Lorand, 1990; Luguet & Lorand, 1998). Thus, as proposed by Lorand (1990), sulphur has been leached out by

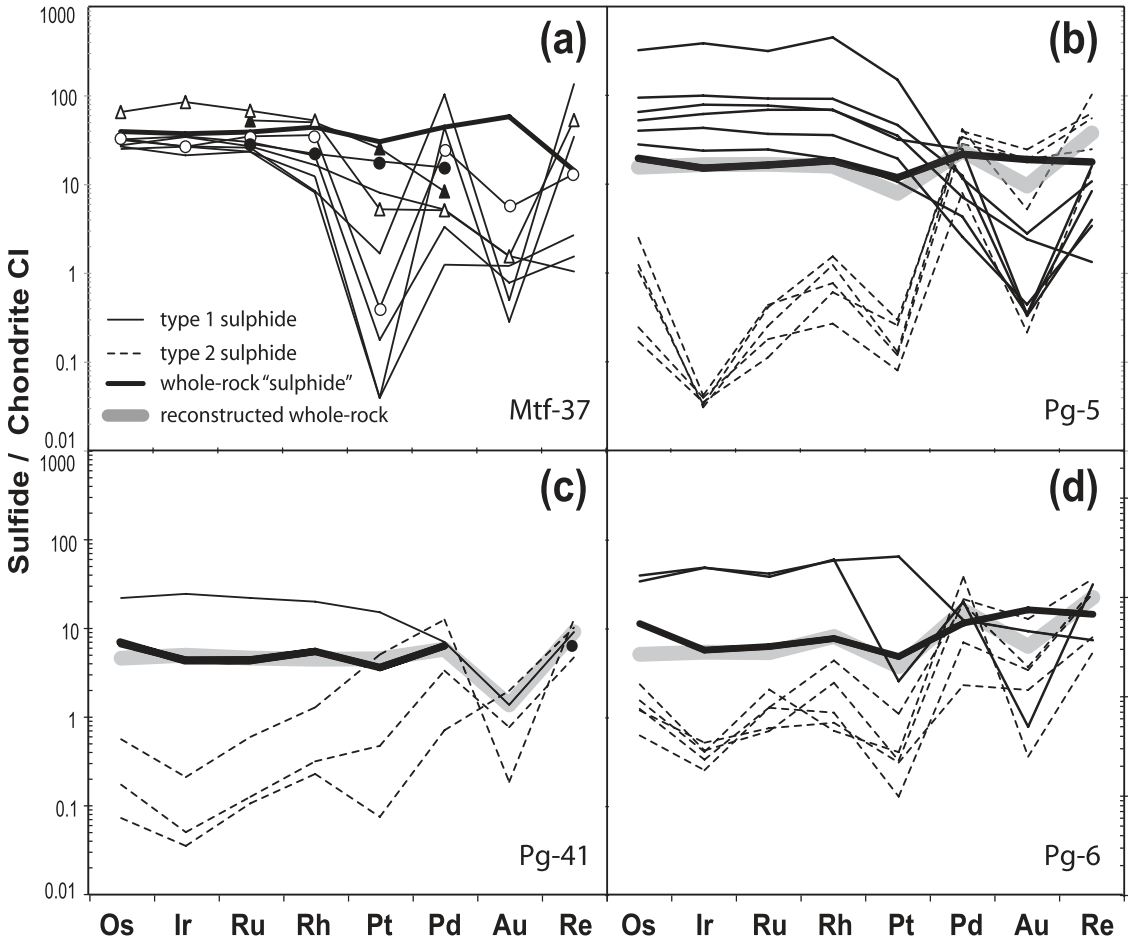

Fig. 14. HSE abundances in individual interstitial sulphides determined by LA-ICP-MS and proton microprobe. Fine continuous lines, Type-1 (see text) sulphide composition; dashed lines, Type-2 sulphides (see text). Bold black line denotes whole-rock HSE patterns recalculated as a homogeneous 'bulk' sulphide, assuming all HSE are in sulphide; sulphide abundance is derived from whole-rock S* (Table 1) and the S content of the bulk sulphide (Tables 2 and 3), Thick grey line is the reconstructed bulk sulphide obtained as follows: HSE compositions from each Type-1 and -2 sulphide are averaged for each sample (Table 5), then the proportion of each of the two sulphide pattern types is obtained by least-squares methods to provide the best fit to the whole-rock pattern; the proportion of each sulphide type (i.e. X_1 and X_2) is given for each sample below except for Mtf-37, in which distinction between Type-1 and -2 sulphide was not possible. (a) Mtf-37; two sulphides (triangles, MTF-37-S3; circles, Mtf-37-S1) were first analysed by proton probe (filled symbols) before LA-CPMS analyses (open symbols) (see also Fig. 14 and Table 5); (b) Pg-5, $X_1 = 0{\cdot}312$, $X_2 = 0{\cdot}688$; for such proportions the reconstructed whole-rock (RWR) HSE composition is $Os_{RWR} = 2{\cdot}8$, $Ir_{RWR} = 2{\cdot}8$, $Ru_{RWR} = 4{\cdot}4$, $Rh_{RWR} = 0{\cdot}76$, $Pt_{RWR} = 2{\cdot}9$, $Pd_{RWR} = 4{\cdot}9$, $Au_{RWR} = 0{\cdot}51$; $Re_{RWR} = 0{\cdot}57$ in ppb; (c) Pg-41, $X_1 = 0{\cdot}186$, $X_2 = 0{\cdot}914$; for such proportions the reconstructed whole-rock HSE composition is $Os_{RWR} = 2{\cdot}9$, $Ir_{RWR} = 2{\cdot}9$, $Ru_{RWR} = 4{\cdot}3$, $Rh_{RWR} = 0{\cdot}8$, $Pt_{RWR} = 6{\cdot}1$, $Pd_{RWR} = 4{\cdot}5$, $Au_{RWR} = 0{\cdot}27$; $Re_{RWR} = 0{\cdot}51$ in ppb; (d) Pg-6, $X_1 = 0{\cdot}137$, $X_2 = 0{\cdot}863$; for such proportions the reconstructed whole-rock HSE composition is $Os_{RWR} = 2{\cdot}4$, $Ir_{RWR} = 2{\cdot}3$, $Ru_{RWR} = 3{\cdot}5$, $Rh_{RWR} = 0{\cdot}9$, $Pt_{RWR} = 3{\cdot}6$, $Pd_{RWR} = 6{\cdot}9$, $Au_{RWR} = 0{\cdot}8$; $Re_{RWR} = 0{\cdot}68$ in ppb. All data are normalized to CI-chondrite abundances, values after McDonough & Sund (1995).

pervasive weathering (hydrous iron hydroxide contains less than 0·5 wt % of S). Because the affinity for O decreases from S to Se, and SeO_2 is a solid compound in contrast to SO_2 and SO_3 (see Dreibus *et al.*, 1995), Se is more resistant to supergene weathering. Therefore Se is a more robust indicator of chalcogenide abundance than S (Lorand *et al.*, 2003*a*). This conclusion is reinforced by the fact that the S*/Se ratio (S* = S abundance corrected for the percentage of weathering; see Table 1) of the breccia-hosted xenoliths is within error of the primitive mantle ratio. Furthermore, LA-ICP-MS analyses of variably altered sulphides in Mtf-37 do not show Se variation. The abundance of Cu in both breccia and basalt-hosted xenoliths shows similar ranges, suggesting that Cu is not affected at the whole-rock scale by supergene weathering (Handler *et al.*, 1999). The similarity in HSE abundance between the two groups of xenoliths and the lack of correlation with LOI indicates that HSE abundances are insensitive to weathering. Therefore no specific HSE fractionation, including Os and Pd, the most mobile HSE, can be ascribed to weathering. For instance, the whole-rock analysis of Mtf-37 displays broadly chondritic

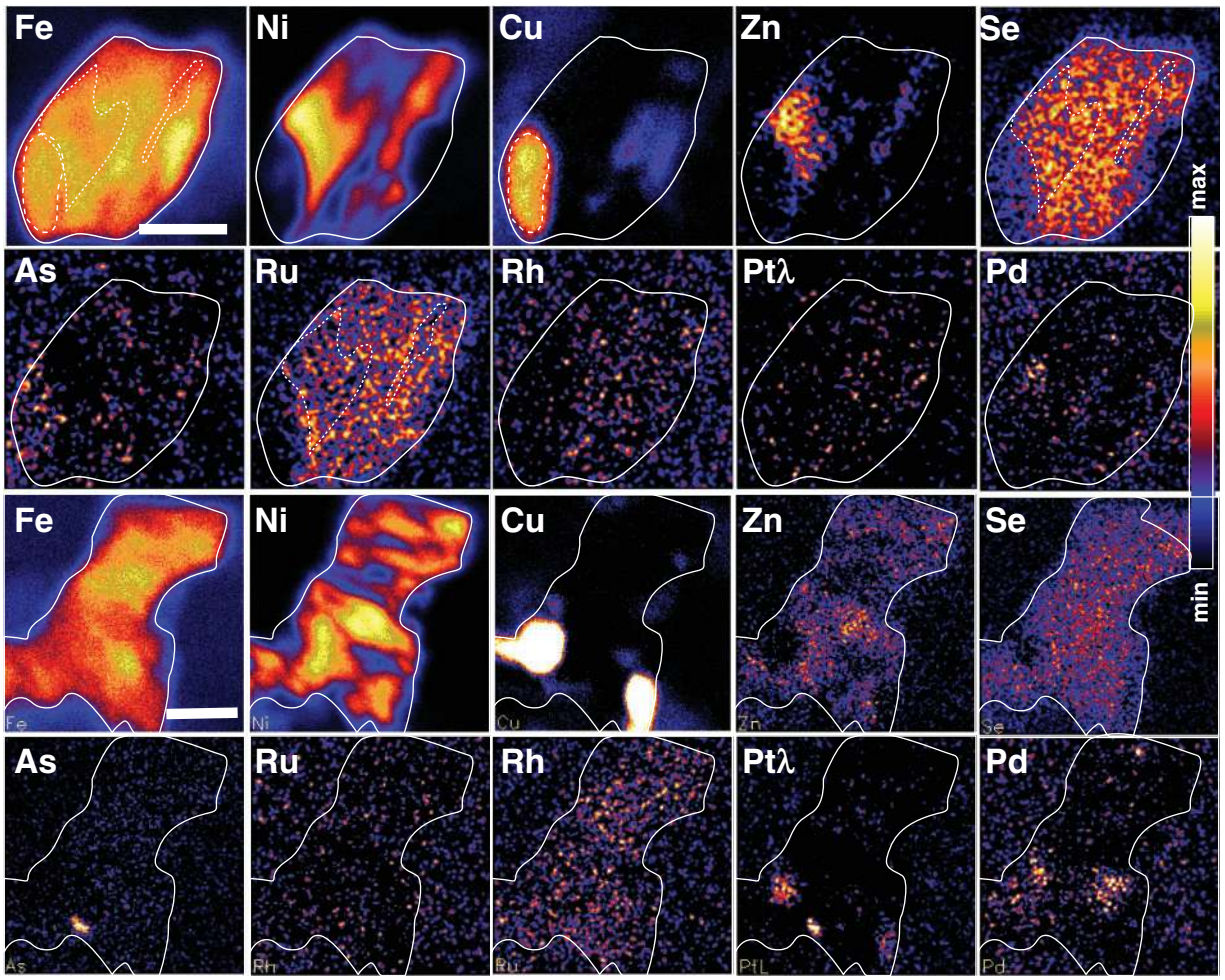

Fig. 15. Proton-induced X-ray emission element maps of sulphides S1 and S2 from sample Mtf-37, showing the distribution of siderophile and chalcophile elements. Analyses were performed at the Nuclear Microprobe facility at the CSIRO–GEMOC analytical unit (North Ryde, Australia). Data are reported in Table 5. (Note the difference in distribution between Pt and Ru and/or Rh.). White scale bars are 50 μm.

Os/Ir and superchondritic Pd/Ir, despite *c.* 73% sulphide alteration. This is in contrast to the loss of both elements relative to Ir expected from alteration (Handler *et al.*, 1999; Pearson *et al.*, 2004). In fact, unlike xenoliths ejected along with oxidized scoria, the Montferrier xenoliths probably escaped high-temperature devolatilization of S, Se, Os and Pd (Lorand *et al.*, 2003*a*).

Such a categorical conclusion cannot be reached for Re. Indeed, breccia-hosted samples, which have the most altered sulphides, also have the lowest bulk-rock Re contents and Re/Os well below primitive mantle values. This relationship could suggest the loss of Re during sulphide alteration. However, these samples have low Se and S* abundances suggesting low primary chalcophile-element and Re abundances owing to partial melting. Given the highly radiogenic composition of the crust (Esser & Turekian, 1993), the radiogenic compositions of several of the whole-rock aliquots (as high as 0·175) could be related to supergene weathering. However, the less altered xenoliths (basalt-hosted) show the most radiogenic compositions. Following a similar line of reasoning we conclude that the highly radiogenic Os-isotope composition is also not related to serpentinization, as this process affects nearly all of the samples to some extent, rather than being limited to the radiogenic samples.

The Montferrier 'protolith'

Numerous similarities have been recognized between the Montferrier xenoliths and the Pyrenean orogenic peridotites (e.g. Fabriès *et al.*, 1987). These include: (1) the highly fertile compositions of the lherzolites; (2) abundant sheared microstructures; (3) pressure and temperature conditions (i.e. spinel peridotite and garnet pyroxenite); (4) the occurrence of disseminated amphibole; (5) high modal proportions of sulphide, mostly in intergranular positions. Although our study is not focused on this issue,

Table 6: $^{187}Re/^{188}Os$ and $^{187}Os/^{188}Os$ of sulphide grain in Montferrier obtained by LA-MC-ICP-MS

Sample	Sulf	$^{187}Re/^{188}Os$	±2SE	$^{187}Os/^{188}Os$	±2SE	Sample	Sulf	$^{187}Re/^{188}Os$	±2SE	$^{187}Os/^{188}Os$	±2SE
Pg-5	A-s1	0·222	0·008	0·1291	0·0014	Mtf-37	C-s3	0·137	0·008	0·1361	0·0014
Pg-5	B-s4	0·108	0·022	0·1258	0·0016	Mtf-37	E-s9	0·310	0·030	0·1151	0·0032
Pg-5	B-s7	0·388	0·062	0·1308	0·0028	Mtf-37	E-s1	0·256	0·002	0·1194	0·0024
Pg-5	B-s11	0·026	0·007	0·1172	0·00072	Mtf-37	E-s6	0·240	0·012	0·1267	0·0010
Pg-45	A-s3	0·027	0·000	0·1175	0·0005	Mtf-37	E-s4	0·186	0·002	0·1175	0·0017
Pg-45	A-s4	0·205	0·013	0·1298	0·0032	Pg2	A-s2	0·073	0·004	0·1277	0·0005
Pg-45	A-s5	0·072	0·005	0·1211	0·0018	Pg2	A-s1	0·095	0·005	0·1290	0·0010
Pg-45	B-s1	0·243	0·014	0·1278	0·0024	Pg-2	A-s3a	0·041	0·006	0·1444	0·0028
Pg-45	B-s4	0·050	0·007	0·1183	0·0006	Pg-2	A-s5	0·224	0·016	0·1210	0·0015
Pg-45	B-s5	0·172	0·009	0·1264	0·0019	Pg-2	A-s4	0·061	0·007	0·1357	0·0022
Pg-45	B-S6	0·067	0·011	0·1239	0·0011	Pg-43	A-s1	0·063	0·002	0·1228	0·0009
Pg-45	C-s2	0·216	0·005	0·1274	0·0016	Pg-43	A-s2	0·027	0·001	0·1193	0·0005
Pg-45	C-s4	0·149	0·005	0·1267	0·0009	Pg-43	A-s3	0·067	0·011	0·1239	0·0011
Pg	A-s1	0·208	0·008	0·1239	0·0007	Pg-43	As-4	0·012	0·002	0·1240	0·0036
Pg	A-s2	0·767	0·042	0·1273	0·0058	Pg-43	As-5	0·099	0·004	0·1236	0·0010
Pg	A-s3	0·716	0·130	0·1227	0·0028	Pg-43	As-6	0·072	0·005	0·1211	0·0018
Pg	A-s4	0·122	0·007	0·1192	0·0018	Pg-43	A-s8	0·516	0·009	0·1403	0·0098
Pg	A-s5	0·141	0·006	0·1229	0·0008	Pg-43	B-s2a	0·671	0·030	0·1192	0·0028
Pg	A-s6	0·377	0·010	0·1224	0·0034	Pg-43	B-s2b	0·651	0·048	0·1214	0·0054
Pg	A-s7	0·370	0·024	0·1265	0·0028	Pg-43	B-s5	0·214	0·014	0·1328	0·0013
Pg	A-s8	0·200	0·015	0·1232	0·0034	Pg-43	B-s6	0·841	0·062	0·1489	0·0078
Pg	A-s9	0·063	0·002	0·1231	0·0019	Pg-43	B-s8	0·229	0·014	0·1461	0·0044
Pg-46	A-s1	0·355	0·008	0·1201	0·0010	Pg-43	B-s10	0·139	0·010	0·1412	0·0032
Pg-46	A-s2	0·267	0·010	0·1171	0·0030	Pg-43	B-s11	0·184	0·012	0·1303	0·0020
Pg-46	A-s6	0·492	0·012	0·1262	0·0020	Pg-43	B-s14	0·106	0·021	0·1474	0·0042
Pg-46	A-s3	0·242	0·006	0·1222	0·0020	Pg-6	A-s1	0·721	0·032	0·1425	0·0062
Mtf-37	A-s2	0·060	0·010	0·1337	0·0034	Pg-6	A-s5	0·361	0·014	0·1263	0·0013
Mtf-37	A-s1	0·072	0·012	0·1316	0·0042	Pg-6	A-s11	0·788	0·082	0·1610	0·0138
Mtf-37	A-s3	0·211	0·008	0·1209	0·0026	Pg-6	A-s12	0·135	0·008	0·1203	0·0009
Mtf-37	C-s1	0·025	0·011	0·1447	0·0120	Pg-6	A-s18	0·896	0·052	0·1540	0·0076
Mtf-37	C-s2	0·093	0·041	0·1418	0·0140	Pg-6	B-s4	0·106	0·031	0·1306	0·0052
						Pg-6	B-s22	0·831	0·064	0·1721	0·0120

All sulphides are interstitial; A, B, C, D, thick section identifier; s, sulphide number; SE, standard error. Only ratios can be obtained with this technique; Os and Re abundance cannot be computed as no internal standards were analysed during the analysis.

we note that our new data reinforce the resemblance between these two mantle samples. In particular, *in situ* Os data for residual sulphides (see below) yield $^{187}Os/^{188}Os \approx 0{\cdot}115$ as found for the Pyrenean peridotites (Reisberg *et al.*, 1991; Becker *et al.*, 2006). The data indicate that the two mantle segments underwent a major melting event at *c.* $2{\cdot}2 \pm 0{\cdot}2$ Ga (Re-depletion age, T_{RD}). Moreover, whole-rock PGE systematics from the Pyrenean peridotites and the Montferrier xenoliths share the same superchondritic Pd/Ir, Ru/Ir and Rh/Ir. However, Le Roux *et al.* (2007) showed convincingly that the fertile nature of the lherzolites from the type Pyrenean locality (Lherz) is not a primary characteristic, but is due to the percolation of asthenospheric melts through a refractory harzburgite matrix. Therefore what we consider here as a 'protolith' for simplicity's sake, could well be an intensively modified lithospheric mantle.

Metasomatism

Alteration cannot explain the S contents higher than the PM value, nor the extremely high S/Se ratios of some samples. As shown in Fig. 11, the correlations between S, Se

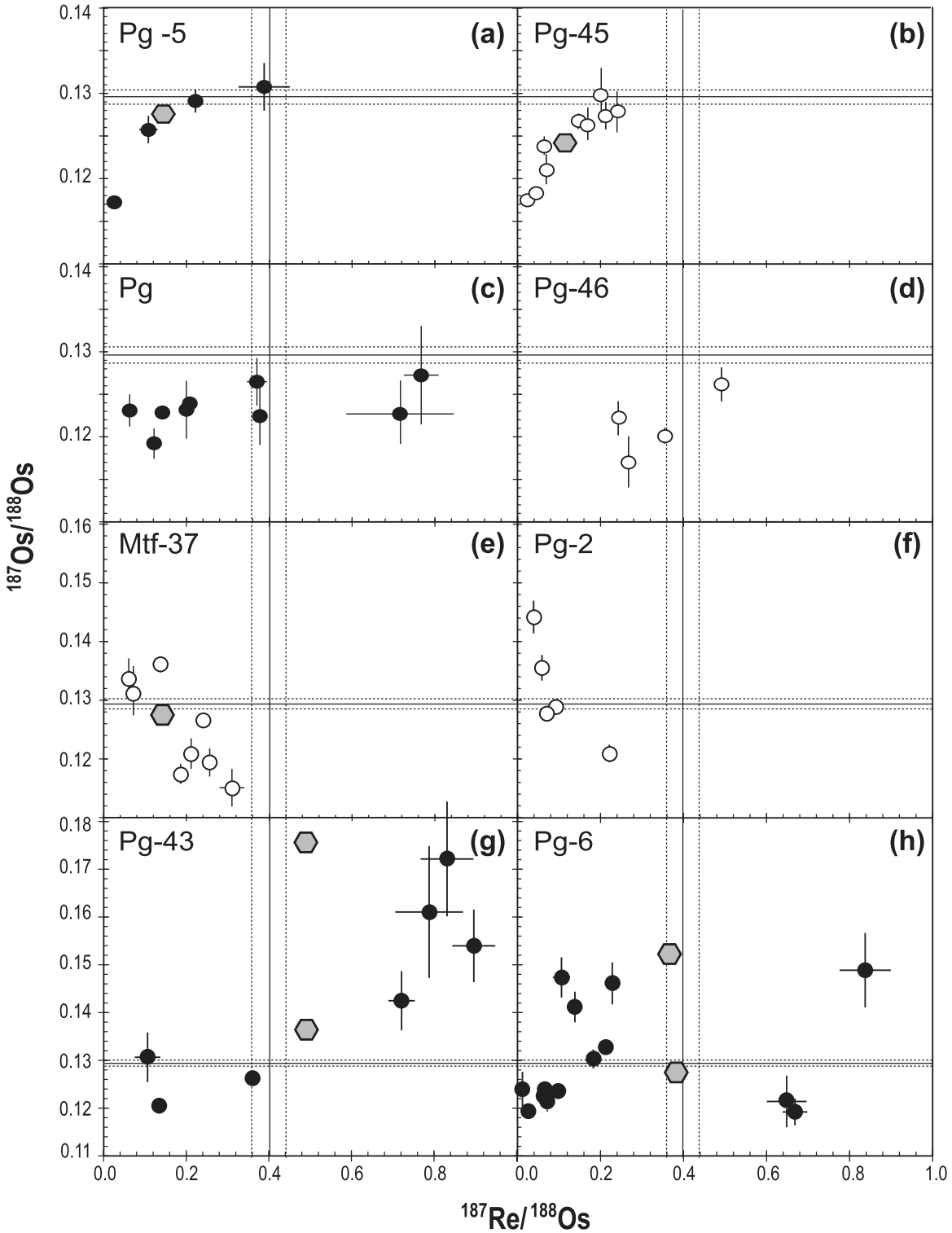

Fig. 16. $^{187}Re/^{188}Os$ vs $^{187}Os/^{188}Os$ for single interstitial sulphide grains obtained by LA-MC-ICP-MS. Grey hexagons, whole-rock composition and duplicate when available; open circles, sulphide from breccia-hosted xenoliths; filled circles, sulphide from basalt-hosted xenoliths. Fine continuous and dashed lines denote the primitive upper mantle estimate (PUM; Meisel *et al.*, 2001).

and La/Sm suggest a relationship between chalcogenide-element enrichment and the metasomatic events recorded by the lithophile trace-element signatures of the silicate minerals.

Lithophile trace element fractionation

Through the study of the incompatible trace element (ITE) patterns (Fig. 3) we can discuss, and partially constrain, the metasomatic history of the Montferrier xenoliths.

First of all, it is apparent from Table 1 that the enriched or depleted LREE characteristics of the Montferrier xenoliths are not related to the occurrence and/or abundance of amphibole. As shown in Fig. 3, the REE fractionation in the Montferrier xenoliths ranges between two types of chondrite-normalized patterns: 'depleted' $[(La/Sm)_N<1]$ and 'enriched' $[(La/Sm)_N>1]$. The evolution from one pattern to the other is continuous and seems to be controlled by a chromatographic effect (Navon & Stolper, 1987). This implies that the peridotite matrix was progressively re-equilibrated with a small fraction (<1%) of fluid, enriched in incompatible trace elements, that percolated through a cold mantle lithosphere. Such a conclusion is in agreement with the low equilibrium temperatures (porphyroclast core compositions) and the lack of obvious related modal metasomatic reactions (except sulphide addition). The LREE-enriched samples also display a pronounced LILE enrichment (especially U and Th) without concomitant HFSE enrichment. Many researchers have ascribed this so-called 'carbonatite' trace-element signature to the percolation of a carbonatite melt (e.g. Yaxley *et al.*, 1991*l*; Dautria *et al.*, 1992; Ionov *et al.*, 1993; Rudnick *et al.*, 1993). However, the LREE-enriched samples from Montferrier lack the metasomatic phases (carbonate and/or secondary diopside) typically associated with carbonatite metasomatism. Furthermore, the constant Nb contents over the large range of LREE variation (Fig. 3) rule out a carbonatitic melt *sensu stricto* (e.g. Frezzotti *et al.*, 2002). Indeed, the exact nature and origin of the percolating melt or fluid is debatable. Carbonatites show a variety of trace-element abundances and fractionations (e.g. Bell *et al.*, 1999), which are not always compatible with those invoked by some models of carbonatite metasomatism. For instance, the fractionation of Nb–Ta is extremely variable relative to the LREE, as is the enrichment of U and Th relative to Nb–Ta and the LREE, in carbonatites worldwide. In addition, as reviewed by Bell *et al.* (1999), carbonatite-like melts could be generated either by partial melting of the mantle or by magmatic differentiation. Similar incompatible trace-element patterns were also predicted by modelling of continuous reactions between a percolating asthenospheric silicate melt and the surrounding lithospheric peridotites (Bedini *et al.*, 1997; Vernieres *et al.*, 1997; Ionov *et al.*, 2005, 2006*a*). Owing to the strong thermal gradient across the SCLM, the rising melt should evolve with decreasing volume through crystallization of successive phases and melt–rock reactions. Through these reactions the residual melt or fluid becomes more and more enriched in volatiles and incompatible elements. In such numerical simulations, LILE enrichment occurs in the upper part of the lithosphere-percolation domain at low rock porosity. The volatile enrichment should also significantly lower the viscosity, dihedral angles and crystallization temperature of the fluid and thus allow it to percolate into the upper and colder part of the SCLM (Minarik & Watson, 1995; Watson & Brenan, 1987). Within this cold domain, fluid–rock exchange of trace elements should be dominated by chromatographic processes (Navon & Stolper, 1987; Bodinier *et al.*, 1990). From this discussion it is apparent that the incompatible trace element patterns of the 'enriched' Montferrier samples could be generated by various melts or fluids and through various processes. However, a common feature of all these fluids is their volatile-rich nature (i.e. C–O–H–S ± Cl).

The LREE-depleted samples display positive U anomalies, with $(U/Th)_{PM}$ as high as 124 for Mtf-37. Such U anomalies have been reported for SCLM peridotites worldwide (e.g. Ionov *et al.*, 1995; Carigan *et al.*, 1996) and are extremely common in the Massif Central and Languedoc peridotite xenoliths (Alard *et al.*, 1996, 1999; Lenoir *et al.*, 2000). Because U is highly mobile in aqueous fluids, several researchers have suggested a supergene origin for such anomalies (e.g. Ionov *et al.*, 1995; Carigan *et al.*, 1996). However, as suggested by Alard *et al.* (1996) and Lenoir *et al.* (2000), this selective U enrichment is probably a mantle feature. The mantle origin of this anomaly is here strongly suggested by the fact that both U and Th contents increase as the LREE enrichment relative to HREE increases. Such LILE and LREE enrichments must occur under mantle conditions. Therefore, two scenarios can be envisioned: first, the U anomaly is an inherited feature that was overprinted to different degrees during the LREE + LILE enrichment described above; second, this anomaly is produced by the same fluid through percolation–reaction and associated trace-element fractionation. The partition coefficient of U is largely dependent on its oxidation state (U^{4+} or U^{6+}; Brenan *et al.*, 1995). Thus, based on the differential behaviour of U and Th, it could be argued that the metasomatic agent must be oxidizing to have U present in its more oxidized form U^{6+}, which will considerably increase the charge mismatch (especially relative to Th^{4+} and La^{3+}) and thus significantly lower $D^{matrix/melt}(U)$ and consequently increase the chromatographic velocity of U. Therefore, the chromatographic front of U will progress further (i.e. to shallower levels) than the chromatographic fronts of La and Th. Within this framework, the fluid responsible for the U anomaly and for the 'carbonatite' signature are genetically linked (Bedini *et al.*, 1997).

Fractionation of siderophile and chalcophile elements

S contents and sulphide abundances are not correlated with the modal proportions of amphibole. Furthermore, there is no preferential and systematic petrographic relationship between sulphide and amphibole. Cabanes & Mercier (1988) described two types of amphibole, Ti-rich and Ti-poor pargasite, which they ascribed to two distinct metasomatic events, postdating and contemporaneous with the deformation, respectively. However, during this study we were not able to establish a clear link between LREE fractionation and/or sulphide abundance and composition on the one hand and the abundance and composition of amphibole on the other. As mentioned above, such amphibole also occurs within the Pyrenean orogenic peridotite massifs and could be part of what we consider here as the 'protolith'.

The net effect of the metasomatic event as estimated from the whole-rock analyses of the Montferrier xenoliths is a clear gain in S, Re, Au, (Se) and an increase in the Pd/Ir and Os/Ir ratios. The latter feature is due to a dilution of Ir, Ru, Rh and Pt at roughly constant Os and Pd contents. These observations suggest that the fluid involved was depleted in Ir, Ru, Rh and Pt, enriched in Os, Pd, Se, Au and Re, and extremely enriched in S. The effect of the volatile-rich metasomatism on the Re–Os isotopic compositions of the whole-rocks and sulphides is discussed elsewhere. Schematically we can consider two non-exclusive end-member scenarios: (1) sulphide precipitated by immiscibility from a volatile rich melt; or (2) pre-existing sulphide re-equilibrated with a volatile-rich fluid phase, with or without sulphidation reactions (i.e. formation of new sulphide).

All PGE, Se, Te and Cu have high sulphide–melt/silicate–melt partition coefficients ($D > 10^3$; e.g. Peach *et al.*, 1990; Fleet *et al.*, 1999). High-density immiscible sulphide melts segregated from magmas do not strongly fractionate chalcophile from highly siderophile elements relative to silicate melt patterns. Re is the exception, as significant partitioning of Re into the silicate phase has been reported (Burton *et al.*, 2002). Additionally, under oxidizing conditions, spinels may potentially host large amounts of Re (Righter *et al.*, 1998). However, the mass-balance calculation, shown in Fig. 14, indicates that all the Re is hosted in sulphide. As far as we know Os and Ir have similar partitioning behaviour in a sulphide solid–sulphide melt system (see Ballhaus *et al.*, 2006; Brenan, 2008). Likewise, sulphide melts in equilibrium with basaltic melts have Pd/Ir ratios within the range 1–100 (Rehkämper *et al.*, 1999; Bézos *et al.*, 2005), not >1200, as shown by the three *in situ* analyses of Type-2 sulphide from sample Pg-5. In contrast to magmatic sulphide melts, vapour deposition of HSE and S can produce strong fractionation among the HSE. It has been suggested that oxidizing volatile-rich fluids can mobilize Os (Brandon *et al.*, 1996). Similar mobility and fractionation of these elements have been ascribed to super-critical fluids in subduction zone settings (Parkinson *et al.*, 1998; McInnes *et al.*, 1999). Furthermore, several studies have suggested that Re could be extremely mobile as a volatile species (e.g. Lassiter, 2003). Experimental work shows that under some conditions Os, Ru and Pd could be mobile in such fluids (Wood, 1987; Fleet & Wu, 1995). Similarly, the most S-rich samples (i.e. the LREE-enriched samples) show S/Se ratios markedly higher than chondritic values (3000–12 000), which are inconsistent with a simple addition of immiscible sulphides via a melt during metasomatism. Previous data obtained for metasomatic sulphides resembling sulphide partial melt (Ballhaus *et al.*, 2001) yield S/Se 2670 ± 525 (Lorand & Alard, 2001), similar to S/Se values (1120–2500) of mantle sulphides residual after melting (Lorand & Alard, 2001; Hattori *et al.*, 2002). This suggests that the metasomatic agent preferentially transported S relative to Se. This difference in behaviour could result from the lesser affinity of Se for oxygen compared with S. Experimental work shows that partial melting of mss will produce a Cu-rich melt (e.g. Ballhaus *et al.*, 2001, 2006); accordingly, most of the metasomatic sulphides associated with melt–rock percolation reaction described so far are Cu-rich (Alard *et al.*, 2000, 2002; Lorand & Alard, 2001; Lorand *et al.*, 2004; Luguet *et al.*, 2004; Powell & O'Reilly, 2007). In the Montferrier samples, sulphide mineralogy and whole-rock chemistry do not show Cu enrichment (Figs 5 and 7–9). Therefore, the fractionation of elements (i.e. Pd, Os and S enrichment relative to Pt, Ir, Se and Cu, respectively), which usually displays similar 'magmatic' behaviour, is inconsistent with a scenario involving simple addition of a sulphide melt. Peregoedova *et al.* (2006) provided experimental evidence for transfer of Au > Ni > Cu > Pd–Pt > Ru–Rh–Ir at 1000–1100°C in magmatic-vapour H_2S, suggesting that other ligands (chlorine) are not necessary for transport of these elements. In more oxidizing highly saline fluids (Ni–NiO–Hematite–Magnetite buffer; i.e. $0 < \Delta \log O_2 < 5$, relative to FMQ calculated at 900°C and 1·5 GPa), such as gas condensates from arc volcanoes, Yudovskaya *et al.* (2008) reported fluid/melt partition coefficients decreasing from Os (54·5) to Ni ($15{\cdot}9 \pm 10{\cdot}7$), Cu ($12{\cdot}4 \pm 6{\cdot}4$), and Re ($12{\cdot}1 \pm 14{\cdot}3$), which show similar solubility to Au, whereas Pd is less concentrated. The covariation of Os/Ir–Pd/Ir–Re with S, coupled with the slight Au enrichment with respect to Pd in the Montferrier xenoliths, is thus consistent with the inferred affinity of these elements for oxidized, sulphurous vapour phases at magmatic temperatures. Thus, as suggested by Lee (2002) and Lorand *et al.* (2004), superchondritic Os/Ir, Pd/Pt and high S/Se (>10 000) could be symptomatic of metasomatism via oxidized fluids. However, the whole-rock budget of the Montferrier xenoliths does not simply result from cryptic re-equilibration between sulphides and a percolating

volatile-rich fluid: it has also been modified through modal metasomatism. Indeed, as demonstrated by the correlations of sulphide modal abundances with whole-rock LREE enrichment, precipitation of S-rich Fe–Ni sulphides has occurred. This suggests that S was a dissolved species in the volatile-rich metasomatic fluid.

In situ PGE analyses identify two types of mantle-derived sulphide. Type-2 patterns (Fig. 14) are characterized by Os enrichment relative to Ir and chondrite-normalized HSE patterns with a marked positive slope [$3{\cdot}8 \leq (Pd/Ir)_N \leq 1280$]. Such HSE abundances are inconsistent with a residual origin and instead indicate a metasomatic origin. The Type-2 metasomatic sulphides are predominant in extremely S-rich samples (i.e. Pg-6) and have been superimposed on a pre-existing sulphide assemblage (Type-1), inherited from the protolith. Type-1 HSE patterns, enriched in compatible PGE (Os, Ir, Ru, Rh) with respect to Pt and Pd, show the characteristics of mss residual after partial melting (e.g. Alard *et al.*, 2000; Ballhaus *et al.*, 2006). The residual origin of Type-1 sulphide is also attested by *in situ* Re–Os isotopic data, which include $^{187}Os/^{188}Os$ compositions as low as 0·117 at low $^{187}Re/^{188}Os$ (down to 0·026; Fig. 16). In 'enriched' samples the two types of sulphide coexist at the thin-section scale; the ratio between Type-2 and Type-1 increases from 68:32 in samples displaying modest LREE enrichment to 86:13 in the most S- and LREE-rich sample, Pg-6. Mass-balance calculations for Pg-6 indicate that 120 ppm of S was inherited from the protolith and 480 ppm of S added through metasomatism.

Metasomatic sulphides are not in equilibrium with coexisting olivine, as shown by their Ni contents. Their bulk Ni contents, as estimated from 'enriched' xenoliths (Table 3), are too low by *c.* 50% compared with sulphides equilibrated with olivine at 900°C, taking into account the Ni contents of Montferrier olivine ($0{\cdot}30 \pm 0{\cdot}03$ wt % NiO) and the olivine–mss partition coefficient $[(X\mathrm{Ni}/\mathrm{XFe})_{\mathrm{sulph}}/(X\mathrm{Ni}/\mathrm{XFe})_{\mathrm{ol}}]$ of 33 (Clark & Naldrett, 1972). The theoretically predicted Ni content is *c.* 30–32 wt %.

Although SO_2 occurs at high fO_2 ($\geq$FMQ+1), H_2S is the main sulphur species in mantle fluids (Eggler & Lorand, 1993). Sulphidation reactions can occur via reactions between fluid and melts (see Ballhaus & Stumpfl, 1986) such as

$$H_2S(f) + BM(f) + O_2^-(m) = BMS(m) + 2OH^-(sil) \quad (1)$$

or, if chlorine was present,

$$H_2S(f) + BMCl(f) + O_2^-(m) = BMS(m) + 2OH^- + 2Cl^-(sil) \quad (2)$$

where BM indicates base metals, Ni, Cu, Fe; f is fluid(s); m is silicate melt; sil is silicates.

Both reactions produce OH^-, which can be accommodated in hydrous silicate minerals such as amphibole or phlogopite. Another mechanism is the sulphidation of olivine into mss and orthopyroxene

$$2Fe_2SiO_4 + S_2 = 2FeSiO_3 + 2FeS + O_2 \quad (3)$$

which was invoked years ago for the generation of magmatic sulphide ores (Naldrett & Gasparini, 1971) and investigated experimentally at 900°C by Libaudé & Sabatier (1980).

Lorand *et al.* (2004) have suggested that because Cu is a trace element in mantle olivine, metasomatic sulphides produced by sulfidation would be Cu-poor but Fe-rich. For 480 ppm S added (e.g., Pg-6), the Ni/S in metasomatic sulphides (13/36) converts to 150–200 ppm Ni added from the silicates; that is, just one-tenth of the bulk-rock Ni (2000 ± 200 ppm). Given the modal abundance of metasomatic BMS, any secondary opx derived from reaction (3) would be of very restricted volume, and would be difficult to detect by petrographic studies. For instance, olivine sulphidation [reaction (3)] produces a maximum of 0·2 wt % FeS (0·00227 mol %), corresponding to 0·00227 mol % of opx.

Conversion of residual sulphides by metasomatic fluids.

'Depleted' samples such as Mtf-37 do not show obvious sulphide enrichment. S* abundance is lower than estimated for the PM and the sulphides do not display Type-2 PGE patterns. However, this sample, and the other LREE-depleted lherzolites, are not devoid of metasomatic fingerprints. First, they display positive U anomalies. Second, whole-rock analyses have $(Os/Ir)_N$, $(Pd/Ir)_N$ and $(Au/Ir)_N > 1$. Third, their sulphide mineralogy is not typical of mantle xenoliths and shows po–pn intergrowths similar to Type-2 metasomatic sulphides. Finally, *in situ* analyses of the Re–Os isotopic composition reveal an inverse relationship between $^{187}Re/^{188}Os$ and $^{187}Os/^{188}Os$, which is hardly compatible with a residual origin for these sulphides.

Although Mtf-37 sulphides display only PGE patterns akin to Type-1 (i.e. high Os, Ir, Ru, Rh content), several sulphides display some coupled Pd + Re enrichment relative to Ir, in addition to micronuggets of arsenic minerals such as $PtAs_2$ (Fig. 15). The latter minerals probably were produced by reactions of Pt-alloys or Pt-bismuthotellurides (identified by spikes in time-resolved LAM-ICP-MS spectra) with an As-bearing vapour phase. Thus, $PtAs_2$ micronuggets crystallized at temperatures below or near 900°C (i.e. below the solidus of Cu–Fe–Ni sulphide assemblages), as Pt–Te–Bi microminerals are not stable at higher temperature in mantle peridotites (Lorand *et al.*, 2008*b*). Gold, Pd, and Re are the most incompatible HSE with respect to mss, as is arsenic, a highly volatile chalcophile element. Thus, we suggest that these selective enrichments of the most incompatible HSE + As, independently of Cu, S and Se, may reflect a type of 'cryptic' metasomatism. In this model, pre-existing

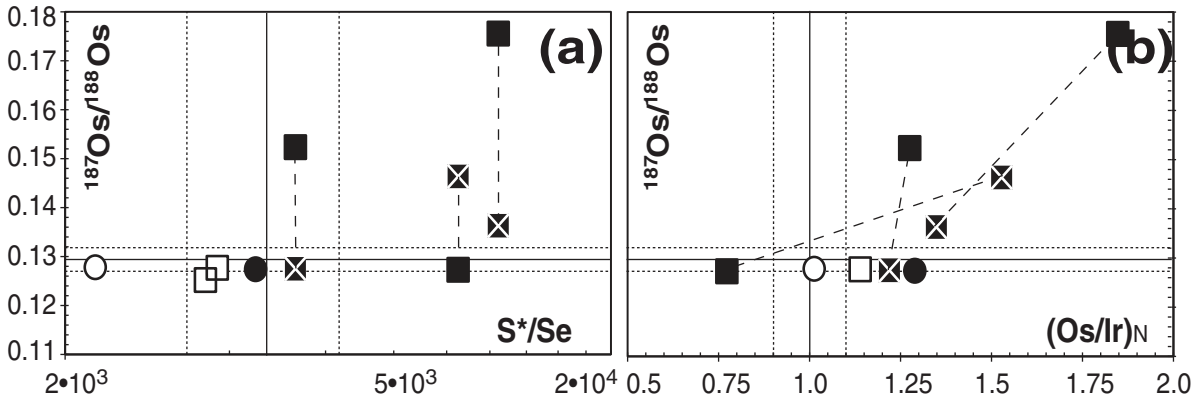

Fig. 17. Whole-rock $^{187}Os/^{188}Os$ vs S*/Se and $(Os/Ir)_N$. Symbols as in Fig. 12. PUM value after McDonough & Sun (1995) and Meisel *et al.* (2001).

(primary) sulphides with sub-chondritic Pd/Ir, Au/Ir and Re/Ir ratios as a result of a previous melting event have been re-equilbrated locally with a percolating fluid rich in Pd–Au–Re–As. Chromatographic effects have been previously proposed as an explanation for the enrichment of specific zones of ore deposits in elements such as Pd or Au (Boudreau, 1999) and for the genesis of the Pd–Au–As magmatic orebodies that are associated with some Betic–Rif orogenic peridotite bodies (Torres-Ruiz *et al.*, 1996; Narbonna-Guttierez *et al.*, 2003). This process must have occurred on a very small scale (thin-section scale), as suggested by the highly variable Pd/Ir and Re/Os ratios of Mtf-37 sulphides and the marginal occurrence of $PtAs_2$ micronuggets. The heterogeneous and discrete enrichment of the most incompatible HSE and fluid-borne elements is consistent with the U enrichment that also characterizes the LREE-depleted samples; we have shown above that the U enrichment is the fingerprint of highly evolved fluids. By analogy with the proposed LREE enrichment mechanism, the HSE compatible in mss (IPGE + Rh + Pt) were readily buffered by the surrounding mss matrix, thus leaving a 'residual' fluid highly enriched in Re, Pd, Au and As in the uppermost part of the rock column.

Re–Os isotopic composition (whole-rock and sulphide)

Sulphide addition via metasomatism obviously has an effect on the Os isotopic composition. Whole-rock $^{187}Os/^{188}Os$ can be as high as 0·1756 (sample Pg-6). The most radiogenic samples are S-rich and LREE-enriched. Figure 17 shows that, despite the extreme heterogeneity between aliquots, the most radiogenic compositions are obtained for samples with high (>PM) S*/Se and Os/Ir. In each of the three samples analysed in duplicate, the analysis with the higher $^{187}Os/^{188}Os$ ratio displays the higher Os concentration (Fig. 13b). These features, along with the correlation between $^{187}Os/^{188}Os$ and S* (Fig. 13d), demonstrate unequivocally that the whole-rock Os-isotope composition was shifted towards extremely radiogenic compositions during the metasomatic process. Although the massive addition of Type-2 sulphide would appear as the most obvious process to explain these trends, mass-balance considerations suggest that another process is required; the low Os contents of Type-2 sulphides need to be balanced by extremely radiogenic compositions. For instance, Type-2 sulphides in Pg-6 represent more than 80% of the sulphide population but contribute only ≈12% of the Os budget. Thus, the whole-rock $^{187}Os/^{188}Os$ composition cannot be accounted for simply by a mixing process via the addition of radiogenic Os. This is also shown by the lack of covariation between 1/Os and $^{187}Os/^{188}Os$ (Fig. 13b).

The positive Re/Os–$^{187}Os/^{188}Os$ correlation found in Pg-6 can be used to illustrate the effect of the sulphide addition process. However, as mentioned above, owing to the analytical technique, and to the extreme compositional heterogeneity of the sulphides, we can assess only a part of the Re–Os isotopic systematics of these samples. This is best demonstrated by comparing the range of Re/Os obtained by LA-ICP-MS and by LA-MC-ICP-MS. LA-ICP-MS analyses of Pg-6 sulphides indicate that Re/Os varies at least between 0·02 and 3·55, whereas we have obtained reliable Re–Os isotopic data only for sulphides having Re/Os below 0·19. Thus we sample mainly Type-1 sulphides. However, such radiogenic Os compositions are unlikely in residual sulphides. Similarly, the $^{187}Re/^{188}Os$–$^{187}Os/^{188}Os$ compositions of the most radiogenic whole-rock aliquots (Pg-6, Pg-43) can be explained only if some sulphides with high Os concentrations and low to moderate Re/Os ratios (i.e. as in Type-1 sulphide) have highly radiogenic compositions. Such sulphides were partly sampled in Pg-43. Thus the whole-rock–sulphide Re–Os isotopic relationships that we have partly unfolded here would suggest a complex interplay between Os

addition via sulphide addition (e.g. Pg and Pg-5) and isotopic re-equilibration of pre-existing sulphide with a radiogenic Os-bearing fluid (e.g. Pg-6 and Pg-43).

Likewise, the negative correlation between $^{187}Re/^{188}Os$ and $^{187}Os/^{188}Os$ obtained for Mtf-37 and Pg-2 is unexpected. Several hypotheses could be put forward, as follows.

(1) This unusual correlation could be due to an analytical artefact. However, the Os and Re voltages and Re/Os ratios are well within the range of the analytical techniques and are comparable with what has been obtained for other sulphide grains in samples not showing such inverse relationships (e.g. Pg-5, Pg-6) analysed during the same day with the same conditions. We also performed high-resolution mass scans on mass 185 to ensure that no interfering element was present. Four scans were performed on three Mtf-37 sulphides showing various degrees of alteration (see below). All scans show a clean ^{185}Re peak without a shoulder or satellite peak. Furthermore, the stable Os isotopic ratios such as $^{186}Os/^{188}Os$ and $^{189}Os/^{188}Os$ are well within the accepted range. Thus, there is no obvious reason to believe that this inverse correlation is due to an analytical artefact.

(2) Re loss during sulphide weathering could also account for this inverse correlation. As discussed above, whole-rock contents of Re and S decrease as the degree of sulphide weathering increases. Mtf-37 and Pg-2 show a clear inverse relationship between Re/Os and $^{187}Os/^{188}Os$; both are breccia- hosted xenoliths with the highest degree of sulphide alteration (*c.* 73 and 68%, respectively). It could be envisaged that Re is leached out by low-temperature water-rich fluid during the formation of Fe-oxyhydroxide (Luguet *et al.*, 1999). This deuteric fluid could be enriched in radiogenic (i.e. crustal) Os. Thus the removal of Re will be accompanied by an increase in radiogenic Os sequestered in the newly formed Fe-oxyhydroxide. However, Re and Se are correlated, and Se is not affected by weathering (Lorand *et al.*, 2003*a*). Re abundances in sulphide grains in Mtf-37 (0·04–5·4 ppm) span the same range as for less altered samples such as Pg-5 (Re = 0·05–4·1 ppm; Alt-S% ≈ 17%). Pg-45 and Pg-46 are also breccia-hosted xenoliths with sulphide alteration levels of 47–45%, and do not show the negative $^{187}Re/^{188}Os$–$^{187}Os/^{188}Os$ correlation. Finally, such negative correlations are also found in a xenolith from Montboissier (French Massif Central) that contains extremely fresh metasomatic sulphides hosted in poikilitic cpx (Alard *et al.*, 2002).

(3) Partial isotopic homogenization of Type-1 sulphide with a radiogenic Os-bearing fluid may also account for such features. We can envision a scenario of local and partial isotopic re-equilibration of pre-existing sulphides (Mtf-37 shows only Type-1 sulphide) with a percolating radiogenic Os-bearing fluid. Recently, Le Roux *et al.* (2009) have shown that the isotopic composition of percolated peridotites in the Lherz massif is best explained by element–isotope decoupling. The extent of this decoupling depends on several parameters including: element diffusivity in minerals; average grain size of minerals; elemental and isotopic compositional contrast between the matrix and the percolating fluid; critical volume of isotopic homogenization; integrated fluid/rock ratio. Thus, although the contrast in Os abundance between the fluid and the matrix (i.e primary sulphide) is not favourable ($[Os]_{fluid}/[Os]_{sulph} = 10^{-6}$–$10^{-8}$) there are several characteristics inherent in the Os-sulphide system, as well as several peculiarities of the Montferrier xenoliths, that may counterbalance this unfavourable ratio. First, Os diffusivity in sulphide and especially in pyrrhotite (i.e. $n \times 10^{-14}\ m^2\ s^{-1}$; Brenan et al., 2000) is higher by three orders of magnitude than typical REE diffusivity (i.e. $n \times 10^{-17}\ m^2\ s^{-1}$; Van Orman et al., 2001). Furthermore, sulphides have typical grain sizes between 50 and 100 μm, and are thus 10–100 times smaller than typical silicate phases. In Montferrier more than 95% of the sulphides are interstitial and thus could be readily equilibrated. In this process, the low Os concentration of the fluid would be compensated by the integrated fluid/sulphide ratio. Sulphides are trace phases (<0·1% by volume of the whole-rock); this low sulphide volume significantly reduces the fluid/sulphide ratio required for re-equilibration. In addition, as discussed below, the Os isotopic composition of such metasomatic fluids could be extremely radiogenic (i.e $^{187}Os/^{188}Os \gg 1$); thus the fluid/sulphide ratio needed to significantly increase the $^{187}Os/^{188}Os$ ratio of the sulphide might not be very high. Finally, the peculiar sheared microstructure of the xenoliths, and the geodynamic context of the Montferrier volcanic province, notably its connection with the Cevennes Fault (Fig. 1), suggest the existence of a major lithospheric shear zone beneath Montferrier. Mantle fluid flux was probably focused and enhanced within such a structure. We also noted that all samples showing this inverse Re–Os relationship have high U/Th ratios, including the Montboisssier sample (Mbs-1; Alard *et al.*, 2002). The U fractionation relative to Th has been here tentatively ascribed to the occurrence of U in the mestasomatic fluid in its most oxidized form U^{6+} instead of U^{4+}. The fO_2 may have an influence on the behaviour of Re and Os in this fluid and relative to the sulphide matrix. Re may become more incompatible and partition more readily into the fluid. In this scenario, the extent to which each sulphide in its microstructural environment would be isotopically homogenized

would depend on the fluid path and on the connectivity of the system. The latter parameter should be high given the deformed nature of the Montferrier xenoliths. Although this scenario is qualitatively attractive, it remains a hypothesis and requires further testing, which is beyond the scope of this study, given the number and variety of parameters that must be tested, and the lack of partition coefficient data between such fluids and sulphides for HSE. Nevertheless, the percolating fluid must have had a highly radiogenic composition ($^{187}Os/^{188}Os > 0{\cdot}18$).

Relationships between sulphide, siderophile and chalcophile elements and metasomatic processes

Reports of metasomatic alteration(s) of the chalcophile and HSE abundances of various mantle sections have significantly increased in recent years (Brandon *et al.*, 1996; Alard *et al.*, 2000, 2002; Lorand & Alard, 2001*l*; Lee, 2002; Lorand *et al.*, 2003*b*, 2008*a*, 2009; Chesley *et al.*, 2004; Luguet *et al.*, 2004; Pearson *et al.*, 2004; Powell & O'Reilly, 2007). The Montferrier xenolith suite arguably represents the best-documented example of sulphide metasomatism. Indeed, with S contents as high as 622, and with $(Pd/Ir)_N$ and $^{187}Os/^{188}Os$ reaching 2 and 0·17, respectively, the Montferrier xenoliths provide an extreme example of metasomatic alteration of chalcophile elements and HSE. However, numerous studies have reported similar metasomatic enrichment in LILE and LREE, without massive sulphide enrichment or significant HSE fractionation (we consider here only peridotite xenoliths hosted in alkali basalts).

The most patent effect of metasomatism is the crystallization of metasomatic phases (i.e. modal metasomatism) such as amphibole, phlogopite, feldspar, apatite or carbonate. In this respect we would argue that the relationship with 'hydrated' minerals such as amphibole or phlogopite is not really established. For instance, amphibole-bearing samples in the Massif Central or from the Nógrád–Gömör volcanic field (Hungary–Slovakia) do not show higher sulphide abundances than the amphibole-barren ones (Szabo & Bodnar, 1995; Lorand & Alard, 2001*l*; Lorand *et al.*, 2003*a*). Wilson *et al.* (1996) reported occasional sulphide–amphibole associations in a xenolith suite from Dish Hill (California); these contain up to 20% amphibole, yet S contents remained below the primitive upper mantle (PUM) value and only one amphibole-rich sample showed a significantly fractionated PGE pattern. Those workers concluded that overall, amphibole-bearing REE-rich samples did not show appreciable enrichment or fractionation of PGE.

In contrast, the relationship between carbonate and sulphide is almost systematic. Several reserchers (e.g. Dautria *et al.*, 1992, 2006; Ionov *et al.*, 1993; Kogarko *et al.*, 1995; Jakni *et al.*, 1996; Lorand *et al.*, 2004; Powell & O'Reilly, 2007) have described sulphide globules associated with newly formed phases directly related to the percolation–reaction of carbonatite melt such as carbonate and/or wehrlitic reaction zones containing cpx II ± olivine II ± phlogopite and/or amphibole ± (K-)feldspar or glass ± Ti-oxide ± Cr-spinel (II). In most cases the sulphide assemblage is metal-rich (pn–cp ± po) and especially Cu-rich (i.e. cp ≥ 10%). When data are available, whole-rock S contents are relatively high, at least 50–100 ppm more than in non-metasomatized peridotites from the same locality. In agreement with their sulphide mineralogy (cp ≥ 10%) such samples often show high whole-rock Cu contents and high Pd/Ir (Alard *et al.*, 2000; Lorand & Alard, 2001*l*; Lorand *et al.*, 2004; Powell & O'Reilly, 2007). However, S/Se remains within error of or slightly lower than the chondritic ratio (Lorand & Alard, 2001*l*; Lorand *et al.*, 2003*a*, 2004), in agreement with the preferential partitioning of Se into Cu-rich sulphides (Peach *et al.*, 1990). Cu-rich pentlandites in such metasomatic carbonate/wehrlitic reaction zones have high $(Pd/Ir)_N$ and $^{187}Os/^{188}Os$ as high as ≈15 and 0·176, respectively (e.g. Alard *et al.*, 2000; Powell & O'Reilly, 2007).

Peridotite xenoliths devoid of such modal metasomatic imprints, but from the same localities, often equilibrated at slightly lower temperature (i.e. $T_{BK90} \leq 950^{\circ}C$); they are characterized by abundant CO_2-rich polyphase inclusions containing minute sulphide blebs. In several cases, sulphide grains (>10 μm) have petrographic and compositional characteristics contrasting with the Cu-rich sulphide associated with the carbonate/wehrlitic reaction zones described above. These sulphides show abundant flame-like pn exsolution within (Ni-rich) po, and low abundances of Cu-rich phases (≤5%), as described from Montferrier. Lorand *et al.* (2004) noted that Kerguelen mantle xenoliths showing such features had high S/Se ratios (up to 10 000), coupled with superchondritic $(Os/Ir)_N$ and strong Pd enrichment. As discussed above, the geochemical characteristics of these sulphides strongly suggest that they are related to C–H–S–O ± Cl-rich fluids and not to a melt. The spatial association of sulphide–CO_2 fluid and sulphide–carbonate–silicate metasomatic assemblages suggests a genetic relationship through 'fractional crystallization' and liquid–liquid immiscibility between these two metasomatic occurrences of sulphide (e.g. Frezzotti *et al.*, 2002).

On the basis of incompatible trace-element patterns, we argued that such metasomatic fluids could be produced by differentiation through melt–rock reaction of a basaltic [ocean island basalt (OIB)-like] melt. This scenario was convincingly proposed for the Sidamo (East Africa) and Tok (Siberia) xenolith suites (Bedini *et al.*, 1997; Ionov *et al.*, 2005, 2006*a*). Apatite-bearing samples from both suites show pronounced enrichments in LILE and LREE

without concomitant enrichment in HFSE, but are in both cases sulphide-poor and show limited HSE fractionation [$(Pd/Ir)_N < 1·6$]. Furthermore, whole-rock $^{187}Os/^{188}Os$ remains below or near the PUM value (Reisberg & Lorand, 1995; Lorand *et al.*, 2003*b*; Ionov *et al.*, 2006*b*), suggesting a completely different source of fluid than at Montferrier.

A key parameter to constrain the origin of the metasomatic agent is its highly radiogenic $^{187}Os/^{188}Os$ composition. Although such highly radiogenic compositions (not supported by high Re/Os) are not unknown especially in sulphides (e.g. Aulbach *et al.*, 2009), as discussed by Chesley *et al.* (2004) they are extremely unusual in 'primary' melts. For instance, OIB display initial $^{187}Os/^{188}Os$ mostly between 0·13 and 0·15 (e.g. Shirey & Walker, 1998), with a peak value at ≈0·135 and ≈0·145 for HIMU lavas (e.g. Brauns *et al.*, 2000). Thus, the highly radiogenic composition of the inferred metasomatic fluid argues against derivation from an OIB-type melt. We note that the metasomatized Tok and Sidamo xenolith suites do not show $^{187}Os/^{188}Os$ higher than estimated for the PUM; this is consistent with a metasomatic melt or fluid derived from an OIB-type melt.

One obvious candidate is melt or fluid derived from subducted material. According to Faccenna *et al.* (2003) and references therein, the SW Mediterranean subduction zone was initiated in early Paleocene–late Cretaceous times, and extended from Gibraltar to the Ligurides, deepening to the NW. Around 30 Myr ago, the southward retreat of the subduction front triggered the opening of the Gulf of Lyon and the formation of the Oligocene graben in which the Montferrier volcano erupted (Séranne, 1999). Therefore, at the time of the Montferrier eruptions (≈25 Ma) the subduction trench was ~400 km to the south. Although very unlikely, it is possible that a subducted slab could have been present ~200 km beneath the Gulf of Lyon. However, there is no evidence of the chemical imprint of subducted materials on the lavas and xenoliths of the Languedoc area, including Montferrier (Dautria *et al.*, 2010). The Nd–Sr–Pb isotopic compositions of the 'depleted' and 'enriched' Montferrier xenoliths ($0·70297 \leq {}^{87}Sr/^{86}Sr \leq 0·70319$; $0·513106 \leq {}^{143}Nd/^{144}Nd \leq 0·513336$; $18·134 \leq {}^{206}Pb/^{204}Pb \leq 18·487$; $15·598 \leq {}^{207}Pb/^{204}Pb \leq 15·620$; $37·963 \leq {}^{208}Pb/^{204}Pb \leq 38·374$; Dautria *et al.*, 2010) do not suggest the involvement of an enriched reservoir (i.e. EM or HIMU) but rather a DMM-like composition. This suggests that the LREE enrichment and LILE fractionation documented in the Montferrier xenoliths are recent. Similarly, a detailed Sr isotopic study of mineral separates (cpx, amphibole) and an acid-leaching study carried out by Cabanes & Briqueu (1986) did not reveal ($^{87}Sr/^{86}Sr \leq 0·7035$) any evidence for a radiogenic Sr component that would be expected if subduction-related fluids were involved.

There are only few Re–Os data in the literature that allow us to assess the Os-isotope composition of carbonatites or related melts. Pearson *et al.* (1995) reported $^{187}Re/^{188}Os = 6130$ and $^{187}Os/^{188}Os = 9·31 \pm 0·21$ for a Quaternary carbonatite from Uganda (Fort Portal). Two carbonatites from Cape Verde have $^{187}Re/^{188}Os$ and initial $^{187}Os/^{188}Os$ ranging between 184 and 387 and *c.* 0·17, respectively (Escrig *et al.*, 2005). Blusztajn & Hegner (2002) reported $^{187}Re/^{188}Os$ and initial $^{187}Os/^{188}Os$ for 14 melilitites from SW Germany, in the range of 6–231 and 0·119–0·225, respectively. Carbonatites may have also extremely fractionated PGE patterns, with $(Pd/Ir)_N$ as high as 1000 (Xu *et al.*, 2008). Thus the highly radiogenic compositions of carbonatites and related melts are consistent with the inferred minimum $^{187}Os/^{188}Os$ ratio of the metasomatic fluids. However, the development of such radiogenic signatures requires the storage of a high Re/Os component for at least few million years depending on the Re/Os of the stored material.

Several workers have proposed that carbonatites are the products of partial melting of metasomatized segments of the lithospheric mantle (e.g. Bell *et al.*, 1999; Blusztajn & Hegner, 2002). The presence of carbonated and/or volatile-rich mantle beneath the Languedoc area is attested by the occurrence of leucite (Lc)- and nepheline (Ne)-bearing lavas, with normative abundance of [Lc + Ne] in excess of 22% (Liotard *et al.*, 1999). Furthermore, sulphide–carbonate occurrences have been reported in the Languedoc area (Jakni *et al.*, 1996; Dautria *et al.*, 2006). These were found first in the Lodevois xenoliths, equilibrated at $T_{BK90} \approx 1000 \pm 50^{\circ}C$, which contain abundant pockets formed of carbonate, secondary cpx, phlogopite and sulphide ± oxides (Jakni *et al.*, 1996; J.-M. Dautria & O. Alard, unpublished data). Samples equilibrated at lower temperatures (i.e. $T_{BK90} \approx 920 \pm 40^{\circ}C$) do not show such extensive mineralogical reaction and secondary cpx is lacking (Dautria *et al.*, 2006); however, metasomatic sulphides still occur. Thus, considering the gradation with temperature and depth of the metasomatic products, Dautria *et al.* (2006, 2010) proposed that a 'carbonatitic' component was stored within the SCLM beneath Languedoc. Through adiabatic decompression or heating (e.g. thinning of the Gulf of Lyon lithosphere), decarbonation of this enriched level occurred, leading to the release of a volatile-rich, CO_2-bearing melt (Falloon & Green, 1990; Canil, 1995). This fluid then percolated through the upper levels of the SCLM, as shown by the Languedoc xenoliths at equilibrium temperatures of ≈900°C. Within this framework, the Montferrier xenoliths, which are devoid of secondary Cpx and carbonate and were equilibrated at $T_{BK90} = 860 \pm 21^{\circ}C$, would represent the uppermost mantle level affected by such a fluid, after it had undergone further differentiation during its ascent through the mantle column. The oxygen fugacity constraints

derived from the enclosed sulphides ($fO_2 \approx FMQ+2$, Eggler & Lorand, 1993) are consistent with oxidizing conditions generated by CO_2-bearing fluids and with experimental work on siderophile and chalcophile element mobility discussed above (Wood, 1987). In this scenario, the highly radiogenic Os isotope composition could have been inherited directly from the carbonatite component or developed during the storage of a high-Re/Os carbonatite-like compound in the deeper levels of the mantle lithosphere.

Our data emphasize once again the strong relationships between C-bearing fluids and S. This association is also reminiscent of the overabundance of sulphide inclusions in diamond (e.g. Deines & Harris, 1995), which also indicates a relationship between these two phases. However, the exact nature of this relationship remains unclear. Are they both major components of the same mantle fluid, or does sulphide play only a catalytic role in diamond formation, notably through a reduction effect on CO_2 (e.g. Palyanov *et al.*, 2007)? Our study as well as the numerous occurrences of S- and C-bearing metasomatic assemblages and fluid inclusions reported in the literature testify that S and C are significant components of mantle fluids (Andersen *et al.*, 1987; Kovalenko *et al.*, 1987; O'Reilly & Griffin, 1988; Dautria *et al.*, 1992, 2006; Ionov *et al.*, 1993; Kogarko *et al.*, 1995; Jakni *et al.*, 1996; Alard *et al.*, 2000; Lorand & Alard, 2001; Frezzotti *et al.*, 2002; Lorand *et al.*, 2004; Frezzotti & Peccerillo, 2007; Powell & O'Reilly, 2007; Montanini *et al.*, 2011). Several researchers have suggested that CO_2 is the prevailing deep fluid component and exerts a strong control on mantle melting (e.g. Presnall & Gudfinnsson, 2005; Dasgupta & Hirschmann, 2006). We also suggest that S-compounds (H_2S, SO_2, S_2, etc.) could also be significant components of such fluids and may modify the systematics of chalcophile and siderophile elements in the Earth's mantle.

CONCLUDING REMARKS

The Montferrier xenoliths demonstrate that the sulphur content and sulphide abundance and composition, as well as the HSE systematics and Os isotopic composition of the upper mantle, can be significantly modified through metasomatism, even with small melt volumes and/or volatile-rich fluids and without obvious mineralogical reactions in the percolated rock (i.e. cryptic metasomatism from the silicate point of view).

The exact nature and origin of the percolating melt or fluid responsible for the so-called 'carbonatite' trace element signature is debatable. For instance, recently Ionov *et al.* (2006*a*,*b*) argued that the presence of apatite or the replacement of opx by cpx (i.e. 'wehrlitization') and 'carbonatite' trace element signatures are not unambiguous indices of carbonatite metasomatism, but instead are more likely to be produced by reaction with evolved SiO_2-undersaturated alkali silicate melts. Our results, combined with literature data, suggest that a distinction between the different types of metasomatic agent could be possible using sulphide and HSE characteristics. Percolation–reaction of carbonatite melt or derived fluids in the lithospheric mantle leads to significant enrichment in sulphide, pronounced fractionation of the HSE, and Os-isotope compositions more radiogenic than the PUM and most OIB lavas (i.e. $\geq 0{\cdot}14$). In contrast, interactions with OIB-type SiO_2-undersaturated alkali silicate melts do not lead to massive sulphide crystallization, large fractionations of the HSE, or significantly radiogenic Os-isotope signatures ($^{187}Os/^{188}Os \leq 0{\cdot}14$).

The abundances of chalcophile and siderophile elements and the Re–Os isotopic composition of the Montferrier sulphides clearly have been extensively modified by volatile-rich metasomatism. The exact modality and effects of this metasomatic alteration remain complex and partly elusive. The data presented here suggest that the observed PGE–Os fractionation probably occurred through two non-exclusive processes: sulphide addition and sulphide re-equilibration. However, the peculiar sulphide mineralogy and the specific fractionations observed in chemical proxies such as S/Se, Os/Ir and Pd/Pt suggest that these enrichments in the Montferrier xenoliths probably did not occur via a sulphide melt. Rather, these geochemical features suggest that S and other chalcophile and siderophile elements were present as dissolved species in an oxidizing ($\geq FMQ+1$), volatile-rich fluid.

ACKNOWLEDGEMENTS

Trace element data were obtained using the AETE platform facilities, Montpellier (France). This work greatly benefited from the help of Christophe Nevado and Dorianne Delmas for thin sections; Claude Merlet for electron probe analyses and imaging; Michel Gros for S and PGE analyses; and Liliane Savoyant, Simone Pourtales and Olivier Bruguier for ICP-MS. We also thank Norman J. Pearson for assistance with MC-ICP-MS at the GEMOC Analytical Unit (Macquarie University); Catherine Zimmermann and Anne-Catherine Pierson-Wickmann for technical assistance during Re–Os chemistry and analyses at the CRPG (Nancy); Ian Parkinson and Bruce Schaefer for assistance with N-TIMS at the Open University; and C. Ryan (CSIRO) for PMP imaging. This paper has greatly benefited from constructive and insightful reviews by Sonja Aulbach, Dmitri Ionov and an anonymous reviewer. Dominique Weis is acknowledged for her helpful editorial comments. Comments by W. L. Griffin were greatly appreciated. This is Contribution 677 from the ARC National Key Centre for Geochemical Evolution and Metallogeny of Continents.

FUNDING

In situ Re–Os data were obtained using instrumentation funded by ARC LIEF, and DEST Systemic Infrastructure Grants and Macquarie University. Financial support was obtained partly through a SEDIT grant from the Institut National des Sciences de l'Univers (France).

REFERENCES

Alard, O., Dautria, J.-M. & Bodinier, J.-L. (1996). Nature and metasomatic processes of the lithospheric mantle on either part of Sillon Houiller (French Massif Central). *Comptes Rendus de l'Academie des Sciences, Série IIa* **323**, 763–770.

Alard, O., Bodinier, J.-L., Lenoir, X. & Dautria, J.-M. (1999). Uranium enrichment in the lithospheric mantle: evidence from French Massif Central. *Ofioliti* **24**, 49–50.

Alard, O., Griffin, W. L., Lorand, J.-P., Jackson, S. E. & O'Reilly, S. Y. (2000). Non-chondritic distribution of the highly siderophile elements in mantle sulphides. *Nature* **407**, 891–894.

Alard, O., Griffin, W. L., Pearson, N. J., Lorand, J.-P. & O'Reilly, S. Y. (2002). New insights into the Re–Os systematics of sub-continental lithospheric mantle from *in situ* analysis of sulphides. *Earth and Planetary Science Letters* **203**, 651–663.

Andersen, T., O'Reilly, S. Y. & Griffin, W. L. (1987). Primary sulphide melt inclusions in mantle-derived megacrysts and pyroxenites. *Lithos* **20**, 279–294.

Aulbach, S., Stachel, T., Creaser, R. A., Heaman, L. M., Shirey, S. B., Muehlenbachs, K., Eichenberg, D. & Harris, J. W. (2009). Sulfide survival and diamond formation during formation and evolution of Archaean subcontinental lithosphere: A comparison between the Slave and Kaapvaal Cratons. *Lithos* **112**, 747–757.

Ballhaus, C. & Stumpfl, E. F. (1986). Sulfides and platinum mineralization in the Merensky Reef: evidence from hydrous silicates and fluids inclusions. *Contributions to Mineralogy and Petrology* **94**, 193–204.

Ballhaus, C. B., Berry, R. F. & Green, D. H. (1991). High pressure experimental calibration of the olivine–orthopyroxene–spinel oxygen barometer—implications for redox conditions in the upper mantle. *Contributions to Mineralogy and Petrology* **107**, 27–40.

Ballhaus, C., Tredoux, M. & Spaeth, A. (2001). Phase relation in the Fe–Ni–Cu–PGE–S system at magmatic temperature and application to massive sulfide ores of Sudbury Igneous Complex. *Journal of Petrology, Special Lherzolites Issue* 1991–2026.

Ballhaus, C., Bockrath, C., Wohlgemuth-Ueberwasser, C., Laurenz, V. & Berndt, J. (2006). Fractionation of the noble metals by physical processes. *Contributions to Mineralogy and Petrology* **152**, 667–684.

Becker, H., Horan, M. F., Walker, R. J., Gao, S., Lorand, J.-P. & Rudnick, R. L. (2006). Highly siderophile element composition of the Earth's primitive upper mantle; constraints from new data on peridotite massifs and xenoliths. *Geochimica et Cosmochimica Acta* **70**, 4528–4550.

Bedini, R. M., Bodinier, J.-L., Dautria, J.-M. & Morten, L. (1997). Evolution of LILE-enriched small melt fractions in the lithospheric mantle: a case study from the East African Rift. *Earth and Planetary Science Letters* **153**, 67–83.

Bell, K., Kjarsgaard, B. A. & Simonetti, A. (1999). Carbonatites—into the twenty-first century. *Journal of Petrology* **39**, 1839–1845.

Bellon, H. (1976). *Séries magmatiques Néogènes et Quaternaires du pourtour de la Méditerranée occidentale comparées dans leur cadre géologique: Implications géodynamiques*. Ph.D. thesis, Orsay: Université Paris-Sud, 367 p.

Bézos, A., Lorand, J. P., Humler, E. & Gros, M. (2005). Platinum-group element systematics in mid-oceanic ridge basaltic glasses from the Pacific, Atlantic, and Indian Oceans. *Geochimica et Cosmochimica Acta* **69**, 2613–2627.

Birck, J. L., Roy Barman, M. & Capmas, F. (1997). Re–Os isotopic measurements at the femtomole level in natural samples. *Geostandards Newsletter* **20**, 19–27.

Blusztajn, J. & Hegner, E. (2002). Osmium isotopic systematics of melilitites from the Tertiary Central European Volcanic Province in SW Germany. *Chemical Geology* **189**, 91–103.

Bodinier, J. L., Vasseur, G., Vernieres, J., Dupuy, C. & Fabries, J. (1990). Mechanisms of mantle metasomatism—geochemical evidence from the Lherz orogenic peridotite. *Journal of Petrology* **31**, 597–628.

Boudreau, A. E. (1999). Chromatographic separation of the platinum-group elements, gold, base metals and sulfur during degassing of a compacting and solidifying igneous crystal pile. *Contributions to Mineralogy and Petrology* **134**, 174–185.

Brandon, A. D., Creaser, R. A., Shirey, S. B. & Carlson, R. W. (1996). Osmium recycling in subduction zones. *Science* **272**, 861–864.

Brauns, C. M., Hergt, J. M., Woodhead, J. D. & Maas, R. (2000). Os isotopes and the origin of the Tasmanian dolerites. *Journal of Petrology* **41**, 905–918.

Brenan, J. M. (2008). Re–Os fractionation by sulfide melt–silicate melt partitioning: A new spin. *Chemical Geology* **248**, 140–165.

Brenan, J. M., Shaw, H. F., Ryerson, F. J. & Phinney, D. L. (1995). Mineral–aqueous fluid partitioning of trace elements at 900°C and 2·0 GPa: Constraints on the trace element chemistry of mantle and deep crustal fluids. *Geochimica et Cosmochimica Acta* **59**, 3331–3350.

Brenan, J. M., Cherniak, D. J. & Rose, L. A. (2000). Diffusion of osmium in pyrrhotite and pyrite: implications for closure of the Re–Os isotopic system. *Earth and Planetary Science Letters* **180**, 399–413.

Brey, G. P. & Köhler, T. (1990). Geothermobarometry in four-phase lherzolites II: New thermobarometers and practical assessment of existing thermobarometers. *Journal of Petrology* **31**, 1353–1378.

Burton, K. W., Gannoun, A., Birck, J.-L., Allègre, C. J., Schiano, P., Clocchiatti, R. & Alard, O. (2002). The compatibility of rhenium and osmium in natural olivine and their behaviour during mantle melting and basalt genesis. *Earth and Planetary Science Letters* **198**, 63–76.

Cabanes, N. & Briqueu, L. (1986). Hydration of an active shear zone: interactions between deformation, metasomatism and magmatism—the spinel-lherzolites from the Montferrier (southern France) Oligocene basalts. *Earth and Planetary Science Letters* **81**, 233–244.

Cabanes, N. & Mercier, J.-C. (1988). Chimie des phases minérales et conditions d'équilibre des enclaves de lherzolite à spinelle de Montferrier (Herault, France). *Bulletin de Minéralogie* **111**, 65–77.

Canil, D. (1995). Experimental study bearing on the absence of carbonate in mantle derived xenoliths. *Geology* **8**, 1011–1013.

Carigan, J., Ludden, J. & Francis, D. (1996). On the recent enrichment of subcontinental lithosphere: A detailed U–Pb study of spinel lherzolite xenoliths, Yukon, Canada. *Geochimica et Cosmochimica Acta* **60**, 4241–4252.

Chesley, J., Righter, K. & Ruiz, J. (2004). Large-scale mantle metasomatism: a Re–Os perspective. *Earth and Planetary Science Letters* **219**, 49–60.

Clark, A. H. & Naldrett, A. J. (1972). The distribution of Ni and Fe between synthetic olivine and sulfide at 900°C. *Economic Geology* **67**, 932–952.

Cohen, A. S. & Waters, F. G. (1996). Separation of osmium from geological materials by solvent extraction for analysis by thermal ionisation mass spectrometry. *Analytica Chimica Acta* **332**, 269–275.

Creaser, R. A., Papanastassiou, D. A. & Wasserburg, G. J. (1991). Negative thermal ion mass spectrometry of osmium, rhenium and iridium. *Geochimica et Cosmochimica Acta* **55**, 397–401.

Dasgupta, R. & Hirschmann, M. M. (2006). Melting in the Earth's deep upper mantle caused by carbon dioxide. *Nature* **440**, 659–662.

Dautria, J. M., Dupuy, C., Takherist, D. & Dostal, J. (1992). Carbonate metasomatism in the lithospheric mantle: peridotitic xenoliths from a melilitic district of the Sahara Basin. *Contributions to Mineralogy and Petrology* **111**, 37–52.

Dautria, J.-M., Bosch, D. & Liotard, J. M. (2006). Role of secondary carbonation mechanism in the upper mantle of Languedoc (south France). *Comptes Rendus Géoscience* **338**, 527–536.

Dautria, J.-M., Liotard, J.-M., Bosch, D. & Alard, O. (2010). The Languedoc volcanic line (South of France): A unique 160 My-long episodic magmatic activity recording the advent of the Central Atlantic Plume Head beneath Western Europe. *Lithos* , doi:10.1016/j.lithos.2010.04.009.

Deines, P. & Harris, J. W. (1995). Sulfide inclusion chemistry and carbon isotopes of African diamonds. *Geochimica et Cosmochimica Acta* **59**, 3173–3188.

Dreibus, G., Palme, H., Spettel, B., Zipfel, J. & Wanke, H. (1995). Sulfur and selenium in chondritic meteorites. *Meteoritics* **30**, 439–445.

Eggler, D. H. & Lorand, J. P. (1993). Mantle sulfide geobarometry. *Geochimica et Cosmochimica Acta* **57**, 2213–2222.

Escrig, S., Doucelance, R., Manuel, M. & Allègre, C. J. (2005). Os isotope systematics in Fogo Island: Evidence for lower continental crust fragments under the Cape Verde Southern Islands. *Chemical Geology* **219**, 93–113.

Esser, B. K. & Turekian, K. K. (1993). The osmium isotopic composition of the continental crust. *Geochimica et Cosmochimica Acta* **57**, 3093–3104.

Fabries, J., Figueroa, O. & Lorand, J. P. (1987). Petrology and thermal history of highly deformed mantle xenoliths from the Montferrier basanites, Languedoc, Southern France: a comparison with ultramafic complexes from the North Pyrenean Zone. *Journal of Petrology* **28**, 887–919.

Faccenna, C., Jolivet, L., Piromallo, C. & Morelli, A. (2003). Subduction and the depth of convection in the Mediterranean mantle. *Journal of Geophysical Research* **108**, doi:10.1029/2001JB001690.

Falloon, T. J. & Green, D. H. (1990). Solidus of carbonated fertile peridotite under fluid-saturated conditions. *Geology* **18**, 195–199.

Fleet, M. E. & Wu, T.-W. (1995). Volatile transport of precious metals at 1000°C: Speciation, fractionation, and effect of base-metal sulfide. *Geochimica et Cosmochimica Acta* **59**, 487–495.

Fleet, M. E., Crocket, J. H., Liu, M. & Stone, W. E. (1999). Laboratory partitioning of platinum-group elements (PGE) and gold with application to magmatic sulfide–PGE deposits. *Lithos* **47**, 127–142.

Frey, F. A. & Green, D. H. (1974). The mineralogy, geochemistry and origin of lherzolite inclusions in Victorian basanites. *Geochimica et Cosmochimica Acta* **38**, 1023–1059.

Frezzotti, M. L. & Peccerillo, A. (2007). Diamond-bearing COHS fluids in the mantle beneath Hawaii. *Earth and Planetary Science Letters* **262**, 273–283.

Frezzotti, M. L., Andersen, T., Neumann, E.-R. & Simonsen, S. L. (2002). Carbonatite melt–CO_2 fluid inclusions in mantle xenoliths from Tenerife, Canary Islands: a story of trapping, immiscibility and fluid–rock interaction in the upper mantle. *Lithos* **64**, 77–96.

Gastaud, J. (1981). Le volcanisme des Causses et du Bas-Languedoc, géochronologie et relations avec les paléocontraintes. Ph.D. Thesis, Université de Nice, 152 p.

Godard, M., Jousselin, D. & Bodinier, J.-L. (2000). Relationships between geochemistry and structure beneath a palaeo-spreading centre: a study of the mantle section in the Oman ophiolite. *Earth and Planetary Science Letters* **180**, 133–148.

Griffin, W.L., Powell, W. J., Pearson, N. J. & O'Reilly, S. Y. (2008). GLITTER: data reduction software for laser ablation ICP-MS. In: Sylvester, P. (ed.) *Laser Ablation–ICP–MS in the Earth Sciences. Mineralogical Association of Canada, Short Course Series* **40**, Appendix 2, 204–207.

Gros, M., Lorand, J. P. & Luguet, A. (2002). Analysis of platinum group elements and gold in geological materials using NiS fire assay and Te coprecipitation; the NiS dissolution step revisited. *Chemical Geology* **185**, 179–190.

Gros, M., Lorand, J.-P. & Bezos, A. (2005). Determination of the total sulfur contents in the international rock reference material SY-2 and other mafic and ultramafic rocks using an improved scheme of combustion/iodometric titration. *Geostandards and Geoanalytical Research* **29**, 123–130.

Handler, M. R., Bennett, V. C. & Dreibus, G. (1999). Evidence from correlated Ir/Os and Cu/S for late-stage Os mobility in peridotite xenoliths: Implications for Re–Os systematics. *Geology* **27**, 75–78.

Hattori, K. M., Arai, S. & Clarke, D. B. (2002). Selenium, tellurium, arsenic and antimony contents of primary mantle sulfides. *Canadian Mineralogist* **40**, 637–650.

Ionov, D. A., Hoefs, J., Wedepohl, K. H. & Wiechert, U. (1992). Content and isotopic composition of sulphur in ultramafic xenoliths from central Asia. *Earth and Planetary Science Letters* **111**, 269–286.

Ionov, D. A., Dupuy, C., O'Reilly, S. Y., Kopylova, M. G. & Genschaft, Y. S. (1993). Carbonated peridotite xenoliths from Spitsbergen: implications for trace element signature of mantle carbonate metaspmatism. *Earth and Planetary Science Letters* **119**, 283–297.

Ionov, D. A., O'Reilly, S. Y. & Ashchepkov, I. V. (1995). Feldspar-bearing lherzolite xenoliths in alkali basalts from Hamar-Daban, southern Baikal region, Russia. *Contributions to Mineralogy and Petrology* **122**, 174–190.

Ionov, D. A., Chanefo, I. & Bodinier, J. L. (2005). Origin of Fe-rich lherzolites and wehrlites from Tok, SE Siberia by reactive melt percolation in refractory mantle peridotites. *Contributions to Mineralogy and Petrology* **150**, 335–353.

Ionov, D. A., Chazot, G., Chauvel, C., Merlet, C. & Bodinier, J.-L. (2006*a*). Trace element distribution in peridotite xenoliths from Tok, SE Siberian craton: a record of pervasive, multi-stage metasomatism in shallow refractory mantle. *Geochimica et Cosmochimica Acta* **70**, 1231–1260.

Ionov, D. A., Shirey, S. B., Weiss, D. & Brugmann, G. (2006*b*). Os–Hf–Nd isotope and PGE systematics of spinel peridotite xenoliths from Tok, SE Siberian craton: effects of pervasive metasomatism in shallow refractory mantle. *Earth and Planetary Science Letters* **241**, 47–64.

Jakni, B., Dautria, J.-M., Liotard, J.-M. & Briqueu, L. (1996). Metasomatose carbonatée sous la lithosphère du Languedoc (France). *Comptes Rendus de l'Academie des Sciences, Série IIa* **323**, 33–40.

Kogarko, L. N., Henderson, C. M. B. & Pacheco, H. (1995). Primary Ca-rich carbonatite magma and carbonate–silicate–sulphide liquid immiscibility in the upper mantle. *Contributions to Mineralogy and Petrology* **121**, 267–274.

Kovalenko, V. I., Solovova, I. P., Ryabchikov, I. D., Ionov, D., Bogatikov, O. A. & Naumov, V. B. (1987). Fluidized CO_2–sulphide–silicate media as agents of mantle metasomatism and megacrysts formation: evidence from a large druse in a spinel-lherzolite xenolith. *Physics of the Earth and Planetary Interiors* **45**, 280–293.

Lassiter, J. C. (2003). Rhenium volatility in subaerial lavas: constraints from subaerial and submarine portions of the HSDP-2 Mauna Kea drillcore. *Earth and Planetary Science Letters* **214**, 311–325.

Lee, C.-T. Y. A. (2002). Platinum-group element geochemistry of peridotite xenoliths from the Sierra Nevada and the Basin and Range, California. *Geochimica et Cosmochimica Acta* **66**, 3987–4005.

Lenoir, X., Garrido, C. J., Bodinier, J.-L. & Dautria, J.-M. (2000). Contrasting lithospheric mantle domains beneath the Massif Central (France) revealed by geochemistry of peridotite xenoliths. *Earth and Planetary Science Letters* **181**, 359–375.

Le Roux, V., Bodinier, J.L. & Alard, O. (2009). Isotopic decoupling during porous melt flow: a case study in the Lherz peridotite. *Earth and Planetary Science Letters* **279**, 79–85.

Le Roux, V., Bodinier, J. L., Tommasi, A., Alard, O., Dautria, J.-M., Vauchez, A. & Riches, A. J. V. (2007). The Lherz spinel lherzolites: refertilised rather than pristine mantle. *Earth and Planetary Science Letters*, doi:10.1016/j.epsl.2007.05.026.

Libaudé, J. & Sabatier, G. (1980). Contribution à l'étude de la sulfuration des olivines nickelifères en phase vapeur. *Mémoire du Bureau des Recherches Géologiques et Minières* **97**, 252–253.

Liotard, J. M., Briqueu, L., Dautria, J. M. & Jakni, B. (1999). Basanites et néphélinite du Bas-Languedoc (France): contamination crustale et hétérogénéite de la source mantellique. *Bulletin de la Société Géologique de France* **170**, 423–433.

Lorand, J. P. (1989). Abundance and distribution of Cu–Fe–Ni sulfides, sulfur, copper and platinum-group elements in orogenic-type spinel lherzolite massifs of Ariege (northeastern Pyrenees, France). *Earth and Planetary Science Letters* **93**, 50–64.

Lorand, J. P. (1990). Are spinel lherzolite xenoliths representative of the abundance of sulfur in the upper mantle? *Geochimica et Cosmochimica Acta* **54**, 1487–1492.

Lorand, J.-P. & Alard, O. (2001). Platinum-group element abundances in the upper mantle: new constraints from *in situ* and whole-rock analyses of Massif Central xenoliths (France). *Geochimica et Cosmochimica Acta* **65**, 2789–2806.

Lorand, J. P. & Conquéré, F. (1983). Contribution à l'étude des sulfures dans les enclaves de lherzolite à spinelle des basaltes alcalins (Massif Central et Languedoc, France). *Bulletin de Minéralogie* **106**, 585–606.

Lorand, J.-P., Pattou, L. & Gros, M. (1999). Fractionation of platinum-group elements and gold in the upper mantle: a detailed study in Pyrenean orogenic lherzolites. *Journal of Petrology* **40**, 957–981.

Lorand, J.-P., Alard, O., Luguet, A. & Keays, R. R. (2003*a*). Sulfur and selenium systematics of the subcontinental lithospheric mantle: Inferences from the Massif Central xenolith suite (France). *Geochimica et Cosmochimica Acta* **67**, 4137–4151.

Lorand, J. P., Reisberg, L. & Bedini, R. M. (2003*b*). Platinum-group elements and melt percolation processes in Sidamo spinel peridotite xenoliths, Ethiopia, East African Rift. *Chemical Geology* **196**, 57–75.

Lorand, J. P., Delpech, G., Gregoire, M., Moine, B., O'Reilly, S. Y. & Cottin, J. Y. (2004). Platinum-group elements and the multistage metasomatic history of Kerguelen lithospheric mantle (South Indian Ocean). *Chemical Geology* **208**, 195–215.

Lorand, J.-P., Luguet, A. & Alard, O. (2008*a*). Platinum-Group Elements: A new set of key tracers for the Earth's interior. *Elements* **4**, 247–252.

Lorand, J.-P., Luguet, A., Alard, O., Bézos, A. & Meisel, T. (2008*b*). Abundance and distribution of platinum-group elements in FON-B 93, a matrix-matched orogenic lherzolite (Ariège, French Pyrénées). *Chemical Geology* **248**, 174–194.

Lorand, J.-P., Alard, O. & Godard, M. (2009). Platinum-group element signature of the primitive mantle rejuvenated by melt–rock reactions: evidence from Sumail peridotites (Oman Ophiolite). *Terra Nova* **21**, 35–40.

Luguet, A. & Lorand, J.-P. (1998). Supergene weathering and sulphur contents of basalt-hosted mantle xenoliths: an appraisal from Montferrier lherzolites (Languedoc, France). *Comptes Rendus de l'Academie des Sciences, Série IIa* **327**, 519–525.

Luguet, A., Lorand, J.-P., Alard, O. & Cottin, J.-Y. (2004). A multi-technique study of platinum-group elements systematic in some Ligurian ophiolitic peridotites, Italy. *Chemical Geology* **208**, 175–194.

McDonough, W. F. & Sun, S.-S. (1995). The composition of the Earth. *Chemical Geology* **120**, 223–253.

McInnes, B. I. A., McBride, J. S., Evans, N. J., Lambert, D. D. & Andrew, A. S. (1999). Osmium isotope constraints on ore metal recycling in subduction zones. *Science* **286**, 512–516.

Meisel, T. & Moser, J. (2004). Reference materials for geochemical PGE analysis: new analytical data for Ru, Rh, Pd, Os, Ir, Pt and Re by isotope dilution ICP-MS in 11 geological reference materials. *Chemical Geology* **208**, 319–338.

Meisel, T., Walker, R. J., Irving, A. J. & Lorand, J.-P. (2001). Osmium isotopic compositions of mantle xenoliths: a global perspective. *Geochimica et Cosmochimica Acta* **65**, 1311–1323.

Meisel, T., Reisberg, L., Moser, J., Carignan, J., Melcher, F. & Brugmann, G. (2003). Re–Os systematics of UB-N, a serpentinized peridotite reference material. *Chemical Geology* **201**, 161–179.

Minarik, W. G. & Watson, E. B. (1995). Interconnectivity of carbonate melt at low melt fraction. *Earth and Planetary Science Letters* **133**, 423–437.

Montanini, A., Tribuzio, R. & Bersani, D. (2011). Insights into the origin of mantle graphite and sulfides in garnet pyroxenites from the external ligurides peridotites (Northern Apenine, Italy). In: Coltorti, M., Downes, H., Gregoire, M. & O'Reilly, S.Y. (eds) *Petrological evolution of the European Lithospheric Mantle. Geological Society of London, Special publication, London*, 87–105.

Morgan, J. W. (1986). Ultramafic xenoliths: clues to Earth's late accretionary history. *Journal of Geophysical Research* **91**, 12375–12387.

Naldrett, A. J. & Gasparini, E. L. (1971). Archean nickel sulfide deposits in Canada: their classification, geological setting and genesis; with some suggestion as to exploration. In: Glover, J.E. (ed.) *Geological Society of Australia, Special Publications: Proceeding of the 1st Symposium on Archean Rocks, Adelaide*, 423–424.

Narbonna-Guttierez, R., Lorand, J.-P., Gervilla, F. & Gros, M. (2003). New data on base metal minerals and platinum-group elements in the Ojen chromitites (Southern Spain). *Neues Jahrbuch für Mineralogie, Abhandlungen* **179**, 143–173.

Navon, O. & Stolper, E. (1987). Geochemical consequences of melt percolation: the upper mantle as a chromatographic column. *Journal of Geology* **95**, 285–307.

Nickel, K. G. & Green, D. H. (1985). Empirical geothermobarometry for garnet peridotites and implications for the nature of the lithosphere, kimberlites and diamonds. *Earth and Planetary Science Letters* **73**, 158–170.

Norman, M. D., Pearson, N. J., Sharma, A. & Griffin, W. L. (1996). Quantitative analysis of trace elements in geological materials by laser ablation ICPMS: Instrumental operating conditions and calibration values of NIST glasses. *Geostandards Newsletter* **20**, 247–261.

O'Reilly, S. Y. & Griffin, W. L. (1988). Mantle metasomatism beneath western Victoria, Australia, I: Metasomatic processes in Cr-diopside lherzolites. *Geochimica et Cosmochimica Acta* **52**, 433–447.

Palyanov, Y. N., Borzdov, Y. M., Bataleva, Y. V., Sokol, A. G., Palyanova, G. A. & Kupriyanov, I. N. (2007). Reducing role of sulfides and diamond formation in the Earth's mantle. *Earth and Planetary Science Letters* **260**, 242–256.

Parkinson, I. J., Hawkesworth, C. J. & Cohen, A. S. (1998). Ancient mantle in a modern arc: osmium isotopes in Izu–Bonin–Mariana forearc peridotites. *Science* **281**, 2011–2013.

Peach, C. L., Mathez, E. A. & Keays, R. R. (1990). Sulphide melt–silicate melt distribution coefficients for the noble metals and other chalcophile metals as deduced from MORB: Implications for partial melting. *Geochimica et Cosmochimica Acta* **54**, 3379–3389.

Pearson, D. G., Shirly, S. B., Carlson, R. W., Boyd, F. R., Pokhilenko, N. P. & Shimizu, N. (1995). Re–Os, Sm–Nd, and Rb–Sr isotope evidence for the thick Archaean lithospheric mantle beneath the Siberian craton modified by multistage metasomatism. *Geochimica et Cosmochimica Acta* **59**, 959–977.

Pearson, N. J., Alard, O., Griffin, W. L., Jackson, S. E. & O'Reilly, S. Y. (2002). *In situ* measurement of Re–Os isotopes in mantle sulfides by laser ablation multicollector-inductively coupled plasma mass spectrometry: Analytical methods and preliminary results. *Geochimica et Cosmochimica Acta* **66**, 1037–1050.

Pearson, D. G., Irvine, G. J., Ionov, D. A., Boyd, F. R. & Dreibus, G. E. (2004). Re–Os isotope systematics and platinum group element fractionation during mantle melt extraction: a study of massif and xenolith peridotite suites. *Chemical Geology* **208**, 29–59.

Pearson, N. J., Griffin, W. L., Alard, O., O'Reilly, S. Y., Schaefer, B. F. & Payne, J. L. (2009). The accuracy and precision of *in situ* Re–Os isotopic measurements by laser ablation MC-ICPMS19th Annual V. M. Goldschmidt Conference, *Davos. Switzerland. Geochimica et Cosmochimica Acta A1005.*

Peregoedova, A., Barnes, S. J. & Baker, D. R. (2006). An experimental study of mass transfer of platinum-group elements, gold, nickel and copper in sulfur-dominated vapor at magmatic temperatures. *Chemical Geology* **235**, 59–75.

Peslier, A., Reisberg, L., Ludden, J. & Francis, D. (2000). Os isotopic systematics in mantle xenoliths; age constraints on the Canadian Cordillera lithosphere. *Chemical Geology* **168**, 85–101.

Powell, W. & O'Reilly, S. Y. (2007). Metasomatism and sulfide mobility in lithospheric mantle beneath eastern Australia: Implications for mantle Re–Os chronology. *Lithos* **94**, 132–147.

Presnall, D. C. & Gudfinnsson, G. H. (2005). Carbonate-rich melts in the seismic low vicosity zone and deep mantle. In: Foulger, G. R., Natland, J. H., Presnall, D. C. & Anderson, D. L. (eds) *Plates, Plumes, and Paradigms. Geological Society of America, Special Papers* **388**, 207–216.

Rehkämper, M., Halliday, A. N., Fitton, J. G., Lee, D.-C., Wieneke, M. & Arndt, N. T. (1999). Ir, Ru, Pt and Pd in basalts and komatiites: new constraints from the geochemical behaviour of the platinum-group elements in the mantle. *Geochimica et Cosmochimica Acta* **63**, 3915–3935.

Reisberg, L. & Lorand, J.-P. (1995). Longevity of sub-continental mantle lithosphere from osmium isotope systematics in orogenic peridotite massifs. *Nature* **376**, 159–162.

Reisberg, L., Allègre, C. J. & Luck, J. M. (1991). The Re–Os systematics of the Ronda ultramafic complex of southern Spain. *Earth and Planetary Science Letters* **105**, 196–213.

Righter, K., Chesley, J. T., Geist, D. & Ruiz, J. (1998). Behaviour of Re during magma fractionation: an example from Volcan Alcedo, Galapagos. *Journal of Petrology* **39**, 785–795.

Rudnick, R. L., McDonough, W. F. & Chappell, B. W. (1993). Carbonatite metasomatism in the northern Tanzanian mantle: petrographic and geochemical characteristics. *Earth and Planetary Science Letters* **114**, 463–475.

Séranne, M. (1999). The Gulf of Lion continental margin (NW Mediterranean) revisited by IBS: an overview. In: Durand, B., Jolivet, L., Horvath, F. & Séranne, M. (eds) *The Mediterranean Basins: Tertiary Extension within the Alpine Orogen. Geological Society, London, Special Publications* **156**, 15–36.

Shirey, S. B. & Walker, R. J. (1995). Carius tube digestion for low-blank rhenium–osmium analysis. *Analytical Chemistry* **67**, 2136–2141.

Shirey, S. B. & Walker, R. J. (1998). The Re–Os isotope system in cosmochemistry and high-temperature geochemistry. *Annual Review of Earth and Planetary Sciences* **26**, 423–500.

Szabo, C. & Bodnar, R. J. (1995). Chemistry and origin of mantle sulfides in spinel peridotite xenoliths from alkaline basaltic lavas, Nograd–Gomor Volcanic Field, northern Hungary and southern Slovakia. *Geochimica et Cosmochimica Acta* **59**, 3917–3927.

Torres-Ruiz, J., Garuti, G., Gazzotti, M., Gervilla, F. & Hach-Ali, P. F. (1996). Platinum-group minerals in chromitites from the Ojen lherzolite massif (Serrania de Ronda, Betic Cordillera, Southern Spain). *Mineralogy and Petrology* **56**, 25–50.

Van Orman, J. A., Grove, T. L. & Shimizu, N. (2001). Rare earth element diffusion in diopside: influence of temperature, pressure, and ionic radius, and an elastic model for diffusion in silicates. *Contributions to Mineralogy and Petrology* **141**, 687–703.

Vernieres, J., Godart, M. & Bodinier, J.-L. (1997). A plate model for the simulation of trace-element fractionation during partial melting and magma transport in the Earth's upper mantle. *Journal of Geophysical Research* **102**, 24771–24784.

Walker, R. J., Horan, M. F., Morgan, J. W., Becker, H., Grossman, J. N. & Rubin, A. E. (2002). Comparative ^{187}Re–^{187}Os systematics of chondrites: Implications regarding early solar system processes. *Geochimica et Cosmochimica Acta* **66**, 4187–4201.

Watson, E. B. & Brenan, J. M. (1987). Fluids in the lithosphere, 1. Experimentally-determined wetting characteristics of CO_2–H_2O fluids and their implications for fluid transport, host-rock physical properties and fluid inclusion formation. *Earth and Planetary Science Letters* **85**, 497–515.

Wilson, M. R., Kyser, T. K. & Fagan, R. (1996). Sulfur isotope systematics and platinum group element behavior in REE-enriched metasomatic fluids: A study of mantle xenoliths from Dish Hill, California, USA. *Geochimica et Cosmochimica Acta* **60**, 1933–1942.

Wood, S. A. (1987). Thermodynamic calculations of the volatility of the platinum group elements (PGE): The PGE content of fluids at magmatic temperatures. *Geochimica et Cosmochimica Acta* **51**, 3041–3050.

Xu, C., Qi, L., Huang, Z., Chen, Y., Yu, X., Wang, L. & Li, E. (2008). Abundances and significances of platinum group elements in carbonatites from China. *Lithos* **105**, 201–207.

Yaxley, G. M., Crawford, A. J. & Green, D. H. (1991). Evidence for carbonatite metasomatism in spinel peridotite xenoliths from western Victoria, Australia. *Earth and Planetary Science Letters* **107**, 305–317.

Yudovskaya, M. A., Tessalina, S., Distler, V. V., Chaplygin, I. V., Chugaev, A. V. & Dikov, Y. (2008). Behaviour of highly-siderophile elements during magma degassing: a case study at the Kudryavy volcano. *Chemical Geology* **248**, 318–341.